



UNIVERSITY *of the*
WESTERN CAPE

TARGETED DELIVERY OF EMBELIN TO CANCER CELLS

ZAAKIYAH EMJEDI



A thesis submitted in partial fulfilment of the requirements for the degree
Magister Scientiae in the Department of Biotechnology, University of the
Western Cape

Supervisor: Dr. Mervin Meyer

Co-supervisor: Dr. Abram Madiehe

May 2013

ABSTRACT

TARGETED DELIVERY OF EMBELIN TO CANCER CELL

Z. Emjedi

MSc thesis, Department of Biotechnology, Faculty of Natural Science, University of the Western Cape, South Africa.

Apoptosis or programmed cell death is vital to the development of organisms as they maintain the balance between cell death and cell growth. Failure to activate apoptosis has been implicated in carcinogenesis and often results from the over expression of anti-cancer proteins such as the X-linked inhibitor of apoptosis protein (XIAP). XIAP is over expressed in certain cancers and is a potent inhibitor of the initiator caspase 9 and effector caspases 3 and 7. The increased expression of XIAP in cancer cells result in the resistance to apoptosis. The control of XIAP is therefore considered as a target for anti-cancer drug development. Embelin or 2,5-dihydroxy-3-undecyl-1,4-benzoquinone is a dihydroxyquinone compound that was previously shown to inhibit XIAP. This drug was discovered by structure based computational screening. The binding of embelin to XIAP displaces XIAP from caspases, consequently eliminating the inhibitory effect of XIAP on apoptosis.

The objective of this study was to develop a gold nanoparticle that can be used for the targeted delivery of embelin to cancer cells thereby enhancing pro-apoptotic effects of the pro-apoptotic drug, ceramide. XIAP expression levels were investigated by Western blot analysis in a panel of human cancer cell lines available in the laboratory to identify two cell lines that can be used as low and high XIAP expression controls. Gold nanoparticles were synthesized and conjugated with embelin and a cancer targeting peptide with the amino acid sequence LTVSPWY. The biconjugated nanoparticles were used to co-treat MCF7 and HepG2 cells with ceramide. Apoptosis was quantified using flow cytometry. The uptake of gold nanoparticles was investigated using HR-TEM and ICP-OES. This study showed that gold nanoparticles conjugated with the LTVSPWY peptide is specifically targeted to and taken up by cancer cells. Gold nanoparticles conjugated with embelin promoted ceramide induced apoptotic cell death of cancer cells. However, it was observed that gold nanoparticles biconjugated with the LTVSPWY peptide and embelin failed to enhance the pro-apoptotic effects of ceramide.

This study successfully demonstrated that gold nanoparticles conjugated with embelin could be used to enhance the effects of anti-cancer drugs using ceramide as an example.



KEYWORDS

Apoptosis

Carcinogenesis

Initiator Caspase

Effector Caspase

Pro-apoptotic

Biconjugated nanoparticles

Gold nanoparticles

Embelin

Ceramide



DECLARATION

I declare that “**Targeted delivery of embelin to cancer cells**” is my own work, that it has not been submitted for any degree or examination in any other university, and that all the sources I have used or quoted have been indicated or acknowledged by complete references.

ZAAKIYAH EMJEDI

Signed.....



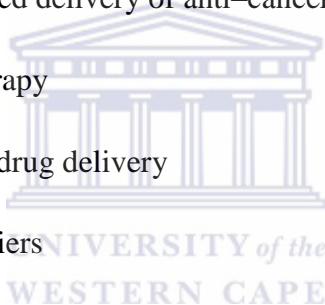
May 2013

TABLE OF CONTENTS	PAGE
ABSTRACT	ii
KEYWORDS	iv
DEDICATION	v
TABLE OF CONTENTS	vi
LIST OF TABLES	xiii
LIST OF FIGURES	xiv
ABBREVIATIONS	xvii
ACKNOWLEDGEMENTS	xix

CHAPTER 1: INTRODUCTION

1.1. Cancer and associated risk factors	1
1.1.1 Cancer development	1
1.1.2 Global statistics for breast and liver cancer	2
1.1.3 Impact of genetics and lifestyle on cancer development	3
1.2. Apoptosis	3
1.2.1 Apoptotic cell death	3
1.2.2 Apoptosis pathways	4
1.2.3 Ceramide as an inducer of apoptosis	6
1.2.3.1 Ceramide generation	6
1.2.3.2 Effects of ceramide and ceramide analogues treatments	7
1.2.4. Defective apoptosis	8
1.3. Relations between inhibitor of apoptosis proteins and cancer	9

1.3.1	Inhibitor of apoptosis proteins	9
1.3.2	X–chromosome linked inhibitor of apoptosis protein (XIAP) and its relation to cancer	10
1.4.	Embelin: an inhibitor of XIAP	11
1.4.1	Structure of embelin	11
1.4.2	Embelin as an inhibitor of XIAP	12
1.5.	Embelin targets XIAP via its BIR3 domain	12
1.5.1	Relation between XIAP’s BIR3 and Smac/DIABLO	12
1.5.2	BIR3 inhibition of XIAP leads to apoptosis	15
1.6.	Nanotechnology for targeted delivery of anti–cancer drugs	15
1.6.1	Goal of cancer therapy	15
1.6.2	Nanoparticles and drug delivery	18
1.6.3.	Nanoparticles as drug carriers	19
1.7.	Aims of this study	20
1.8.	Thesis outline	20
CHAPTER 2: MATERIALS AND METHIODS		
2.1.	Materials used and suppliers	24
2.1.1	List of kits used	27
2.2.	Solutions and buffers	27
2.3.	Cell culture	29
2.3.1	Thawing MCF7 and HepG2 cells	29
2.3.2	Trypsinization of MCF7 and HepG2 cells	29



2.3.3	Seeding of cells	30
2.3.4.	Synthesis of embelin conjugated nanoparticles	30
2.4.	Synthesis of embelin conjugated nanoparticles	30
2.5.	Investigating the toxicity of embelin and embelin conjugated nanoparticles	30
2.6.	Investigating the concentration and percentage of gold in treated cancer cells by Inductively Coupled Plasma–Optical Emission Spectrometry (ICP–OES)	31
2.7.	Investigating uptake of nanoparticles in treated cancer cells by transmission electron microscopy (TEM)	31
2.8.	Statistical analysis	32
2.9.	RNA isolation	32
2.9.1	Agarose electrophoresis of RNA	33
2.10.	cDNA synthesis	33
2.11.	Primers	34
2.12.	Polymerase chain reaction (PCR) amplification of DNA	35
2.13.	Agarose gel electrophoresis of PCR product	36
2.14.	Gel purification of amplified PCR product	36
2.15.	DNA cloning	36
2.15.1	pGEM®–T Easy vector system	36
2.15.2	Ligation of PCR product into pGEM®–T Easy vector	37
2.15.3	Transformation of competent <i>E. coli</i> MC1061 competent cells	38
2.15.4	Colony PCR amplification	38
2.15.5	Culturing of transformed MC1061 <i>E. coli</i> cells	38
2.15.6	Plasmid DNA isolation and purification	39



2.15.7	Restriction digestion of pGEM–XIAP	40
2.16.	DNA sub–cloning	40
2.16.1	pET28a Cloning Vector	40
2.16.2	Restriction Digestion of pET28a	41
2.16.3	Ligation of the released pGEM–XIAP product into the pET28a vector	41
2.16.4	Transformation of BL21 (DE3) pLysS <i>E. coli</i> competent cells with pET28a–XIAP construct	42
2.16.5	Colony PCR amplification	42
2.16.6	Culturing of transformed BL21 (DE3) pLysS <i>E. coli</i> cells	44
2.17.	Mini expression screen for recombinant His–XIAP protein	43
2.18.	Purification of recombinant His–XIAP protein	43
2.18.1	Cell extract preparation and protein purification as per Ni–NTA His–Bind Resins	44
2.19.	Expression and purification of GST–XIAP protein	45
2.19.1	Transformation of <i>E. coli</i> BL21 (DE3) pLysS competent cells with pGEX–XIAP construct	45
2.19.2	Expression screen for recombinant GST–XIAP protein	45
2.19.3	Expression of GST–XIAP recombinant protein	46
2.19.4	Cell extract preparation and protein purification as per BugBuster® GST–Bind purification kit	46
2.20.	Protein extraction from cultured human cancerous cells	47
2.21.	One Dimensional SDS Polyacrylamide Gel Electrophoresis	47
2.21.1	Gel preparation	47
2.21.2	Sample preparation and gel loading	49


2.21.3	Gel staining	49
2.22.	Analysis of XIAP expression by Western Blot	50
2.22.1	Blot transfer of proteins onto PVDF membrane	50
2.22.2	Analysis of XIAP expression	50
2.22.3	Exposure of membrane	50
2.23.	Densitometric Analysis of Western Blot	50
2.24.	Evaluating the interaction of recombinant GST–XIAP protein and embelin	51

CHAPTER 3: RESULTS

3.1.	Evaluating the expression levels of XIAP in human cancer cells	54
3.1.1	Introduction	54
3.1.2	Western blot analysis of XIAP expression in various human cancer cell lines	54
3.2.	Evaluating the apoptotic effects of ceramide as an apoptotic inducer	56
3.2.1	Introduction	56
3.2.2	Characterization of conjugated nanoparticles	57
3.2.3	Morphological changes in MCF7 and HepG2 cancer cells upon treatment	59
3.2.4	Induction of apoptosis on MCF7 and HepG3 cancer cells as a result of the treatment options	62
3.2.5	Evaluating the cellular uptake of AuNP–E and AuNP–P–E	64
3.2.5.1	Inductively Coupled Plasma–Optical Emission Spectrometry	64
3.2.5.2	Transmission Electron Microscopy	64
3.3.	Cloning of XIAP into His–tagged expression vector system	68

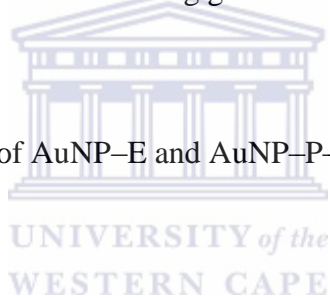
3.3.1	Introduction	68
3.3.2	The isolation of total RNA from MCF7 breast cancer cells	68
3.3.3	PCR amplification of XIAP	68
3.3.4	Sub-cloning of XIAP into pGEM-T Easy vector	69
3.3.5	Colony PCR screening of XIAP positive clones	69
3.3.6	Sequence analysis of XIAP positive clones	70
3.3.7	XIAP release from pGEM-XIAP by restriction digestion	72
3.3.8	Preparation of the pET28a expression vector for DNA ligation	73
3.3.9	Screening of XIAP positive clones by colony PCR	74
3.4.	Affinity purification of recombinant His-XIAP	75
3.4.1	Introduction	75
3.4.2	Screening for the expression of XIAP	75
3.4.3	Purification of His-XIAP recombinant protein using the Ni-NTA His-Bind® resins	76
3.5.	Affinity purification for recombinant GST XIAP	77
3.5.1	Introduction	77
3.5.2	Expression screen of GST-XIAP	77
3.5.3	Sequence analysis of GST-XIAP	78
3.5.4	Purification of GST-XIAP using BugBuster® GST-Bind Purification Kit	79
3.6.	Evaluating the interaction between the recombinant GST-XIAP Protein and embelin and embelin Conjugated Nanoparticles by Isothermal Titration Calorimetry (ITC)	80
3.6.1	Introduction	80
3.6.2	ITC analysis	80

CHAPTER 4:DISCUSSION

4.1.	Synthesis and characterization of gold nanoparticles	86
4.2.	The expression levels of XIAP in human cancer cell lines	87
4.3.	The cytotoxic effects of AuNP–E and AuNP–P–E	88
4.4.	Evaluating cellular uptake of AuNPs	89
4.5.	Expression and purification of recombinant XIAP protein	90
4.6.	Protein–Protein interactions	94
4.6.1	Isothermal Titration Calorimetry	94
4.6.2	Applications of ITC to study the Protein–Nanoparticle interactions	94
4.7.	Investigating the binding between the recombinant GST–XIAP and embelin	95
4.8.	Conclusion	96
4.9.	Future Directions	97
		
	REFERENCES	98

LIST OF TABLES

Table 2.1:	Reagents utilized in cDNA synthesis reaction.	34
Table 2.2:	XIAP gene specific primers used in PCR reactions.	34
Table 2.3:	PCR primers as at 35 cycles.	35
Table 2.4:	Reagents utilized in PCR reactions.	35
Table 2.5:	Reagents utilized in the ligation reaction of XIAP and pGEM®-T Easy vector system.	38
Table 2.6:	Reagents used in ligation of pET28a expression vector and XIAP.	42
Table 2.7:	Stock solutions for the 12% separating gel solution.	48
Table 2.8:	Stock solution for the 5% stacking gel solution.	49
Table 3.1:	Optical properties of AuNP-E and AuNP-P-E.	58



LIST OF FIGURES

Figure 1.1:	Pathway leading to cancer following DNA damage.	1
Figure 1.2:	Process of apoptotic cell death.	4
Figure 1.3:	The two major apoptotic pathways.	5
Figure 1.4:	Structure of ceramide.	6
Figure 1.5:	Pathways of ceramide generation.	7
Figure 1.6:	Functional domains of the XIAP protein.	11
Figure 1.7:	Chemical structure of embelin.	12
Figure 1.8:	NMR structure of XIAPs BIR3–Smac/DIABLO complex.	14
Figure 1.9:	Structure of a nanoparticle for targeted drug delivery.	17
Figure 2.1:	A circular map and sequence reference points of pGEM®–T Easy vector system.	37
Figure 2.2:	A circular map and sequence referencing points of pET28a expression vector system.	41
Figure 3.1:	1D SDS polyacrylamide gel electrophoresis of proteins extracted from available mammalian cancer cells.	55
Figure 3.2:	Western blot of XIAP expression in mammalian cancer cells.	55
Figure 3.3:	Densitometry data for XIAP protein expression.	56
Figure 3.4:	A schematic representation of gold nanoparticles before and after conjugation.	58
Figure 3.5:	UV Vis spectra for (a) AuNP–E and (b) AuNP–P–E.	58
Figure 3.6:	TEM data for (a) AuNP–E and (b) AuNP–P–E.	59

Figure 3.7:	Morphology of HepG2 liver cancer cells treated with embelin, AuNP-E or AuNP-P-E as well as co-treatments with ceramide.	60
Figure 3.8:	Morphology of MCF7 breast cancer cells treated with embelin, AuNP-E or AuNP-P-E as well as co-treatments with ceramide.	61
Figure 3.9:	Indications of apoptosis of (a) HepG2 and (b) MCF7 cancer cells as a result of the various treatment options.	63
Figure 3.10:	Evaluating the presence of gold in MCF7 breast and HepG2 liver cancer cells treated with AuNP-E and AuNP-P-E.	66
Figure 3.11:	Evaluating the uptake of AuNP-E and AuNP-P-E in HepG2 and MCF7 cells.	67
Figure 3.12:	Total RNA isolated from MCF7 mammalian breast cancer cells.	68
Figure 3.13:	PCR amplification of XIAP with the use of gene specific primers.	69
Figure 3.14:	Colony PCR screening for XIAP positive clones.	70
Figure 3.15:	BLAST sequence analysis of a positive clone 3 for XIAP.	71
Figure 3.16:	Pairwise protein sequence of the translated DNA sequence obtained for a positive XIAP clone and XIAP protein sequence.	72
Figure 3.17:	Restriction digestion of pGEM-XIAP. Plasmid DNA was digested with <i>XhoI</i> and <i>NdeI</i> .	73
Figure 3.18:	Restriction digestion of the pET28a expression vector.	74
Figure 3.19:	Colony PCR screen for XIAP positive clones.	75
Figure 3.20:	Expression screen for His-XIAP protein.	76
Figure 3.21:	Purification of the His-XIAP protein using Ni-NTA His-Bind® Resin.	77
Figure 3.22:	Expression screen for GST-XIAP protein.	78
Figure 3.23:	Pairwise protein sequence of the translated DNA sequence for a positive clone of XIAP from the pGEX-4T-2 vector.	79

Figure 3.24: Purification of the GST–XIAP protein using the BugBuster® GST–Bind Purification Kit.	80
Figure 3.25: ITC titration data describing the interaction of EDTA with calcium.	82
Figure 3.26: ITC titration data describing the interaction of recombinant GST–XIAP protein and embelin.	83



ABBREVIATIONS

APS	Ammonium Persulphate
AuNP	Gold Nanoparticle
AuNP-E	Embelin conjugate Gold Nanoparticle
AuNP-P-E	Biconjugated Gold Nanoparticle
bp	Base Pair
BSA	Bovine Serum Albumin
cDNA	Complementary Deoxyribonucleic Acid
CO ₂	Carbon Dioxide
DEPC	Diethylpyrocarbonate
DNA	Deoxyribonucleic Acid
DTT	Dithiothreitol
DMSO	Dimethyl Sulfoxide
DMEM	Dulbecco's Modified Eagle's Medium
EDTA	Ethylene Diamine Tetra-Acetic Acid
FBS	Fetal Bovine Serum
IAPs	Inhibitor of Apoptosis Proteins
IPTG	Isopropyl β -D-1-thiogalactopyranoside
kb	Kilobyte
kDa	Kilo Dalton
NaOH	Sodium Hydroxide
ng	Nanogram
nm	Nanometer



PBS	Phosphate Buffered Saline
RNA	Ribonucleic Acid
SD	Standard Deviation
SDS	Sodium Dodecyl Sulphate
SDS PAGE	Sodium Dodecyl Sulphate Polyacrylamide Gel Electrophoresis
TBS	Tris Buffered Saline
TBETween	Tris Buffered Saline containing Tween20
TEMED	N,N,N',N'-Tetramethylethylenediamine
Tris	Tris (hydroxymethyl) aminoethane
μ l	Microliter
μ M	Micrometer
UV	Ultraviolet
v/v	volume to volume
w/v	weight to volume
XIAP	X-linked Inhibitor of Apoptosis Protein



ACKNOWLEDGEMENTS

First and foremost I would like to say thank you to my Creator for leading me the right way and giving me the strength and perseverance to see this study through.

I would like to thank my supervisor for allowing me the opportunity to carry out this study in his laboratory. I would like to express my sincerest gratitude to Dr. Meyer for his supervision, knowledge, support, encouragement, critique as well as the opportunities he presented me with. I acknowledge him for proofreading my thesis.

I would like to extend my gratitude to my co-supervisor Dr. Abram Madiehe for making this project possible. I would like to thank Dr. Madiehe for his support, encouragement and critic. I acknowledge him for proofreading my thesis.

I would like to express my sincerest gratitude to all those involved, past and present, in the DST/Mintek NIC Biolabels Group (UWC). Your advice, support and encouragement will always be appreciated.

I would like to thank the staff and students, past and present, of the Biotechnology Department for their support and encouragement.

I would like to thank the following people: Mr. Ronald Dreyer for his assistance with the FACS analysis, Mrs. Nolan Muller for her assistance with the TEM imaging and Prof. L. Petrik for her assistance for the ICP-OES analysis. I would also like to thank Dr. James Fredericks, Mr. Mustafa Drah, Mr Francois Taute for their contribution to this work. Lastly, I would like to thank the late Mr. Stonard Kanyanda for his patience, assistance and guidance with regard to the cell culture experiments and FACS.

My sincerest gratitude goes to The National Research Foundation (NRF) and DST/Mintek NIC for the financial assistance.

CHAPTER 1: INTRODUCTION

- 1.1. Cancer and associated risk factors
 - 1.1.1 Cancer development
 - 1.1.2 Global statistics for breast and liver cancer
 - 1.1.3 Impact of genetics and lifestyle on cancer development
- 1.2. Apoptosis
 - 1.2.1 Apoptotic cell death
 - 1.2.2 Apoptosis pathways
 - 1.2.3 Ceramide as an inducer of apoptosis
 - 1.2.3.1 Ceramide generation
 - 1.2.3.2 Effects of ceramide and ceramide analogues treatments
 - 1.2.4. Defective apoptosis
- 1.3. Relations between inhibitor of apoptosis proteins and cancer
 - 1.3.1 Inhibitor of apoptosis proteins
 - 1.3.2 X–chromosome linked inhibitor of apoptosis protein (XIAP) and its relation to cancer
- 1.4. Embelin: an inhibitor of XIAP
 - 1.4.1 Structure of embelin
 - 1.4.2 Embelin as an inhibitor of XIAP
- 1.5. Embelin targets XIAP via its BIR3 domain
 - 1.5.1 Relation between XIAP’s BIR3 and Smac/DIABLO
 - 1.5.2 BIR3 inhibition of XIAP leads to apoptosis
- 1.6. Nanotechnology for targeted delivery of anti–cancer drugs

1.6.1 Goal of cancer therapy

1.6.2 Nanoparticles and drug delivery

1.6.3. Nanoparticles as drug carriers

1.7. Aims of this study

1.8. Thesis outline



1.1.Cancer and associated risk factors

1.1.1. Cancer development

Cancer is a group of diseases which are characterized by the uncontrolled growth of cells with abnormal DNA. When a cell detects DNA damage, it triggers its DNA repair mechanism. Failure of the cell to repair DNA damage results in the instability in its genome. Under normal conditions, apoptosis is triggered to ensure that the damaged cells do not survive and multiply. In the event where these cells are not destroyed by apoptosis cancer can develop (Figure 1.1) (Gotter, 2009). Cancer arises from various factors including inherited mutations, immune disorders, hormone imbalances, tobacco, chemicals, as well as radiation (Cretney *et al.*, 2007). Cancer cell proliferation arises as a result of the interaction between the DNA damaged cell and the non-damaged cell. As a result of the interaction, practically all types of human tumours, especially their metastatic outgrowths, continue to spread the defects to various cell types resulting in the formation of malignant growth (Hanahan and Weinberg, 2000).

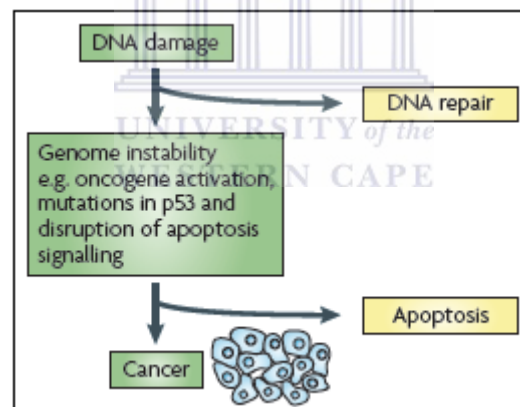


Figure 1.1: Pathway leading to cancer following DNA damage. When the DNA of a cell is damaged, signalling cascades are triggered to repair the damaged DNA. If DNA repair is unsuccessful, the genome becomes unstable which, under normal conditions, trigger apoptosis. Should the events leading to apoptosis are terminated the result will be the development of cancer (Gotter, 2009).

According to Ferlay and colleagues more than 85% of the “global cancer burden”, for liver cancer, occurs in developing countries. Regions regarded as being high risk for liver cancer, are Eastern and Western Africa, Southern Africa, South Central Asia, Central Africa and Southern America where the cumulative risk of developing cancer range from 3.8 (highest) to 2.5 (lowest). Regions regarded as being low risk are Western Asia, North America and

Australia/New Zealand where the risk of developing cancer was constant at 0.5% (Ferley *et al.*, 2010).

1.1.2. Global statistics for breast and liver cancer cells

According to Ferlay and colleagues, the 2008 statistics shows that lung cancer remains the most common cancer in the world as it has a number 1.6 million cases which accounts for 12.7% of all cancers and with a death toll of 1.4 million (18.2% of all deaths). The second most common cancer overall is breast cancer. It has 1.4 million cases (10.9%) but is the fifth highest cause of death (458 000 deaths, 6.1%). Regarding the incidence of cancer, colorectal cancer has been reported to be responsible for 608 000 deaths, stomach cancer 738 000 deaths, prostate cancer 261 000 deaths and liver cancer 695 000 deaths (Ferlay *et al.*, 2010).

The global cancer statistics of 2008 supports statistics the study conducted by Parton and colleagues where breast cancer was identified as the most common and frequent malignancy among women (Parton *et al.*, 2001; Ferley *et al.*, 2010). Parton and colleagues identified breast cancer to comprise 18% of all cancers in women (Parton *et al.*, 2001) where one in eight women will develop breast cancer in their lifetime (Johnson and Guthrie, 2000). For the purpose of this study, focus will be on breast and liver cancer.

During 2008 approximately 1.38 million new breast cancer cases were diagnosed. Therefore with an overall global percentage incidence of 10.9% breast cancer ranks second when comparing all cancers. With an estimate of 690 000 new cases of breast cancer in both developed and developing countries, breast cancer is emerging as the most common cancer in a population ratio of 1:4 for developed and developing countries respectively. As a results of 458 000 deaths due to breast cancer, when compared to other cancer related deaths breast cancer ranks fifth. However it must be noted that breast cancer is the most frequent cause of death among women in developing countries where accounting for 269 000 deaths or a total percentage of 12.7% within developing regions alone (Ferlay *et al.*, 2010).

According to the global statistics, liver cancer is the fifth most common cancer in men and seventh most common in women. It is the third most common cause of cancer related deaths worldwide. Most of the liver cancer cases diagnosed have been reported in developing countries where regions of high incidence are Eastern and South–Eastern Asia, Central and Western Africa, Melanesia and Micronesia–Polynesia (Ferlay *et al.*, 2010).

1.1.3. Impact of genetics and lifestyle on cancer development

The risk of developing breast cancer depends on a number of factors. While age and gender are the two pre-dominant cancer risk factors (Carter and Church, 2009), Trentham–Dietz and colleagues suggested that a family history in the case of breast cancer as well as potentially modifiable characteristics such as body weight, alcohol consumption and post-menopausal hormone use may be associated with a secondary risk of developing breast cancer (Trentham–Dietz *et al.*, 2007). The link between cancer and socio-economic conditions suggest that lifestyle may also impact on the risk of developing cancer. Together with pre-existing risk factors may it bring about a change in the incidence of cancer, especially in the developing countries with regard to the use of tobacco, alcohol consumption, nutritional habits as well as physical activity (Ferley *et al.*, 2010).

1.2. Apoptosis

1.2.1. Apoptotic cell death

According to Fry and Vassiley the development and progression of cancer is associated with irregularities in biochemical pathways (Fry and Vassiley, 2005). One of the biochemical pathways that are often affected in cancer cells is the apoptotic pathways.

Programmed cell death or apoptosis are descriptive definitions of a specific form of cell death (Kroemer *et al.*, 2005) which have been implicated in a variety of both physiological and pathological process (Green and Martin, 1995).

Apoptosis is a multi-stage process characterized by cell shrinkage, chromatin condensation as well as nuclear and cell fragmentation. The final stage of apoptosis is characterized by the formation of apoptotic bodies (Figure 1.2) which are engulfed by neighbouring phagocytic cells (Gewies, 2003; Gotter, 2009).

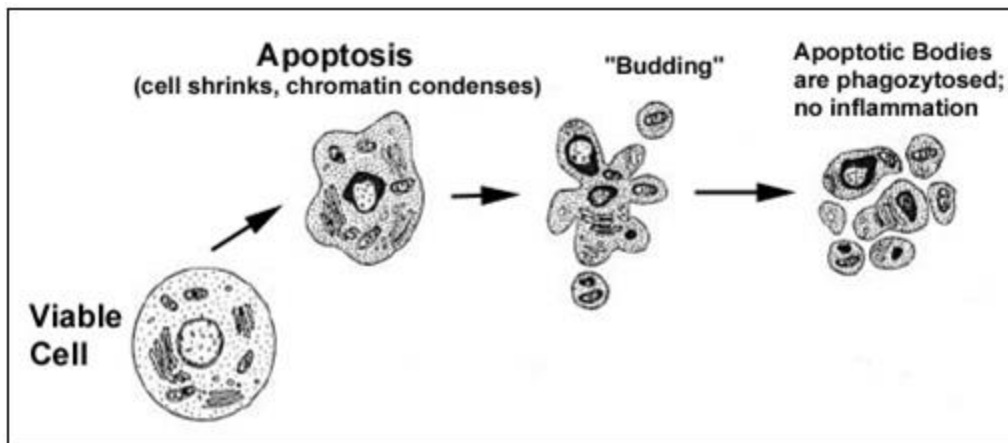


Figure 1.2: Process of apoptotic cell death. Apoptotic cells differ from viable cells in that apoptotic cells shrink upon deformation caused by chromatic condensation and nuclear cell fragmentation, which is followed by the plasma membrane “budding” resulting in cell fragmentation and finally the formation of membrane enclosed structures known as apoptotic bodies [adapted from Gewies, 2003].

This fast and effective form of cell death is an ordered set of events responsible for cell death during the development of multicellular organisms (Blagosklonny, 2004) and thereby control the development of the organism (Fisher and Schulze–Osthoﬀ, 2005¹; Gotter, 2009).

Apoptosis is essential in the development of the immune system (Fisher and Schulze–Osthoﬀ 2005²). Apoptosis controls the cell number (Gotter, 2009) as it maintains the balance between cell death and cell proliferation (Fisher and Osthoﬀ, 2005²). Apoptosis has become a key interest in biomedical research as it plays a central role in physiological processes such as morphogenesis, negative selection in the immune system as well as cancer surveillance (Hengartner, 1996).

1.2.2. Apoptosis pathways

Apoptosis induction may be achieved by the increased expression of pro–apoptotic factors whilst reducing the expression of anti–apoptotic factors (Ghavami *et al.*, 2009). As deregulation of apoptosis is implicated in a number of diseases, apoptosis is seen as a target for the development of alternative therapeutic strategies (Fisher and Schulze–Osthoﬀ, 2005¹).

Apoptosis is executed via two distinct signalling pathways, namely the intrinsic or the mitochondrial pathway and the extrinsic or death receptor pathway (Figure 1.3) (Fisher and Schulze–Osthoﬀ, 2005²). A third pathway, known as the granzyme B pathway also exist (Salvesen and Dixit, 1997; Thornberry and Lazebnik, 1998).

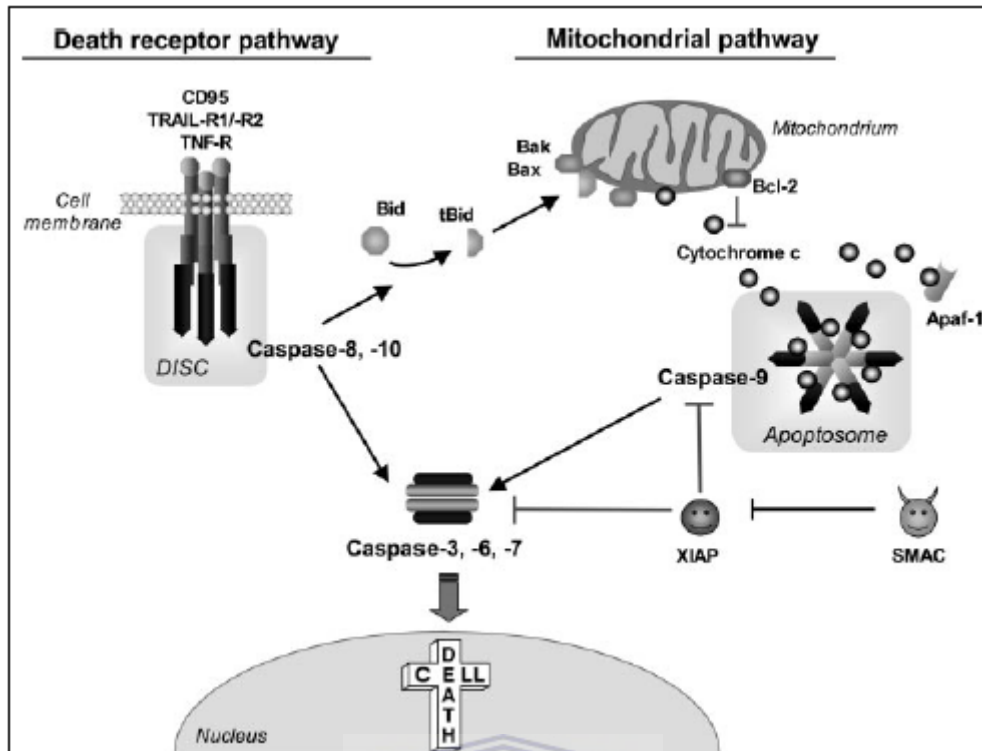


Figure 1.3: The two major apoptotic pathways. The extrinsic (or death receptor pathway) and the intrinsic (or mitochondrial) pathways leading to apoptosis appear on the left and right, respectively. It must be noted that the extrinsic and intrinsic pathways both converge at the stage of caspase activation which activates the same downstream caspases resulting in apoptotic cell death (Fisher and Schulze–Osthoﬀ, 2005²).

The extrinsic pathway is initiated by the ligation of death receptors such as Fas/CD95, TNF receptor and/or TRAIL receptor. Death receptors function in activating initiator caspases 8 and 10 which, in turn, directly activates eﬀector caspases 3 and 7 (Nachmais *et al.*, 2004; Salvesen and Dixit, 1997; Thornberry and Lazebnik, 1998; Raychaundhuri, 2010).

The intrinsic pathway is initiated in response to intracellular stresses such as DNA damage, hypoxia and/or growth factor deprivation (Sousa and Espreafico, 2006). The caspase cascade is triggered by an increase in the permeability of the mitochondrial membrane and the release of cytochrome c. These mitochondrial changes result in the formation of apoptosomes consisting of pro-caspase 9, Apaf-1, cytochrome c and dATP. The formation of the apoptosome results in caspase 9 activation, which in turn activates caspase 3 (Salvesen and Dixit, 1997; Thornberry and Lazebnik, 1998; Nachmias *et al.*, 2004). Caspase 3 cleaves and/or degrades cellular substrates (Fisher and Schulze–Osthoﬀ, 2005²; Friedrich *et al.*, 2001) thereby inactivating enzymes or disassembling cellular structures (Friedrich *et al.*, 2001).

1.2.3. Ceramide as an inducer of apoptosis

Apoptosis can be triggered either by activating the extrinsic pathway by the presence of death receptors. Alternatively, the intrinsic or mitochondrial pathway may also be activated in response to DNA damage. Apoptosis may also be triggered *in vitro* using anti-tumour agents. Some examples of anti-tumour agents used in human cancer models are doxorubicin, paclitaxel, daunorubicin, and ceramide (Monrad and Cabot, 2013).

Ceramide, a product resulting from sphingolipid metabolism, consist of N-acetylated (14 to 16 carbons) sphingosine (18 carbons). It is comprised of hydroxyl groups situated at carbons 1 and 3, a *trans* double bond between carbons 4 and 5 which is important for its biological activity as well as an amino group positioned at carbon 2 (Figure 1.4) (Pettus, 2002; Ogretmen and Hannun, 2004).



Figure 1.4: Structure of ceramide. Ceramide is comprised of sphingosine and a fatty acid. An important feature to note is the *trans* double bond present between carbons 4 and 5 (Radin, 2003).

Sphingomyelin is the main lipid in the plasma membrane of mammalian cells. Hydrolysis of sphingomyelin is the major source of ceramide (Hannun, 1996; Herr and Debatin, 2001). *In vivo* ceramide generation may be achieved through multiple pathways. The *de novo* and sphingomyelin pathways are mainly involved in increasing exogenous ceramide levels (Figure 1.5) (Hannun, 1996; Ogretmen and Hannun, 2004).

1.2.3.1. Ceramide generation

Ceramide generation via the *de novo* pathway is as a result of serine and palmitoyl-CoA reacting with serine palmitoyl transferase to generate 3-ketosphinganine (Figure 1.5). The resulting shinganine is converted to dihydroceramide due to the action of fatty acyl coenzyme A and dihydroceramide kinase. Ceramide results from the action of dihydroceramide desaturase on dihydroceramide (Ogretman and Hannun, 2004). Ceramide generation also

involves the activation of the enzyme sphingomyelinase or SMase (Hannun, 1996; Jiang *et al.*, 2000, Ogretman and Hannun, 2004) in response to TNF and other cytokines (Hannun, 1996). Upon SMase activation sphingomyelin is cleaved thereby releasing phosphocholine and ceramide (Andrieu–Abadie *et al.*, 2001).

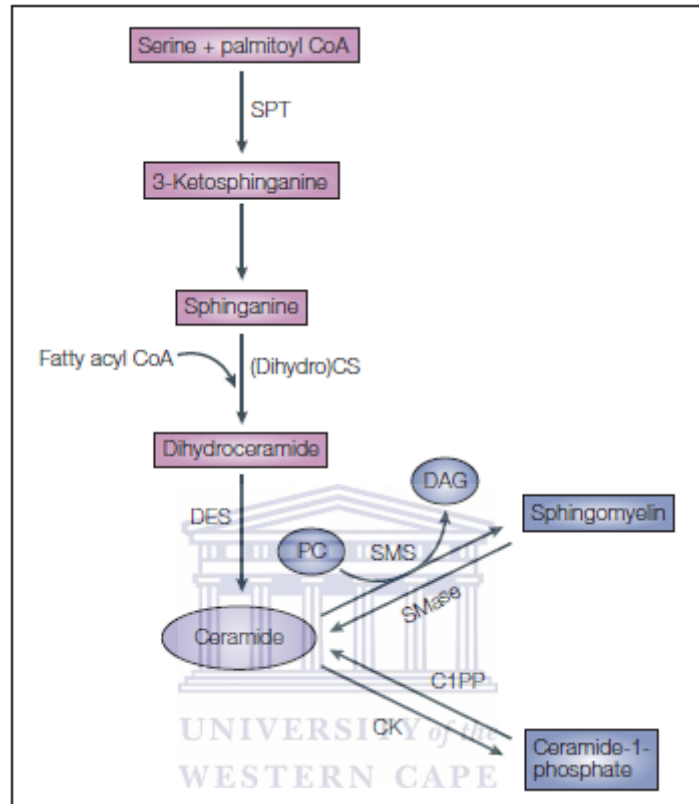


Figure 1.5: Pathways of ceramide generation. A major source of ceramide generation occurs via sphingomyelin hydrolysis. *In vivo* ceramide generation is generated by the *de novo* pathway [adapted from (Ogretman and Hannun, 2004)].

1.2.3.2. Effects of ceramide and ceramide analogues treatments

C2– and C6– ceramide are short chain analogues of ceramide. These two short chain ceramides mimic some of the signalling events of endogenous ceramide. It must be noted that endogenous ceramide is a hydrophobic molecule whereas the short chain ceramides are water soluble molecules. Therefore, it is unlikely that these short chain ceramides carries out all the biological functions of endogenous ceramide (Wagenknecht *et al.*, 2001).

Initiators of apoptosis such as TNF, daunorubicin, γ and ultraviolet (UV) radiation as well as growth factor removal are associated with an increase in the production of ceramide (Jiang *et al.*, 2000). Intracellular levels of ceramide increase in response to many chemotherapy drugs,

ionizing radiation as well as cytokines. These responses induce morphological changes in the cells which are indicative of apoptosis (Shabbits *et al.*, 2003).

According to Radin apoptosis almost always occurs when cancer cells are treated *in vitro* with exogenous ceramide (Radin, 2003). According to Hannun and Luberto apoptosis among most cancer cells triggered by ceramide may be accompanied by cell cycle arrest (Hannun and Luberto, 2000).

Treatment with exogenous ceramide analogues enables ceramide to mimic the role of apoptosis inducers via direct molecular interactions. In these cases, ceramide exerts its killing effect on specific targeting molecules thereby activating subsequent signalling cascades (Shabbits *et al.*, 2001). In an experiment carried out by Jiang and colleagues, HeLa cells were treated the 50 μM C2-ceramide and no obvious morphological changes were observed within the first three hours. However, after six hours crevices appeared between the cells where some of the cells resembled a rounded shape. It was also reported that many reflective organelles that were not visible in the untreated cells were visible in the treated cells. Within 24 hours more than 90% of HeLa cells were detached whilst the untreated HeLa cells grew into a compact monolayer. To confirm that the morphological changes in HeLa cells treated with ceramide was due to apoptosis, cells were fixed with glutaraldehyde and examined under a transmission electron microscope (Jiang *et al.*, 2000). Therefore apoptosis results due to the relationship between ceramide production and subsequent cell death (Jiang *et al.*, 2000).

1.2.4. Defective pathways

Incorrect or inaccurate regulation of apoptosis may result in pathological conditions. Acute pathologies such as stroke, heart attack or liver failure are associated with the sudden death of tissues within organs through the activation of apoptosis (Fisher and Schulze-Osthof, 2005²). When comparing pathological conditions to neurodegenerative syndromes, some syndromes results from the slow progression of neuronal cell death. Inappropriate low apoptotic rates may promote survival and accumulation of abnormal cells which may result in tumour formation or autoimmune diseases. Therefore it may be summarized that too little or too much cell death may contribute to medical illnesses (Fisher and Schulze-Osthof, 2005²).

Both the development and the unimpaired state of multicellular organisms are affected by the inactivation of apoptosis. Besides developmental abnormalities, defective or inactive

apoptosis pathways may lead to tumourigenesis, autoimmune diseases and other serious health problems. Defective apoptosis pathways may also be the leading cause of chemoresistance in cancer therapy (Ghavami *et al.*, 2009). A common feature of cancer cells is their ability to evade apoptosis as a result of alterations that block cell death signalling pathways (Meng *et al.*, 2006). The inactivation of apoptosis pathways is central to the development of cancer. The disabling of apoptotic responses may be a major contributor both to resistance to treatment and to the observation that, in many tumours, apoptosis is not the main mechanism for the death of cancer cells in response to common treatment regimens (Brown and Attardi, 2005).

1.3.Relations between Inhibitor of Apoptosis Proteins and cancer

The X-linked inhibitor of apoptosis protein (XIAP) is a protein that has been shown to be over expressed in malignant cancers progression (Tamm *et al.*, 2000; Liu *et al.*, 2011). XIAP has been reported to inhibit both the intrinsic or mitochondrial and extrinsic or death receptor pathways by inhibiting caspase activity.

According to LaCasse and colleagues evidence exist for the involvement of inhibitor of apoptosis proteins (IAPs) in cancer. They reported the cancer specific expression of the IAP Survivin which is not normally expressed in differentiated tissue and the anti-apoptotic effects of IAPs are mediated via the NF- κ B transcription factor (LaCasse *et al.*, 1998).

1.3.1. Inhibitor of apoptosis proteins

IAP family members are defined by one or more repeats of a highly conserved region approximately 70 amino acids long, termed the baculovirus IAP repeat or BIR domain (Deveraux *et al.*, 1999; Nachmias *et al.*, 2003) located at the amino terminus (Nachmias *et al.*, 2003) and consists of cysteine and histidine residues within their core sequence $C_{X2}C_{X6}W_{X3}D_{X5}H_{X6}C$ where X can be any amino acid (Deveraux and Reed, 1999; Holcik *et al.*, 2001). The following eight human IAPs have been identified: c-IAP1, c-IAP2, NAIP, Survivin, XIAP, Bruce, ILP-2 and Livin. With the exception of NAIP and Survivin, human IAPs also contain a conserved sequence known as the RING finger located at the carboxyl terminus (Nachmias *et al.*, 2003).

IAPs are a family of anti-apoptotic proteins. Their main function is to regulate caspase activity. IAPs regulate apoptosis by inhibiting caspase 3 and /or caspase 7. IAPs also prevent the initiation of the intrinsic pathway by directly inhibiting caspase 9 (Riedl *et al.*, 2001).

IAPs have been shown to protect cells against apoptosis induced by the Fas ligand, TNF α , transducers of the TNF receptor super-family namely RIP, RIP2/RICK/CARDIAK, FADD and v-Rel, Bcl-2 pro-apoptotic family members, chemotherapeutic drugs such as etoposide, cisplatin, taxol, actinomycin D and adramycin, ionizing or UV radiation, oxidative stress, ischemia, potassium withdrawal, growth factor withdrawal, caspases, and *Drosophila* death receptors (LaCasse *et al.*, 1998).

1.3.2. X-chromosome linked inhibitor of apoptosis protein (XIAP) and its relation to cancer

Among the human IAPs, X-chromosome linked inhibitor of apoptosis protein (XIAP) is the best and most thoroughly characterized (Holcik *et al.*, 2003; Fischer and Schulze-Osthoff, 2005²). It was shown that XIAP over expression protects cancerous cells from apoptotic triggers induced by UV-irradiation, γ -irradiation as well as chemotherapeutic drugs. The ability to adjust XIAP activity via a subset of cellular proteins would be essential for maintaining control of apoptosis. But, if XIAP is left unchecked, it may lead to cancer (Holcik *et al.*, 2003).

XIAP is comprised of three BIR domain regions as well as a RING domain (Figure 1.6) (Holcik *et al.*, 2003; Schimmer, 2004) and it was the first IAP to be characterized (Schimmer, 2004).

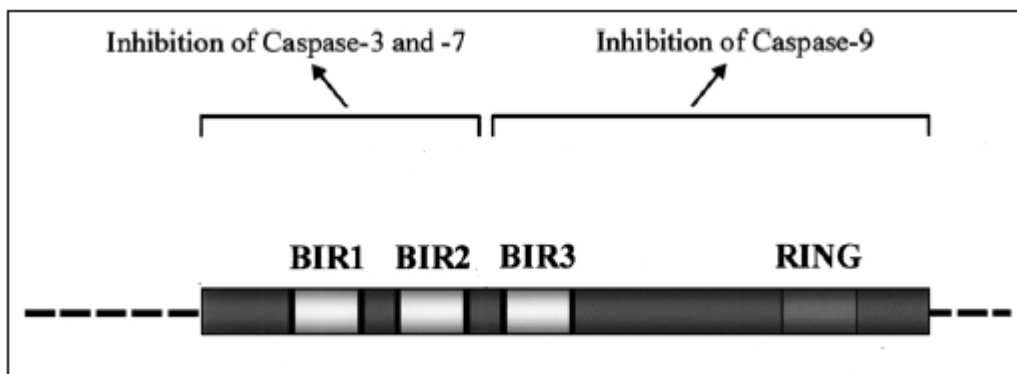


Figure 1.6: Functional domains of the XIAP protein. XIAP is comprised of three BIR domains as well as a RING domain. BIR regions 1 and 2 inhibit the intrinsic or mitochondrial pathway, of apoptosis, by blocking caspases 3 and 7. The extrinsic apoptotic pathway is inhibited by caspase 3 and the RING domain blocking caspase 9 [adapted from (Holcik *et al.*, 2001)].

In an experiment carried out by Tamm and colleagues, it was observed that XIAP was widely expressed in the NCI panel of 60 human tumour cell lines. It was noted that XIAP and c-IAP1 were widely expressed among tumour cell lines (Tamm *et al.*, 2000). The expression of XIAP prevents the activation of caspases, and hence blocks the activation of apoptosis by anti-cancer drugs. Inhibition of XIAP binding to caspases may help restore sensitivity to apoptosis and thus promote the action of anti-cancer drugs.

1.4. Embelin: an inhibitor of XIAP

1.4.1. Structure of embelin

The fruit of the plant *Embelia ribes*, from the Myrsinaceae family (Pathan and Bhandari, 2011), has been used for thousands of years in the treatment of fever and inflammation. The bio active component isolated from this plant is embelin (Siegelin *et al.*, 2009) or 2,5-dihydroxy-3-undecyl-1,4-benzoquinone (Joshi *et al.*, 2007; Pathan and Bhandari, 2011).

Embelin consist of a dihydroxyquinone core and an 11-carbon alkyl side chain (Schimmer *et al.*, 2006) (Figure 1.7) which possesses hydrophobic characteristics (Chen *et al.*, 2006).

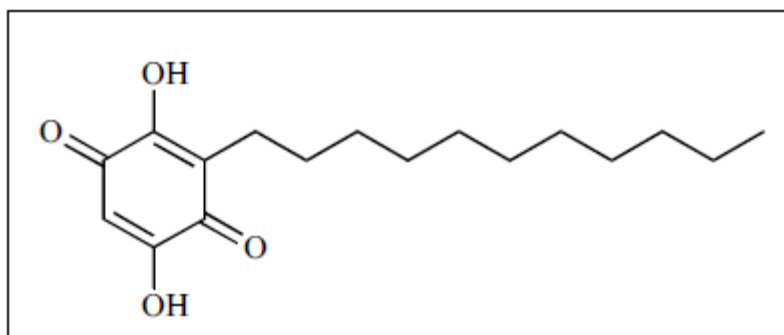


Figure 1.7: Chemical structure of embelin. Embelin consists of a quinone core to which a hydrophobic chain is attached (Nikolovska–Coleska *et al.*, 2004²).

Many naturally occurring anti-cancer substances are quinone containing compounds. Some examples of these anti-cancer drugs include Adramycin, daunorubicin, mitomycin C, streptonigrin, and lapachol (Bachur *et al.*, 1978).

Quinone is a general term used to classify ubiquitous class of compounds common in many natural products and endogenous biochemicals. Quinones are highly redox active molecules which can redox cycle resulting in the formation of reactive oxygen species (ROS) which has been reported to be associated with cancer (Schumacker, 2006). Quinones may be generated via the metabolism of hydroquinones and/or catechols. Quinones are named as derivatives of their parent aromatic systems. An example would be benzoquinones derived from benzene (Bolton *et al.*, 2000).

1.4.2. Embelin as an inhibitor of XIAP

Embelin possess anti-tumour as well as anti-inflammatory properties (Joshi *et al.*, 2007; Siegelin *et al.*, 2009). Embelin is a fairly potent, non-peptidic, cell-permeable, small molecule inhibitor of the anti-apoptotic protein XIAP. It was identified by computational screening of a traditional herbal medicine three-dimensional structure database, consisting of 82221 natural herbal products (Nikolovska–Coleska *et al.*, 2004¹; Nikolovska–Coleska *et al.*, 2004²).

According to Ahn and colleagues embelin not only functions in inhibiting XIAP but also in inhibiting NF- κ B which is a transcription factor that regulates the expression of anti-apoptotic proteins such as Bcl-x1 (Ahn *et al.*, 2007).

Ziedan and colleagues reported that embelin can induce apoptosis in two ways. Firstly embelin was shown to selectively inhibit cell growth in prostate cancer cells. Secondly

embelin was also shown to activate caspase 9 effectively (Ziedan *et al.*, 2008). Xu and colleagues conducted a study investigating the anti-proliferative activity of 5-O-ethylembelin and 5-O-methylembelin in HeLa and HL-60 cells. Both these cell lines were treated with 5-O-ethylembelin and 5-O-methylembelin to a final concentration of 10 μ M for 48 hours. A decrease in cell viability was observed, post 48 hour treatment (Xu *et al.*, 2005).

1.5. Embelin targets XIAP via its BIR3 domain

1.5.1. Relation between XIAP's BIR3 and Smac/DIABLO

Several proteins are released from the mitochondrial intermembrane space into the cytoplasm in response to apoptotic stimuli. These proteins include cytochrome c, second mitochondria-derived activator (Smac/DIABLO), apoptosis inducing factor (AIF), endonuclease G and Omi/HtrA2 (Shiozaki and Shi, 2004).

Smac/DIABLO binds to IAPs and interferes with the ability of IAPs, and more specifically XIAP, to block the activation of caspases 3, 7, and 9 (Hao and Mak, 2010; Riedl *et al.*, 2001; Fesik, 2005). This interference antagonizes the anti-apoptotic activity thereby promoting apoptosis (Riedl *et al.*, 2001; Fesik, 2005). Generally, XIAP inhibition has been thought to facilitate apoptosis (Hao and Mak, 2010). XIAP is neutralized by Smac/DIABLO upon inhibition of caspase 9 as there is competition for the same specific binding site of XIAP with caspase 9 (Gao *et al.*, 2007).

According to Nikolovska-Coleska and colleagues as well as Schimmer and colleagues embelin binds to XIAP's BIR3 domain with an affinity similar to that of Smac/DIABLO (Nikolovska-Coleska *et al.*, 2004²; Schimmer *et al.*, 2006). Schimmer and colleagues go a step further in that they specify that embelin's alkyl side chain binds to the surface groove of XIAP's BIR3 domain (Schimmer *et al.*, 2006).

Liu and colleagues carried out an experiment where they determined the solution structure of XIAP's BIR3 domain using a peptide, comprised of 9 residues, derived from Smac/DIABLO's N terminus in order to understand the structural basis for molecular recognition between Smac/DIABLO and IAPs. From their results, they made the following observations: (i) the Smac/DIABLO protein binds to XIAP's BIR3 domain with the same affinity as Smac/DIABLO peptides, (ii) both Smac/DIABLO proteins and peptides bind more

tightly to XIAP's BIR3 domain than XIAP's BIR2 domain, (iii) XIAP's BIR3–Smac/DIABLO peptide complex, as determined by NMR, indicated that residues 258 – 346 of XIAP's BIR3 domain fits Smac/DIABLO peptide residues 1' – 4' best (Figure 1.8), (iv) XIAP's BIR3–Smac/DIABLO peptide complex was comprised of three stranded β –sheets, five α –helices (Figure 1.8), one turn of a 3_{10} helix as well as a zinc atom that was chelated to three cysteines and a histidine and (v) the ability of mutant proteins to bind to the Smac/DIABLO peptide matched their ability to inhibit caspase 9 which suggests that Smac/DIABLO and caspase 9 bind overlapping sites on XIAP's BIR3 domain. This enables Smac/DIABLO to free caspase 9 from the XIAP/caspase 9 complex in order to fulfil its role in the apoptotic pathway. It must be noted that the binding sites for Smac/DIABLO and caspase 9 are not identical. Liu and colleagues were able to conclude that Smac/DIABLO interacts with IAPs in the same manner as shown by XIAP's BIR3–Smac/DIABLO peptide complex. This was confirmed by primary sequence alignments. Three–dimensional structures in the region of XIAP's BIR3 domain and of other structurally characterized IAPs that bind to Smac/DIABLO are also similar (Liu *et al.*, 2000).

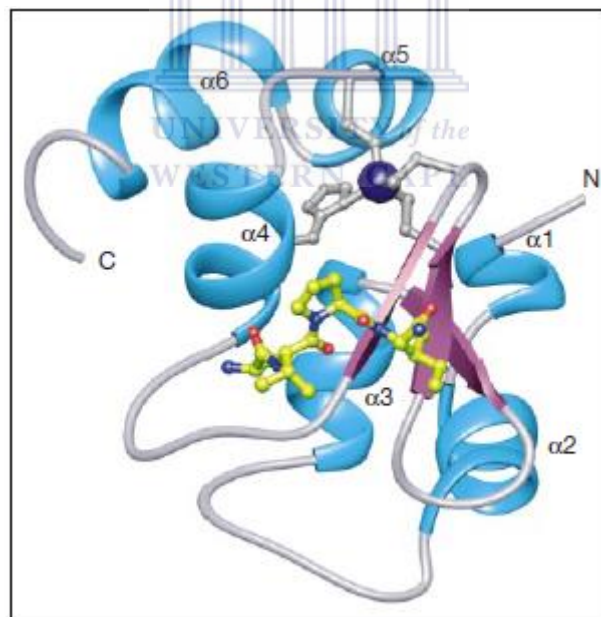


Figure 1.8: NMR structure of XIAP BIR3–Smac/DIABLO complex. This ribbon representation is comprised of residues 258–346 of XIAP's BIR3 domain complexed with residues 1' to 4' of Smac/DIABLO's N terminus (Liu *et al.*, 2000).

A study by Nikolovska–Coleska and colleagues aimed to identify small molecule inhibitors of XIAP by mainly focusing on the BIR3 region as they believed the BIR3 domain has a critical role in apoptosis inhibition based on: (i) BIR3 binding to caspase 9 thereby trapping

caspase 9 in a monomeric inactive form and having the potential to inhibit caspase 9 mediated apoptosis as well as (ii) BIR3 binds to Smac/DIABLO and inhibits the pro-apoptotic activity. Nikolovska-Coleska and colleagues proposed that small molecule inhibitors which bind to XIAP's BIR3 domain can increase cells' sensitivity to apoptotic stimuli via promoting caspase 9 activation as well as Smac/DIABLO's pro-apoptotic activity (Nikolovska-Coleska *et al.*, 2004¹).

1.5.2. BIR3 inhibition of XIAP leads to apoptosis

It has been shown that XIAP over expression renders the cancer cells resistant to drug-induced apoptosis. The binding of embelin to BIR3 inhibits the initiator caspase 9 and effector caspases 3 and 7. Embelin can therefore attenuate or block the protective effects of XIAP and enhance chemodrug-induced apoptosis. Nikolovska-Coleska and colleagues showed that embelin is a fairly potent inhibitor of XIAP and suggested that its anti-cancer activity is mediated at least in part by its direct binding to XIAP and inhibition of the anti-apoptotic function of XIAP protein in cancer cells (Nikolovska-Coleska *et al.*, 2004²).

Other studies focusing on the development of embelin derivative compounds identified new and potent XIAP inhibitors targeting the BIR3 domain as they display enhanced properties within human cancer cells when used in combination with pro-apoptotic drugs (Ziedan *et al.*, 2008).

1.6. Nanotechnology for targeted delivery of anti-cancer drugs

1.6.1. Goal of cancer therapy

The therapeutic goal in cancer treatment is to trigger tumour-selective cell death (Sellers and Fisher, 1999). Cancer treatment most often results in the non-specific distribution of chemotherapeutic drugs and is taken up by both cancerous and non-cancerous cells (Sinha *et al.*, 2006; Yih and Al-Fandi, 2006; Cho *et al.*, 2008). These drugs can therefore also destroy non-cancerous cells (Yih and Al-Fandi, 2006). This gives rise to excessive and increased systemic toxicities and other adverse effects (Sinha *et al.*, 2006; Cho *et al.*, 2008). Therefore, traditional chemotherapy in some cases is not successful (Yih and Al-Fandi, 2006). For cancerous cells to be eliminated rapidly the anti-cancer drugs must be extensively distributed

to target the affected organs and tissues. Consequently, large quantities of the anti-cancer drug need to be administered (Sinha *et al.*, 2006).

Ideally an effective cancer treatment would result in the anti-cancer drug reaching the desired tumour after administration by penetrating the body's barriers while maintaining minimal loss of their activity while circulating through the body. Upon reaching the desired tumour, the anti-cancer drugs should be able to selectively kill the cancerous cells without affecting the non-cancerous cells. These strategies can improve patient survival and quality of life by increasing intra-cellular concentrations of anti-cancer drugs, whilst reducing the dose limiting toxicities (Cho *et al.*, 2008).

Conventionally anti-cancer drugs may either be administered orally or via intravenous routes. Both these methods have disadvantages but traditional intravenous routes are more problematic compared to the oral delivery method. Some conventional intravenous drugs have low specificity thereby resulting in harmful effects to healthy tissues (Sinha *et al.*, 2006; Yih and Al-Fandi, 2006).

When searching for appropriate carriers for drug delivery systems, the main issues to consider are knowledge of drug incorporation and release, formulation stability and shelf life, biocompatibility, biodistribution and targeting as well as functionality (de Jong and Borm, 2008). *In vivo* delivery of therapeutic agents to cancerous targets must overcome drug resistance at the cancerous level due to physiological barriers, drug resistance, biotransformation and clearance of anti-cancer drugs in the body (Brigger *et al.*, 2002).

The field of Nanotechnology is emerging as a technology that can facilitate allows for targeted delivery of anti-cancer drugs to the site of interest. The use of nanoparticles as delivery vehicles for targeted delivery of drugs is generating much interest. Figure 1.9 is a graphical representation of nanoparticles that can be used successfully as targeted delivery vehicles. Anti-cancer drug(s) can be conjugated along with a targeting peptide which specifically bind to a cell surface receptor expressed exclusively on the target cancer cells.

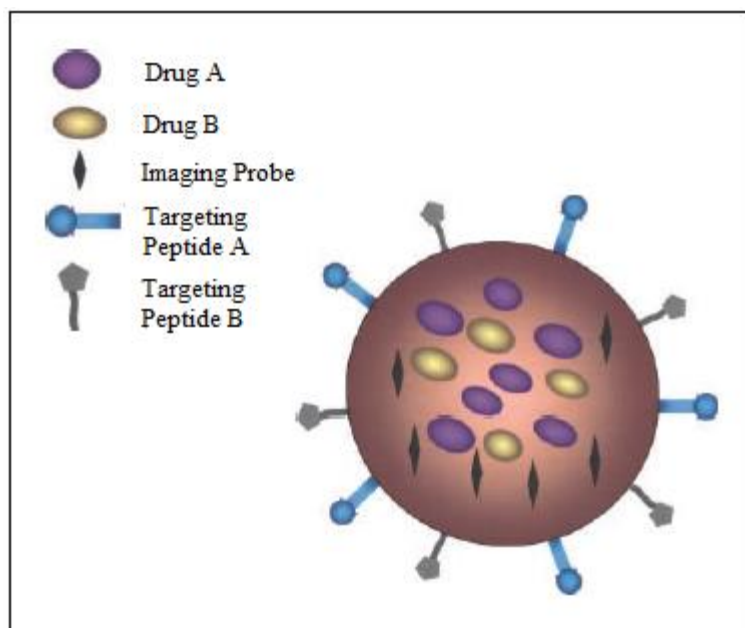


Figure 1.9: Structure of a nanoparticle for targeted drug delivery. From the illustration it can be observed that nanoparticles may be conjugated with targeting peptides (for recognition purposes) and anti-cancer drugs (for apoptosis induction). The targeting peptide and anti-cancer drug used in the conjugation experiments are specific for the cancer of interest [adapted from Cho *et al.*, 2008].

According to Aina and colleagues peptides, peptidomimetics or small molecules are more effective targeting agents in cancer treatment and are therefore regarded as an alternative tool for targeted anti-cancer treatment therapies (Aina *et al.*, 2007). These molecules are chemically stable, small and easy to synthesize. These molecules can easily be conjugated to radionuclides, cytotoxic drugs or toxins.

When comparing the effect of peptides and antibody conjugated nanoparticles, Zambre and colleagues synthesized a series of antibody EGFR and EGFR-peptide conjugated gold nanoparticles to investigate the *in vivo* EGFR targeting characteristics of the conjugates in pancreatic tumour bearing SCID mice models. During their investigation, they observed that the peptide conjugate gold nanoparticles displayed high *in vivo* mobility and targeted the pancreatic tumour effectively (Zambre *et al.*, 2009). Therefore, peptides would serve as a better option as a delivery agents due to their excellent tissue penetration, easy synthesis, easy conjugation to drugs and short oligonucleotides (Shadidi and Sioud, 2002).

1.6.2. Nanoparticles and drug delivery

Advantages of drug delivery systems include improved solubility and biodistribution as well as *in vivo* stability. Loading of pharmaceutical drugs onto the drug delivery system, allows for controlled release of the drug while at the same time maintaining the drug level within the therapeutic dose (Ghosh *et al.*, 2008).

Nanoparticles have the potential to fulfil the requirements for effective drug carrier systems. For delivery of anti-cancer drugs to the targets to be effective, nanoparticles should remain in the blood stream for a significant period of time without the possibility of elimination (Cho *et al.*, 2008) or destruction.

Nanoparticle delivery of anti-cancer drugs to respective target tissues may be achieved in two ways, either via active or passive targeting (Sinha *et al.*, 2006) where a combination of both targeting strategies will allow for an ideal carrier with regards to *in vivo* drug delivery (Ghosh *et al.*, 2008).

Passive targeting occurs when unhealthy tissues, due to extravasion via leaky blood vessels (Ghosh *et al.*, 2008) allow for accumulation of nanocarriers due to their enhanced permeability and retention effect (Garcia *et al.*, 2007). On the other hand, active targeting present ligands on the carrier surface for specific recognition by cell surface receptors (Ghosh *et al.*, 2008) for conjugation purposes (Garcia *et al.*, 2007).

Therefore, the main goals of using nanoparticles in drug delivery would be based on the efficiency as well as specific *in vivo* delivery without toxicity. In relation to this, the dose delivered as well as the therapeutic efficacy may be measured accurately as well as non-invasively over time (Cai *et al.*, 2008).

Nanoparticles may be defined as submicronic colloidal systems (Brigger *et al.*, 2002; Cho *et al.*, 2008). Their submicron sizes range from 3 to 200 nm (Cho *et al.*, 2008). Nanoparticles may be composed of lipids, viruses, ceramics, metals as well as organometallic and biological compounds (Yin and Al-Fandi, 2006; Cho *et al.*, 2008).

Nanoparticle structures may be spherical, branched or shell shaped where each structure offers unique characteristics which makes them appropriate drug delivery candidates for specific therapies (Yih and Al-Fandi, 2006). Nanoparticles may consist of three layers

namely the surface, shell and core where the surface area is often functionalized and the shells material may be added intentionally (Christian *et al.*, 2008).

Anti-cancer drugs may be loaded onto nanoparticles via encapsulation, surface attachment or entrapping. It must be noted that the attachment technique is determined by the nanoparticles architecture and material, drug type as well as the targeted location. Nanoparticles are regarded as an attractive tool for biomedical purposes based on their unique features which include their large surface-to-mass ratio, their quantum properties as well as their ability to absorb and carry other compounds (de Jong and Borm, 2008).

1.6.3. Nanoparticles as drug carriers

By using nanoparticles for delivery of anti-cancer drugs, it provides a more effective and less harmful solution to overcome some of the problems arising from conventional anti-cancer drug delivery methods including severe toxic side effects on healthy organs, difficulties in clinical administration, drug resistance and limited access of the drug to the tumour sites (Sinha *et al.*, 2006; Yih and Al-Fandi, 2006; Utreja *et al.*, 2010).

For successful drug delivery, nanoparticles are required to transport anti-cancer drugs to the targeted area where upon reaching the targeted area, the anti-cancer drug will be released. Therefore for successful and effective drug delivery, biologically inert nanoparticles are required to be formulated with the intention of both transport and release of the anti-cancer drugs (de Jong and Borm, 2008). Nanoparticles may also act at a cellular level where they may be endocytosed or phagocytosed by cells. This results in internalization of the encapsulated anti-cancer drug by the cells (Brigger *et al.*, 2002).

With regard to drug delivery, the primary goals for research into nanobiotechnologies should focus on specific drug targeting and delivery, reduced toxicity while maintaining therapeutic effects, greater safety and biocompatibility as well as faster development with regard to new and safer medicines. The requirements for appropriate carriers in drug delivery systems include knowledge of drug incorporation and release, stability and shelf life, biocompatibility, biodistribution and targeting as well as functionality (de Jong and Borm, 2008).

According to de Jong and Borm, a major challenge in drug delivery is getting the drug to the targeted area without potentially affecting the uninfected area. Therefore the full use of cytotoxic chemotherapeutics is limited due to their therapeutic potential (de Jong and Borm,

2008). Appropriately designed nanoparticles may act as a drug vehicle that is able to target cancerous targets as well as protecting the anti-cancer drug from premature activation during the transport process (Brigger *et al.*, 2002). Increased local drug concentrations, as a result of these forms of targeted drug delivery, provides strategies for more specific therapy. Nanoparticles have specific characteristics that enable these strategies. These characteristics include their small size, binding and stabilization of proteins as well as lysosomal escape post endocytosis (de Jong and Borm, 2008).

1.7.Aims of this study

The objective of this study was to develop gold nanoparticles that can be used for targeted delivery of embelin to cancer cells to improve the effects of pro-apoptotic drugs. This was achieved by biconjugating gold nanoparticles with embelin and a cancer specific targeting peptide.



1.8.Thesis outline

The remainder of this thesis is divided as follows: Chapter 2 describes the materials and methods applied in this work, Chapter 3.1 describes Evaluating the expression levels of XIAP in human cancer cell lines, Chapter 3.2 describes Evaluating the apoptotic effects of ceramide as an apoptotic inducer, Chapter 3.3 describes Cloning of XIAP into a His-tagged expression system, Chapter 3.4 describes Affinity purification of recombinant His-XIAP, Chapter 3.5 describes Affinity purification for recombinant GST-XIAP, Chapter 3.6 describes Evaluating the interaction between recombinant GST-XIAP protein and embelin and embelin conjugated nanoparticles by Isothermal Titration Calorimetry and Chapter 4 summarizes the findings.

CHAPTER 2: MATERIALS AND METHODS

- 2.1. Materials used and suppliers
 - 2.1.1 List of kits used
- 2.2. Solutions and buffers
- 2.3. Cell culture
 - 2.3.1 Thawing MCF7 and HepG2 cells
 - 2.3.2 Trypsinization of MCF7 and HepG2 cells
 - 2.3.3 Seeding of cells
 - 2.3.4. Synthesis of embelin conjugated nanoparticles
- 2.4. Synthesis of embelin conjugated nanoparticles
- 2.5. Investigating the toxicity of embelin and embelin conjugated nanoparticles
- 2.6. Investigating the concentration and percentage of gold in treated cancer cells by Inductively Coupled Plasma–Optical Emission Spectrometry (ICP–OES)
- 2.7. Investigating uptake of nanoparticles in treated cancer cells by transmission electron microscopy (TEM)
- 2.8. Statistical analysis
- 2.9. RNA isolation
 - 2.9.1 Agarose electrophoresis of RNA
- 2.10. cDNA synthesis
- 2.11. Primers
- 2.12. Polymerase chain reaction (PCR) amplification of DNA
- 2.13. Agarose gel electrophoresis of PCR product
- 2.14. Gel purification of amplified PCR product

- 2.15. DNA cloning
 - 2.15.1 pGEM®-T Easy vector system
 - 2.15.2 Ligation of PCR product into pGEM®-T Easy vector
 - 2.15.3 Transformation of competent *E. coli* MC1061 competent cells
 - 2.15.4 Colony PCR amplification
 - 2.15.5 Culturing of transformed MC1061 *E. coli* cells
 - 2.15.6 Plasmid DNA isolation and purification
 - 2.15.7 Restriction digestion of pGEM-XIAP
- 2.16. DNA sub-cloning
 - 2.16.1 pET28a Cloning Vector
 - 2.16.2 Restriction Digestion of pET28a
 - 2.16.3 Ligation of the released pGEM-XIAP product into the pET28a vector
 - 2.16.4 Transformation of BL21 (DE3) pLysS *E. coli* competent cells with pET28a-XIAP construct
 - 2.16.5 Colony PCR amplification
 - 2.16.6 Culturing of transformed BL21 (DE3) pLysS *E. coli* cells
- 2.17. Mini expression screen for recombinant His-XIAP protein
- 2.18. Purification of recombinant His-XIAP protein
 - 2.18.1 Cell extract preparation and protein purification as per Ni-NTA His-Bind Resins
- 2.19. Expression and purification of GST-XIAP protein
 - 2.19.1 Transformation of *E. coli* BL21 (DE3) pLysS competent cells with pGEX-XIAP construct
 - 2.19.2 Expression screen for recombinant GST-XIAP protein

- 2.19.3 Expression of GST–XIAP recombinant protein
- 2.19.4 Cell extract preparation and protein purification as per BugBuster® GST–Bind purification kit
- 2.20. Protein extraction from cultured human cancerous cells
- 2.21. One Dimensional SDS Polyacrylamide Gel Electrophoresis
 - 2.21.1 Gel preparation
 - 2.21.2 Sample preparation and gel loading
 - 2.21.3 Gel staining
- 2.22. Analysis of XIAP expression by Western Blot
 - 2.22.1 Blot transfer of proteins onto PVDF membrane
 - 2.22.2 Analysis of XIAP expression
 - 2.22.3 Exposure of membrane
- 2.23. Densitometric Analysis of Western Blot
- 2.24. Evaluating the interaction of recombinant GST–XIAP protein and embelin



UNIVERSITY of the
WESTERN CAPE

2.1. Materials used and suppliers

Materials

Suppliers

Acetic Acid

Merck

40 % Acrylamide Bis Solution 37:5:1

Bio–Rad

Actin Antibody

Santa Cruz

Agarose

Whitehead Scientific

Ammonium Persulphate

Merck

Ampicillin

Roche

APOPercentage Dye

bioclor

Bacterological Agar

Merck

Boric Acid

Merck

Bovine Serum Albumin (BSA)

Roche

Bradford Reagent

Bio–Rad

Calcium Chloride

Merck

Cesium Chloride

Roche

Coomassie Brilliant Blue R–250

Sigma–Aldrich

CytoBuster™ Protein Extraction Reagent

Novagen

Diethylpyrocarbonate (DEPC)

Merck

Dithiothreitol (DTT)

Fermentas

Dimethyl Sulfoxide (DMSO)

Sigma–Aldrich

Dulbecco's Modified Eagle's Medium (DMEM)

Invitrogen

DreamTaq™ Green PCR Master Mix (2X)

Fermentas

Embelin

Merck



Embelin	Sigma–Aldrich
Ethanol	Merck
Ethidium Bromide	Merck
Ethylene Diamine Tetra–Acetic Acid (EDTA)	Merck
10X FastDigest Green Buffer	Fermentas
FastDigest® <i>Xho</i> I Restriction Enzyme	Fermentas
Fetal Bovine Serum (FBS)	Invitrogen
Glutaraldehyde	Sigma–Aldrich
Goat Anti–Mouse IgG–HRP Antibody: sc–2031	Santa Cruz
6X Gel Loading Dye	Fermentas
GeneRuler™ 1 kb DNA Ladder	Fermentas
Glycerol	Merck
Glycine	Merck
Hydrochloric Acid	Merck
Isopropanol (Propan–2–ol)	Merck
Isopropyl β–D–1–thiogalactopyranoside (IPTG)	Fermentas
Kanamycin sulphate	Roche
Manganese Chloride	Merck
Methanol	Merck
N–Acetyl–D–Sphingosine (C2 Ceramide)	Sigma–Aldrich
N–Acetyl–D–Sphingosine (C2 Ceramide)	Merck
Nitric Acid	Merck
<i>Nde</i> I Restriction Digestion Enzyme	Fermentas



Nuclease Free Water	Fermentas
PageRuler™ Unstained Protein Ladder	Fermentas
Paraformaldehyde	Sigma–Aldrich
pGEM®–T Easy Vector Systems	Promega
Penicillin–Streptomycin (500 Units:5 000 µg/ml)	Invitrogen
pET28a Vector	Novagen
Potassium Acetate	Merck
Potassium Chloride	Merck
Spectra™ Multicolor Broad Range Protein Ladder	Fermentas
Sodium Chloride	Merck
Sodium Dodecyl Sulphate (SDS)	Merck
Sodium Hydroxide	Merck
SuperSignal® West Pico Chemiluminescent Substrate	Thermo Scientific
T4 DNA Ligase	Fermentas
T4 DNA Ligase Buffer	Fermentas
N,N,N',N'–Tetramethylethylenediamine (TEMED)	Sigma–Aldrich
Thrombin	Sigma–Aldrich
Tris (hydroxymethyl) aminoethane (Tris)	Merck
Trypsin	Invitrogen
Tryptone Powder–Pancreatic Casein Powder	Merck
Tween20	Merck
Urea	Merck
XIAP Antibody	Santa Cruz



pGEX–XIAP Construct	Addgene
Yeast Extract Powder	Merck

2.1.1. List of kits used

First Strand cDNA Synthesis Kit for RT–PCR (AMV)	Roche
HIS–Select® Nickel Affinity Gel	Sigma–Aldrich
Novagen GST–Bind™ Kit	Merck
Novagen Ni–NTA His Bind® Resins	Merck
NucleoSpin® Extract II PCR Clean–Up Gel Extraction	Machery–Nagel
NucleoSpin® TriPrep Kit	Machery–Nagel
Wizard® <i>Plus</i> SV Miniprep DNA Purification System	Promega



2.2. Solutions and buffers

Ammonium Persulphate: 10% stock prepared in distilled water, filter sterilized, stored at –20 °C

Ampicillin: 100 mg/ml stock prepared in distilled water, filter sterilized and stored at –20 °C

Coomassie Stain: 0.25% Coomassie Blue R–250, 40% Ethanol, 10% Acetic Acid

C₂–ceramide: 0.005 M stock prepared in DMSO, filter sterilized, stored at –20 °C

DEPC Treated Water: 1 ml dimethyl dicarbonate per 1L distilled water, incubated at 22 °C overnight, autoclaved

Destaining Solution: 10% Acetic Acid and 10% Methanol prepared in distilled water

DTT: 1 M stock prepared in distilled water, filter sterilized, stored at –20 °C

Embelin stock: 0.03 M stock prepared in DMSO, stored at –20 °C

Hydrochloric Acid: 2% (v/v) prepared in distilled water

Gluteraldehyde: 2.5% (w/v) prepared in distilled water, stored at 4 °C

IPTG: 1 M stock prepared in distilled water, filter sterilized, stored at -20 °C

Kanamycin sulphate: 100 mg/ml stock solution prepared in distilled water, filter sterilized, stored at -20 °C

Luria Agar: 10 g Tryptone, 5 g NaCl, 5 g Yeast Extract prepared in 1L distilled water

Luria Broth: 10 g Tryptone, 5 g NaCl, 5 g Yeast Extract, 15 g Bacteriological Agar prepared in 1L distilled water

Nitric Acid: 70% (v/v) prepared in distilled water

Paraformaldehyde: 4% (w/v) prepared in half the final volume distilled water, heat to 60 °C, adjust pH to 7.4, make up to final volume, filter sterilize, stored at 4 °C

0.5 M Phosphate Buffer: 71 g di-sodium hydrogen phosphate, 69 g sodium dighydrogen phosphate prepared in 1L ultrapure (i.e. 18 M Ω) water

0.5 M Phosphate Buffer-DMSO: 71 g di-sodium hydrogen phosphate, 69 g sodium dighydrogen phosphate, 0.15% (v/v) DMSO prepared in 1L ultrapure (i.e. 18 M Ω) water

10X PBS: 81.8 g NaCl, 2 g KCl, 18 g Na₂HPO₄, 2.5 g KH₂PO₄ prepared in 1L distilled water

1X PBS: dilute 10X PBS according to the dilution 1:10 (v/v) in distilled water

10X Running Buffer: 144 g Glycine, 30 g Tris, 10 g SDS prepared in 1L distilled water

1X Running Buffer: dilute 10X Running Buffer according to the dilution 1:10 (v/v) in distilled water

2X Sample Buffer: 4% SDS, 20% glycerol, 100 mM Tris-HCl (pH 6.8), 0.2% bromophenol blue, 200 mM DTT

12% Separating Buffer: 40% Polyacrylamide, 1.5 M Tris-HCl (pH 8.8), 10% Ammonium Persulphate, 10% SDS, 0.002% TEMED

5% Stacking Buffer: 40% Polyacrylamide, 1 M Tris (pH 6.8), 10% Ammonium Persulphate, 10% SDS, 0.002% TEMED

SDS: 10% prepared in distilled water

1X Transfer Buffer: 3.03 g/l Tris, 14.42 g/l Glycine, 40% Methanol

10X TBE: 1M Tris-HCl, 0.5 M EDTA

1X TBE: dilute 10X TBE according to the ration 1:10 (v/v) in distilled water

TE: 10mM Tris-HCl (pH 8), 1 mM EDTA

1X TBSTween: 1 M Tris, 5 M NaCl, 1 ml/l Tween 20

1X TBSTween-BSA: 0.3 g BSA in 1L TBSTween

1X TBSTween-Milk: 0.5 g low fat milk powder in 1L TBSTween

2.3. Cell culture

MCF7 cells (mammalian breast cancer cell line supplied by ATCC®) and HepG2 cells (mammalian liver cancer cell line supplied by ATCC®) were cultured in complete media (i.e. Dulbecco's Modified Eagle's Medium (DMEM) media supplemented with 10% Fetal Bovine Serum (FBS) and 1% penicillin-streptomycin). All cell culture reagents were obtained from Invitrogen.

2.3.1. Thawing MCF7 and HepG2 cells

DMEM complete media (5 ml) was placed at 4 °C. Frozen vials of MCF7 and HepG2 cells were removed from the -150 °C freezer and thawed in a 37 °C water bath. Cells were transferred to 15 ml tubes containing 5 ml pre-cooled DMEM complete media and centrifuged at 3 000×g for 5 minutes. The supernatant was decanted and pelleted. Cells were re-suspended in 5 ml complete media. The latter was transferred to 25 cm² tissue culture flasks. The flask was incubated at 37 °C with 5% CO₂ until 70-90% confluency was reached.

2.3.2. Trypsinization of MCF7 and HepG2 cells

When cells reached confluency the media were discarded and cells were washed once with phosphate buffered saline (PBS). The PBS was discarded and cells were trypsinized with 2X and 1X trypsin for MCF7 and HepG2 cells respectively. Cells were incubated at 37 °C for 2-

3 minutes. DMEM complete media was added to the flask to stop trypsinization. The cells were collected by centrifugation at $3\,000\times g$ for 3 minutes.

2.3.3. Seeding of cells

Once confluency was reached the cells were trypsinized and re-suspended in 10 ml DMEM complete media. Cells were counted with the use of the Countess™ automated cell counter (Invitrogen). Cells were seeded at a density of 2×10^5 live cells/ml for 6 well plates and 5×10^5 live cells/ml for a 25 cm^2 flask.

2.3.4. Freezing of MCF7 and HepG2 cells

For long term storage the cells were trypsinized and harvested by centrifugation. The cell pellet was re-suspended in DMEM complete media containing 10% DMSO. The latter was aliquoted into 2 ml cryo-vials and stored at $-150\text{ }^\circ\text{C}$.

2.4. Synthesis of embelin conjugated nanoparticles

Gold nanoparticles (AuNPs) (14 nm in size) were synthesized and provided by Dr. Franklin Keter (Mintek). Two variants of the AuNPs were prepared. Embelin was conjugated to our batch of the 14 nm AuNPs to form AuNP-E conjugate. Embelin and a cancer targeting peptide LTVSPWY (Shadidi and Sioud, 2003¹) were conjugated to a second batch forming a AuNP-P-E biconjugate. Biconjugation was carried out using the ratio of embelin:peptide:PEG-OH of 10%:1%:89%.

2.5. Investigating the toxicity of embelin and embelin conjugated nanoparticles

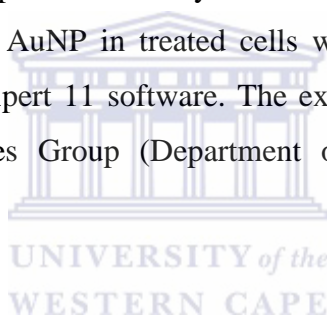
MCF7 breast and HepG2 liver cancer cells were seeded into 6-well plates (**Section 2.3.3**) and cultured to 60 – 70% confluent. Cells were treated for 24 hours in triplicate in one of eight treatment options: 50 μM embelin, 5 nM AuNP, 5 nM AuNP-E or 5 nM AuNP-P-E and co-treatments involving the above mentioned treatments with 50 μM ceramide.

Morphological changes were studied using the Nikon TMS light microscope with a 20X magnification. Images were captured with the aid of the Leica Firecam EC3 Camera.

Apoptosis was assayed by flow cytometry using the FACScan (BD Biosciences) according to the protocol as described by Meyer and colleagues (2008).

2.6. Investigating the concentration and percentage of gold in treated cancer cells by Inductively Coupled Plasma–Optical Emission Spectrometry (ICP–OES)

MCF7 breast and HepG2 liver cancer cells were seeded into 6–well plates (**Section 2.3.3**) and cultured to 60 – 70% confluent. Cells were treated for 24 hours in duplicate with 5 nM AuNP–E and 5 nM AuNP–P–E. Cells were trypsinized (**Section 2.3.2**) and pellets were washed with PBS. For control purposes pellets of AuNP–E and AuNP–P–E were collected by centrifugation. These pellets were washed with PBS. Cell pellets, of treated cells and controls, were re–suspended in 70% nitric acid (2ml) and digested for two hours at 90 °C. The final volume was made up to 10 ml by addition of 2% hydrochloric acid. The concentration and percentage of AuNP in treated cells were determined using the Varian 1600 ES instruments and ICP expert 11 software. The experiments were performed by the Environmental and Nanosciences Group (Department of Chemistry, University of the Western Cape).



2.7. Investigating uptake of nanoparticles in treated cancer cells by Transmission Electron Microscopy (TEM)

MCF7 breast and HepG2 liver cancer cells were seeded into 25 cm² flasks (**Section 2.3.3**) and cultured to 60 – 70% confluent. Cells were treated for 24 hours with 5 nM AuNP and 5 nM AuNP–P–E + 50 µM ceramide co–treatment.

The supernatant of the treated cells were collected and pelleted by centrifugation. The supernatant of the latter was discarded and pellets were stored on ice. Adherent treated cells were washed with PBS and pelleted by centrifugation. Pellets from the respective treatments were collected and added to the adherent cells. To the latter 4% paraformaldehyde (2 ml) was added and flasks were placed on a shaker for 15 minutes at 4 °C. Cell scrapers were used to gather cells. Cells were transferred to labelled 15 ml tubes and pellets were collected by centrifugation at 2 000 rpm for 10 minutes at 4 °C. Pellets were re–suspended in 2.5% glutaraldehyde (100 µl). The uptake of nanoparticles was assessed using the JEOL JEM–

1011 Electron Microscope and cis analysis program iTEM imaging software. Analysis was performed by the National Health Laboratory Services (Tygerberg Hospital, Cape Town).

2.8. Statistical analysis

All data are presented as mean \pm SD. Statistical analysis was performed using one-way ANOVA, followed by Tukey's Test. P-values were $P < 0.05$.

2.9. RNA isolation

The isolation of RNA was carried out with the use of Machery–Nagel's NucleoSpin® Tri Prep Kit according to the manufacturer's guide.

MCF7 cells were cultured in DMEM complete media (**Section 2.3**). Upon reaching approximately 80% confluency MCF7 cells were trypsinized (**Section 2.3.2**). The cell pellet was washed with PBS to remove traces of the 2X trypsin prior to RNA isolation.

The cells were lysed by addition of 350 μ l PR1 buffer and 7 μ l 1 M DTT. The cells were vortexed vigorously for 1 minute. The cell suspension was filtered through a NucleoSpin® Filter (violet ring) by transferring the cell suspension onto the filter and centrifuged at 11 000 \times g at 25 °C. The NucleoSpin® Filter was discarded and 350 μ l 70% ethanol was added to the homogenized lysate (filtrate) and mixed gently. For each preparation, a NucleoSpin® TriPrep Column (light blue ring) was placed in a Collection Tube onto which the lysate was loaded. The samples were centrifuged at 11 000 \times g for 30 seconds at 25 °C. After centrifugation, the NucleoSpin® TriPrep Column was placed into a new Collection Tube.

For RNA extraction: rDNase reaction mixture was prepared first by addition of reconstituted rDNase (10 μ l) and reaction buffer for rDNase (90 μ l) into a sterile 0.2 ml PCR tube. From the rDNase mixture, 95 μ l was added directly onto the center of the silica membrane of the column. The column was incubated at room temperature for 15 minutes. A volume of 200 μ l Buffer RA2 was added to the NucleoSpin® TriPrep Column and centrifuged at 11 000 \times g for 30 seconds at 25 °C. The NucleoSpin® TriPrep Column was placed into a new Collection Tube.

A volume of 600 µl Buffer RA3 was added to the NucleoSpin® TriPrep Column and centrifuged at 11 000×g for 30 seconds at 25 °C. The flow through was discarded and the NucleoSpin® TriPrep Column was returned to the Collection Tube. A volume of 250 µl Buffer RA3 Buffer was added to the NucleoSpin® TriPrep Column and centrifuged at 11 000×g for 2 minutes at 25 °C.

The NucleoSpin® TriPrep Column was placed into a sterile 1.5 ml RNase-free Collection Tube. RNase free water was added to the NucleoSpin® TriPrep Column and centrifuged at 11 000×g for 1 minute. The flow through collected contained the total RNA. The RNA sample was quantified using the NanoDrop ND-100 Spectrophotometer (NanoDrop Technologies).

2.9.1. Agarose gel electrophoresis of RNA

Agarose gels with a percentage of 1% (w/v) were prepared by boiling appropriate amounts of agarose powder in 1X TBE until dissolved. Upon cooling ethidium bromide was added to a final concentration of 1 µg/ml. The prepared 1% agarose were poured into gel casting trays and allowed to solidify. RNA was electrophoresed on a 1% agarose gel to confirm its integrity. Isolated RNA (3.5 µg) was diluted with 6X loading buffer and heated at 95 °C for 2 minutes before loading into the wells. Electrophoresis was carried out at 100 V in 1X TBE electrophoresis buffer. After electrophoresis, the gel was viewed by ultra-visible illumination using a UV trans-illuminator. The gel image was captured with an image capturing system (Kodak Digital Science 1D).

2.10. cDNA synthesis

Roche's First Strand cDNA Synthesis Kit for RT-PCR (AMV) was used for cDNA synthesis according to the manufacturer's guide:

An amount of 0.5 µg of isolated RNA was placed into a sterile 1.5 ml centrifuge tube. The following reagents were added to the tube:

Table 2.1: Reagents utilized in cDNA synthesis reaction

Reagent	Final Concentration
10X Reaction Buffer	1X
25 mM MgCl ₂	5 mM
Deoxynucleotide Mix	1 mM
Oligo-p(dT) ₁₅ Primer	0.8 µg/µl
RNase Inhibitor	50 Units
AMV Reverse Transcriptase	20 Units
Sterile Water	Variable
RNA Sample	Variable

For secondary structure denaturation, the RNA sample was placed on a 65 °C heating block for 15 minutes and subsequently placed on ice for 5 minutes. RNA was added to the mixture followed by a brief centrifugation at 13 200×g for 5 seconds. The reaction mixture was incubated at 25 °C for 10 minutes followed by 42 °C for 60 minutes. The reaction was then incubated at 99 °C for 5 minutes followed by 4 °C for 5 minutes. The cDNA was quantified using the NanoDrop ND-100 Spectrophotometer (NanoDrop Technologies).

2.11. Primers

XIAP gene specific primers for PCR amplification were designed from XIAP's coding region with an accession number NM_001167.2. The forward primer was designed to include the restriction enzyme *NdeI* (CATATG) whereas the reverse primer was designed to include the restriction enzyme *XhoI* (CTCGAG). These gene specific primers were synthesized and purchased from Inqaba Biotech.

Table 2.2: XIAP gene specific primers used in PCR reactions

Primers	Sequence
Forward	5' – GACTCATATGACTTTTAAACAGTTTTGAAGGA – 3'
Reverse	5' – GACTCTCGAGAGACATAAAAATTTTTGCTTGAA – 3'

Table 2.3: PCR parameters as at 35 cycles

Parameter	Temperature	Time
1. Initial Denaturation	95 °C	3 minutes
2. Denaturation	94 °C	30 seconds
3. Annealing	61 °C	30 seconds
4. Elongation	72 °C	45 seconds
5. Final Elongation	72 °C	10 minutes
6. Incubation	4 °C	∞

2.12. Polymerase chain reaction (PCR) amplification of DNA

PCR reactions were carried out using Fermentas 2X DreamTaq™ Green Buffer according to the manufacturer's guide. PCR reactions were prepared according to **Table 2.4** with the use of gene specific primers (**Table 2.2**). The parameters for PCR reactions were according to **Table 2.3**.

Two 1% agarose gels were electrophoresed. The first gel was viewed and images were captured with an image capturing system (Kodak Digital Science 1D). The second gel was used for electrophoresis of the remaining PCR product. This was visualized with a 360 nm UV lamp before the band of interest was excised using a sterile blade and placed in a sterile 1.5 ml microcentrifuge tube. The latter was stored at -20 °C.

Table 2.4: Reagents utilized in PCR reaction

Reagent	Final Concentration
Fermentas 2X DreamTaq™	1X
XIAP Forward Primer	0.4 µM
XIAP Reverse Primer	0.4 µM
DNA	0.8 µg/µl

2.13. Agarose gel electrophoresis of PCR product

Amplified products were analysed post PCR amplification by electrophoresis of 1% agarose gels. Preparation and electrophoresis of 1% agarose gels as well as image capturing are as mentioned in **Section 2.9.1**.

2.14. Gel purification of amplified PCR product

Post PCR amplification, electrophoresis enabled visualization of fragments of interest. These bands were viewed using a 360 nm UV lamp and excised with a sterile blade. DNA was purified using Machery–Nagel’s NucleoSpin® Extract II PCR Clean–Up Gel Extraction Kit according to the manufacturer’s guide.

The excised product of interest was transferred to a sterile 1.5 ml microcentrifuge tube and the weight of the agarose gel was determined. For each 100 mg of the 1% agarose gel containing the product of interest, 200 µl NT buffer was added. The sample was placed on a heating block at 50 °C for 10 minutes whilst vortexing at 2–3 minute intervals until the agarose dissolved completely. The solution was added to the Nucleospin® Extract II Column which was placed in a 2 ml Collection Tube. The tube was centrifuged at 11 000×g for 1 minute and the flow through was discarded. A volume of 700 µl Buffer NT3 was added to the Nucleospin® Extract II Column and centrifuged at 11 000×g for 1 minute. The flow through was discarded. The tube was centrifuged for another 2 minutes at 11 000×g for complete removal of NT3 buffer. The Nucleospin® Extract II Column was placed in a sterile 1.5 ml microcentrifuge tube to which 50 µl NE Buffer was added and the column was incubated on the bench for 1 minute. The latter was centrifuged at 11 000×g for 1 minute. The collected DNA was quantified using the NanoDrop ND–100 Spectrophotometer (NanoDrop Technologies) and stored at –20 °C.

2.15. DNA cloning

2.15.1. pGEM®–T Easy vector system

The pGEM®–T Easy cloning vector from Promega (**Figure 2.1**) was used. pGEM®–T Easy vector is a linearized vector system consisting of a single 3’–terminal thymidine overhang at

the vector's ends. The thymidine overhangs function in improving the ligation efficiency of PCR products by preventing the vector from recircularizing. Hence it provides compatible overhangs for PCR products that have adenosine overhangs generated by thermostable polymerases.

One of the best features of the pGEM®-T Easy vector is that it contains many restriction sites within the multiple cloning region. The multiple cloning region is flanked by recognition sites for the enzymes *BstZ I*, *EcoR I* and *Not I*. These enzymes provide the release of the insert when performing sub-cloning experiments. pGEM®-T Easy vectors are usually supplied with 2X Rapid Ligation Buffer which enable fast and effective incubation periods and increase the number of colonies post transformation.

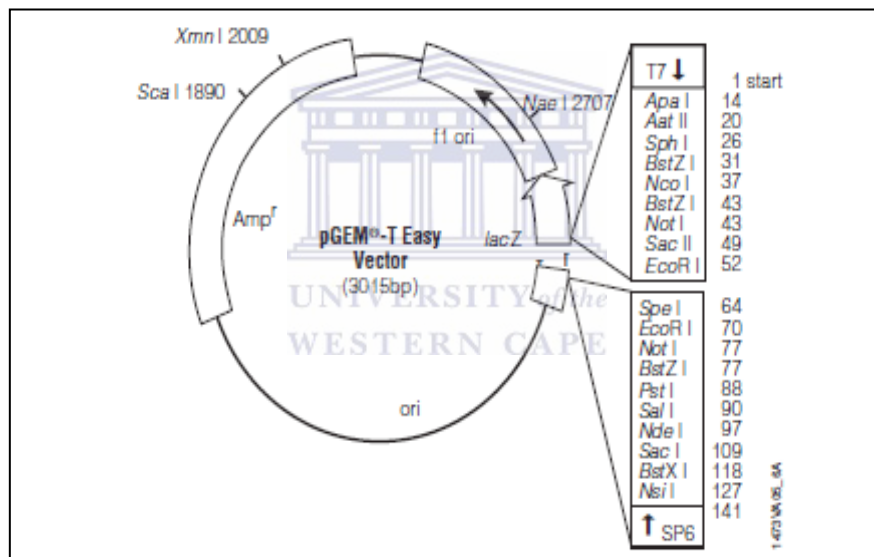


Figure 2.1: A circular map and sequence referencing points of pGEM®-T Easy vector system.

2.15.2. Ligation of PCR product into pGEM®-T Easy vector

The insert, i.e. XIAP PCR product, was purified and quantified using the NanoDrop ND-100 Spectrophotometer (NanoDrop Technologies).

The ligation reaction of XIAP's PCR product and pGEM®-T Easy vector was carried out with the use of Promega's T4 DNA Ligase. The protocol for ligation was performed according to the manufacturer's guide:

The ligation reaction was set up according to the following equation:

$[(\text{ng of vector} \times \text{kb size of insert}) \div \text{kb size of vector}] \times \text{insert:vector ratio}$

The recommended insert:vector ratio used was 3:1. The ligation reaction was prepared according to **Table 2.5**. The reactions were incubated at 4 °C overnight.

Table 2.5: Reagents utilized in the ligation reaction of XIAP and pGEM®-T Easy

Reagents	Experiment	Negative Control
pGEM-T Easy Vector (4 ng/μl)	2 μl	2 μl
XIAP Insert (13.9 ng/μl)	2 μl	-
Promega 2X Ligation Buffer	10 μl	10 μl
Nuclease Free Water	5 μl	7 μl
T4 DNA Ligase (U/ μl)	1 μl	1 μl
TOTAL (μl)	20 μl	20 μl

2.15.3. Transformation of competent *E. coli* MC1061 competent cells

Competent MC1061 *E. coli* cells were thawed on ice. To the ligation reactions, 100 μl of the competent cells were added. Both the experimental and negative control were incubated on ice for 20 minutes. Cells were heat shocked at 42 °C for 45 seconds followed by 5 minute incubation on ice. A volume of 900 μl pre-warmed Luria broth was added to each tube and the latter were incubated at 37 °C for 60 minutes whilst shaking at 700 rpm. After incubation 100 μl of each reaction, were plated on agar plates that contained 100 μg/ml ampicillin. Plates were incubated at 37 °C overnight.

2.15.4. Colony PCR amplification

Post transformation and plating, random colonies were selected from the plates. These colonies were screened for the presence of the XIAP insert by colony PCR amplification. Each colony was inoculated in PCR reaction with a final volume of 25 μl where the colony selected served as the template. The parameters for the PCR reaction were the same as described in **Section 2.12**.

2.15.5. Culturing of transformed MC1061 *E. coli* cells

Luria broth containing 100 µg/ml ampicillin was prepared. Colonies that screened positive for the XIAP insert (**Section 2.15.4**) were used to inoculate 5 ml prepared broth. The culture was incubated at 37 °C overnight whilst shaking at 170 rpm.

2.15.6. Plasmid DNA isolation and purification

From the overnight cultures 2.5 ml was removed and used for the preparation of 20% glycerol stocks (v/v). Glycerol stocks were stored at –80 °C. Plasmid DNA was isolated and purified from remaining overnight cultures (approximately 25 ml) using Promega's Wizard® Plus SV Miniprep DNA Purification System according to the manufacturer's guide.

The overnight bacterial culture was removed from the 37 °C incubator. Approximately 25 ml of the culture was centrifuged at 3 500×g for 15 minutes. The supernatant was discarded and the pellet was resuspended in 250 µl Cell Resuspension Solution by vortexing. A volume of 250 µl Cell Lysis Solution was added to the latter and the tube was inverted 4 times. A volume of 10 µl Alkaline Protease Solution was added and the tube's contents were mixed by inverting the tube 4 times. The cell suspension was incubated at room temperature for 5 minutes. A volume of 350 µl Neutralization Solution was added and the solution was immediately mixed by inverting the tubes 4 times. The bacterial lysate was centrifuged at 13 200×g for 10 minutes.

The cleared lysate were transferred to a prepared Spin Column. The column was centrifuged at 13 200×g for a minute. The flow through was discarded and 750 µl Column Wash Solution was added to the Spin Column. Thereafter, the column was centrifuged at 13 200×g for 1 minute. The flow through was discarded and 250 µl Column Wash Solution was added. The column was centrifuged at 13 200×g for 2 minutes. The Spin Column was transferred to a sterile 1.5 ml microcentrifuge tube. Plasmid DNA was eluted by addition of 100 µl Nuclease Free Water and centrifugation at 13 200×g at room temperature for 1 minute. The purified plasmid DNA was quantified using the NanoDrop ND–100 Spectrophotometer (NanoDrop Technologies) and stored at –20 °C.

2.15.7. Restriction digestion of pGEM–XIAP

Restriction enzymes were used to subclone PCR amplified XIAP product from the vector pGEM–T Easy. pGEM–XIAP plasmid DNA was digested with Fermentas' *XhoI* FastDigest and *NdeI* enzymes according to the manufacturer's guide.

For the first reaction, 1 µg of DNA was digested with 1 Unit of *XhoI* FastDigest in the 10X FastDigest Green Buffer and incubated at 37 °C for 60 minutes. The *XhoI* FastDigest was heat inactivated by incubation at 80 °C for 5 minutes. To the latter, 1 Unit of *NdeI* enzyme was added and incubated at 37 °C overnight. The *NdeI* enzyme was heat inactivated by heat inactivation at 65 °C for 30 minutes.

2.16. DNA sub-cloning

2.16.1. pET28a cloning vector

The expression vector pET28a (**Figure 2.2**) was purchased from Novagen. pET vector systems are regarded as the most powerful systems that have been developed for both cloning and expression of recombinant proteins in *E. coli*. Target genes are cloned in pET plasmids under control of strong bacteriophage T7 transcription and translation signals which are optional. Another important benefit of this system is its ability to maintain target genes transcriptionally silent in the uninduced state.

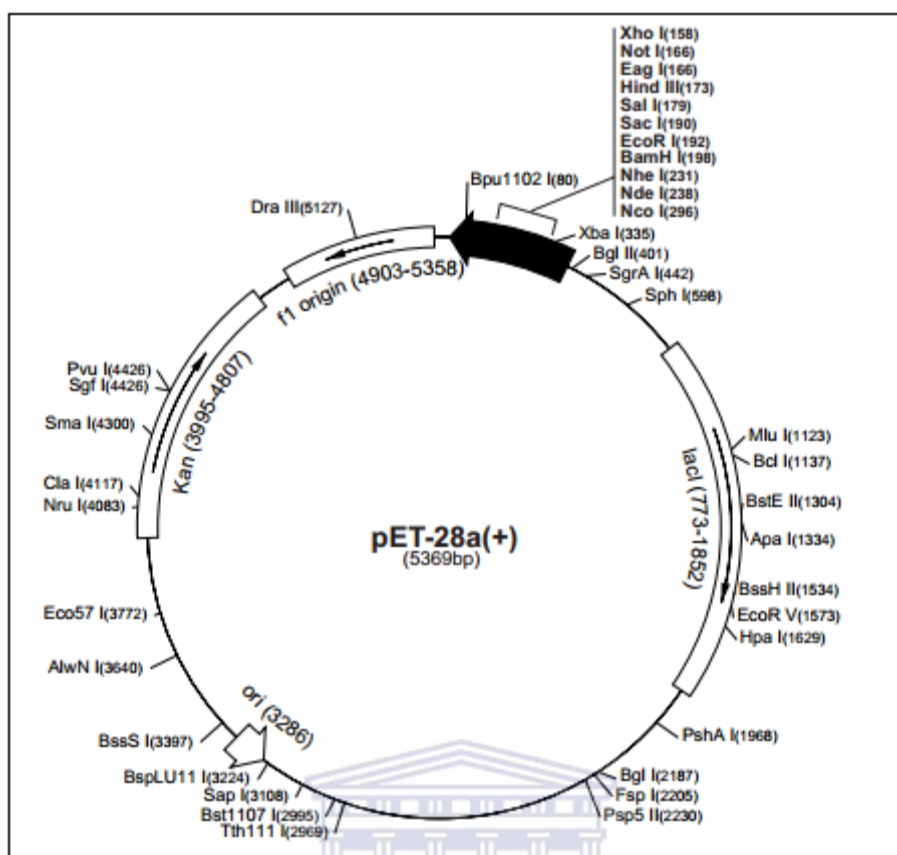


Figure 2.2: A circular map and sequence referencing points of pET28a expression vector system.

UNIVERSITY of the
WESTERN CAPE

2.16.2. Restriction digestion of pET28a

The pET28a expression vector was digested with Fermentas' *XhoI* FastDigest and *NdeI* enzymes as described in **Section 2.15.7**. The linearized vector was gel purified and quantified as described in **Section 2.14**.

2.16.3. Ligation of the released pGEM–XIAP product into the pET28a vector

The ligation of the product released from pGEM–XIAP into the linearized pET28a vector was performed using Promega's T4 DNA ligase according to the manufacturer's guide. The reactions were set up according to the following equation:

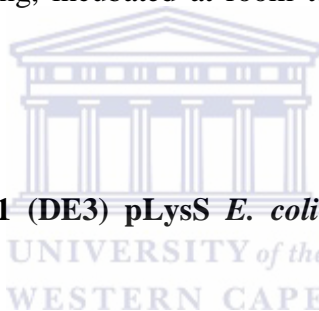
$$[(\text{ng of vector} \times \text{kb size of insert}) \div \text{kb size of vector}] \times \text{insert:vector ratio}$$

The recommended insert:vector ratio used was 3:1. The ligation reactions were prepared according to **Table 2.6**.

Table 2.6: Reagents used in ligation of pET28a expression vector and XIAP

Reagents	Experiment	Enzyme Control	Vector Only Control
pET28a Vector (1.2 ng/μl)	8 μl	8 μl	8 μl
XIAP Insert (1.6 ng/μl)	5 μl	-	-
Fermentas 10X T4 DNA Ligase Buffer	2 μl	2 μl	2 μl
Nuclease Free Water	4 μl	9 μl	10 μl
T4 DNA Ligase (1U/μl)	1 μl	1 μl	-
TOTAL (μl)	20 μl	20 μl	20 μl

Reactions were mixed by pipetting, incubated at room temperature for 1 hour and finally incubated at 4 °C for overnight.



2.16.4. Transformation of BL21 (DE3) pLysS *E. coli* competent cells with pET28a–XIAP Construct

Competent BL21 (DE3) pLysS *E. coli* cells were thawed on ice and 100 μl of the cells were added to the ligation reactions. All reactions were incubated on ice for 20 minutes. Cells were heat shocked at 42 °C for 45 seconds followed by 5 minute incubation on ice. A volume of 900 μl pre-warmed Luria broth was added to each tube and the latter were incubated at 37 °C for 60 minutes whilst shaking at 700 rpm. After incubation 100 μl of each reaction was plated on agar plates that contained 50 μg/ml kanamycin sulphate. Plates were incubated at 37 °C overnight.

2.16.5. Colony PCR amplification

E. coli colonies were screened for the presence of the XIAP insert by colony PCR. The parameters for the PCR reaction were the same as described in **Section 2.12**.

2.16.6. Culturing of transformed BL21 (DE3) pLysS *E. coli* cells

Luria broth containing 50 µg/ml kanamycin sulphate was prepared. Colonies that screened positive for the XIAP insert (**Section 2.15.4**) was used to inoculate prepared broth. The culture was incubated at 37 °C overnight whilst shaking at 170 rpm. From the overnight cultures, 20% glycerol stocks (v/v) were prepared and stored at –80 °C.

2.17. Mini expression screen for recombinant His–XIAP protein

Glycerol stocks containing BL21 (DE3) pLysS *E. coli* cells transformed with pET28a–XIAP were streaked out on Luria agar plates that contained 50 µg/ml kanamycin sulphate. Plates were incubated at 37 °C overnight. Single colonies were picked and cultured in 5 ml Luria broth containing 50 µg/ml kanamycin sulphate at 37 °C whilst shaking at 170 rpm for four hours. Aliquots of 1 ml were transferred to two separate 1.5 ml tubes where IPTG (1 mM) was added to one of the cultures (induced). No IPTG was added to the second culture (uninduced). Both tubes were incubated at 37 °C whilst shaking at 700 rpm for a further four hours.

Cells were harvested by centrifugation at 13200 rpm for 10 minutes in a bench top centrifuge. The supernatant was discarded and pellets were re-suspended in 100 µl of 2X Sample Buffer. The suspension was briefly centrifuged on bench top centrifuge at top speed followed by incubation at 95 °C for five minutes. Samples were analysed by SDS–PAGE gel electrophoresis (**Section 2.21**). The clone that demonstrated the highest level of recombinant protein expression was selected for large scale expression and purification. Additional 20% glycerol stocks (v/v) were prepared for these clones.

2.18. Purification of recombinant His–XIAP protein

A volume of 100 µl of culture of the highest expressing clone of *E. coli* BL21 (DE3) cells (**Section 2.16.6**) was used to inoculate 100 ml Luria broth containing 50 µg/ml kanamycin sulphate. Cells were incubated at 37 °C for 16 hours whilst shaking at 170 rpm. A further 900 ml Luria broth containing 50 µg/ml kanamycin sulphate was added to the primary culture and cells were incubated at 37 °C until OD₆₀₀ was between 0.4 and 0.6. Expression of

recombinant protein was induced by the addition of IPTG to a final concentration of 1 mM and cells were incubated at 25 °C for a further 16 hours.

Cultures were transferred to 250 ml propylene tubes and harvested by centrifugation at 6000×g at 4 °C for 10 minutes. The pellets were either stored at –20 °C or processed further as described in **Section 2.18.1**.

2.18.1. Cell extract preparation and protein purification as per Ni–NTA His–Bind® Resins

Purification of recombinant XIAP was carried out using of Novagen’s Ni–NTA His–Bind® Resins according to the manufacturer’s guide.

Once thawed the respective pellets were weighed to determine the volume of BugBuster reagent to be added. A Protease Inhibitor tablet was re–suspended in 3 ml BugBuster reagent. Thereafter, 1 µl Benzonase was added per 1 ml BugBuster re–suspension reagent. Pellets were allowed to dry and re–suspended in the respective volumes of re–suspension reagent. Cell suspensions were incubated on a slow shaking platform at room temperature for 20 minutes. Cell suspensions were centrifuged at 16 000×g at 4 °C for 20 minutes. The insoluble debris were removed and used for batch purification under native conditions. The pellets were stored at –20 °C.

A volume of 250 µl of 50 % Ni–NTA His–Bind slurry was added to 1 ml 1X Ni–BTA Bind Buffer and mixed gently. The resin was allowed to settle by gravity and 1 ml of the supernatant was removed. The 1 ml cleared lysate was added to the Ni–NTA His–Bind slurry and was mixed gently by shaking at 100 rpm at 4 °C for 60 minutes. The lysate–Ni–NTA His–Bind mixture was loaded onto a column with the bottom outlet capped. The bottom cap was removed to collect the through. The column was washed twice with 1 ml 1X Ni–NTA Wash Buffer and both flowthroughs were collected. The protein was eluted with 4 volumes of 2500 µl 1X Ni–NTA Elution Buffer. All four elutes along with the two washes and flow through were stored at –20 °C for 1D SDS PAGE gel electrophoresis (**Section 2.21**). The column was stored at 4 °C after 10 % ethanol was added.

2.19. Expression and purification of GST–XIAP protein

The pGEX–XIAP construct was purchased from Addgene for expression and purification of the XIAP recombinant protein. *E. coli* containing the pGEX–XIAP construct was streaked on Luria agar plates containing 100 µg/ml ampicillin. Plates were incubated at 37 °C for 16 hours.

Two colonies from each plate were selected and used to inoculate Luria broth (30 ml) containing 100 µg/ml ampicillin. These cultures were incubated at 37 °C whilst shaking at 170 rpm for 16 hours.

Glycerol stocks (20 % v/v) were prepared from the overnight cultures and stored at –80 °C. The remaining cultures were used for plasmid DNA isolation and purification using Promega’s Wizard® Plus SV Miniprep DNA Purification System according to the manufacturer’s guide (Section 2.15.6).

2.19.1. Transformation of *E. coli* BL21 (DE3) pLysS competent cells with the pGEX–XIAP construct

Competent BL21 (DE3) pLysS *E. coli* cells were thawed on ice and 100 µl of the cells were added per 2 µl GST–XIAP plasmid DNA (Section 2.16.4). A negative control consisting of 100 µl of the cells only was used. All reactions were incubated on ice for 20 minutes. Cells were heat shocked at 42 °C for 45 seconds followed by 5 minute incubation on ice. A volume of 900 µl pre-warmed Luria broth was added to each tube and the latter were incubated at 37 °C for 60 minutes whilst shaking at 700 rpm. Plates were incubated at 37 °C overnight.

2.19.2. Expression screen for recombinant GST–XIAP protein

Single colonies were selected from the plates and used to inoculate Luria broth (30 ml) containing 100 µg/ml ampicillin. Cultures were incubated at 37 °C whilst shaking at 170 rpm for four hours. Plates were stored at 4 °C. Glycerol stocks (20% v/v) were prepared from the cultures and stored at –80 °C. Aliquots (1 ml) were transferred into two separate 1.5 ml tubes. Isopropyl β–D–thiogalactopyranoside (IPTG) was added to one of the cultures (induced sample had a final optimized concentration of 0.2 mM IPTG) whereas no IPTG was added to the other sample (uninduced). Both tubes were incubated at 37 °C whilst shaking at 700 rpm for a further four hours.

Cells were harvested by centrifugation for 10 minutes centrifuge at 13 200 rpm in a bench top. The supernatant was discarded and pellets were re-suspended in 100 µl of 2X Sample Buffer. The suspension was briefly centrifuged in a bench top centrifuge at 13000 rpm followed by incubation at 95 °C for five minutes. Samples were analysed by SDS-PAGE gel electrophoresis (**Section 2.21**). The clone that demonstrated the highest level of recombinant protein expression was selected for large scale expression.

2.19.3. Expression of GST-XIAP recombinant protein

A volume of 100 µl of the glycerol stock with the highest expressing clone of *E. coli* BL21 (DE3) pLysS cells (**Section 2.16.6**) was used to inoculate 100 ml Luria broth containing 100 µg/ml ampicillin. Cells were incubated at 37 °C for 16 hours whilst shaking at 170 rpm. A further 900 ml Luria broth containing 100 µg/ml ampicillin was added to the primary culture and cells were incubated at 37 °C until OD₆₀₀ reached between 0.4 and 0.6. Expression of recombinant protein was induced by the addition of IPTG to a final concentration of 0.2 mM and cells were incubated at 25 °C for 16 hours.

Cultures were transferred to 250 ml propylene tubes and harvested by centrifugation at 6000×g at 4 °C for 10 minutes and pellets were stored at -20 °C.

2.19.4. Cell extract preparation and protein purification as per BugBuster® GST-Bind Purification Kit

Purification of recombinant GST-XIAPS was carried out with the use of Novagen's BugBuster® GST-Bind Purification Kit according to the manufacturer's guide.

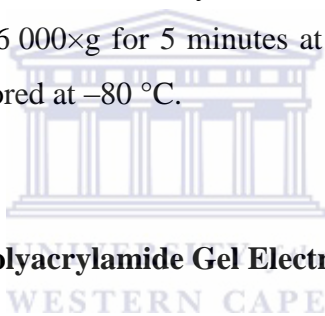
Once thawed the pellets were re-suspended in 4 ml 1X GST Bind/Wash Buffer per 100 ml culture. The sample was sonicated while on ice. The lysate was centrifuged at 10 000×g for 20 minutes. The post-centrifugation supernatant was filtered through 0.45 micron filters.

GST-Bind resin was mixed gently by inversion until the resin was completely suspended. A volume of 2.5 ml of slurry was transferred to the column and the resin was allowed to settle. When the level of storage buffer, containing 20 % ethanol, dropped to the top of the column bed the resin was washed with 12.5 ml 1X GST Bind/Wash Buffer. The GST Bind/Wash Buffer was allowed to drain to the top of the column bed before the prepared extract was loaded. The prepared extract was loaded and the flow through fraction was collected and stored at 4 °C. The column was washed with 25 ml 1X GST Bind/Wash buffer. The wash

was collected and stored at 4 °C. The protein was eluted with 7.5 ml 1X GST Elution Buffer. The eluted fractions were collected and stored at 4 °C. The flow through, wash and eluted fractions were analysed for the presence of the targeted protein via 1D SDS PAGE gel (Section 2.21).

2.20. Protein extraction from cultured human cancerous cells

Various cell lines (A5495, H157, HepG2, HeLa, HT29, KMST and MCF7) were cultured until confluency. The media was decanted and cells were washed with 1X PBS. Protein extraction was carried out with the use of CytoBuster™ Protein Extraction Reagent (Novagen) according to the manufacturer's guide. The recommended amount of CytoBuster™ was added and the cells were placed on a shaker for 5 minutes. Following incubation, the cells were scrapped off in the CytoBuster™ reagent and placed in a 1.5 ml tube. Cells were centrifuged at 16 000×g for 5 minutes at 4 °C. The supernatant containing the proteins were removed and stored at -80 °C.



2.21. One Dimensional SDS Polyacrylamide Gel Electrophoresis

2.21.1 Gel preparation

Proteins were analysed on one dimensional (1D) SDS polyacrylamide gels (PAGE). Glass plates and apparatus (Bio-Rad) used were first cleaned with a soapy wash followed by 70% ethanol to ensure they were free of acrylamide. A 12 % separating gel solution was prepared (Table 2.7). To the separating gel solution, 20 µl TEMED was added and the solution was poured between the gel plates. The separating gel solution was overlaid with 1 ml isopropanol.

Table 2.7: Stock Solutions for the 12 % Separating Gel Solution

Reagent	Volume
Separating Buffer (1.5 M Tris-HCl, pH 8.8)	2.5 ml
40 % Acrylamide-Bis (37:5:1)	3 ml
10 % SDS	0.1 ml
10 % APS	0.2 ml
Distilled Water	4.2 ml
TEMED	0.02 ml
TOTAL VOLUME	10.02 ml

The stacking gel solution was prepared (**Table 2.8**). Once the separating solution was solidified the isopropanol was poured off and the gel was rinsed thoroughly with distilled water. The stacking gel solution was poured above the separating gel, and a 10-well Bio-Rad comb was inserted immediately into the stacking gel. The gel was allowed to solidify for 10 to 15 minutes. Once solidified, the comb was removed and the gel was set-up in a Bio-Rad gel electrophoresis tank. The tank was filled with 1X SDS running buffer and was pre-run at 120 V for 10 to 15 minutes to remove any SDS or liquid acrylamide from the gel wells.

Table 2.8: Stock solution for the 5 % Stacking Gel Solution

Reagent	Volume
Separating Buffer (0.5 M Tris-HCl, pH 6.8)	0.5 ml
40 % Acrylamide-Bis (37:5:1)	0.63 ml
10 % SDS	0.05 ml
10 % APS	0.05 ml
Distilled Water	3.77 ml
TEMED	0.01 ml
TOTAL VOLUME	5.01 ml

2.21.2. Sample Preparation and Gel Loading

In a 1.5 ml eppendorf tube, 10 μ l of the protein sample was mixed with 10 μ l of 2X sample buffer. Samples were boiled at 95 °C for five minutes followed by centrifugation at 14 000 rpm in a benchtop Eppendorf centrifuge for 10 minutes at 4 °C. The protein molecular marker was boiled for 5 minutes at 95 °C. The samples were loaded onto the polyacrylamide gel and were electrophoresed at 100 V until the Coomassie dye front reached the bottom of the gel.

2.21.3. Gel staining

The gel was removed from the gel plates and stained in pre-warmed Coomassie stain for 20 minutes on a shaker. The staining solution was removed and the gel was destained for 1 hour while shaking in destaining solution.

2.22. Analysis of XIAP expression by western blot

2.22.1. Blot transfer of proteins onto PVDF membrane

Proteins were electrophoresed on a 1D SDS PAGE (**Section 2.21**). After electrophoresis proteins were transferred onto BioTrace™'s PVDF membrane by blot transfer. The transfer took place in a tank and interchangeable lid with the vertical electrophoresis unit for 90 minutes at 110 V. The temperature was kept at 2 to 8 °C.

2.22.2. Analysis of XIAP expression

The membrane was blocked in TBS–Tween containing 5 % milk for an hour at room temperature. The membrane was washed thrice in TBS–Tween while shaking at room temperature for five minutes. The membrane was incubated in XIAP monoclonal antibody at a dilution of 1:5000 in TBS–Tween containing 3% BSA while shaking at 4 °C overnight. The membrane was washed in TBS–Tween containing 5% milk powder while shaking at room temperature for five minutes. The membrane was washed twice in TBS–Tween while shaking at room temperature for five minutes. Thereafter, the membrane was incubated in goat anti–mouse IgG–HRP antibody at a dilution of 1:5000 in TBS–Tween containing 3% BSA while shaking for 45 minutes at room temperature. The membrane was washed in TBS–Tween containing 5% milk powder while shaking at room temperature for five minutes. The membrane was washed twice in TBS–Tween while shaking at room temperature for five minutes. The membrane was incubated with 2 ml Thermo Scientific's SuperSignal® West Pico Chemiluminescent Substrate for five minutes in the dark.

2.22.3. Exposure of membrane

The UVP BioSpectrum® Imaging System and Vision Works™ LS Image Acquisition and Analysis Software was used to visualize and capture images of the membrane.

2.23. Densitometric analysis of western blot

ImageJ densitometry software (Version 1.46r, National Institutes of Health, Bethesda, MD) was used for gel band quantitative densitometric analysis. Bands were quantified based on their relevant intensities.

2.24. Evaluating the interaction between the recombinant GST–XIAP protein and embelin

The recombinant GST–XIAP protein was quantified to having a concentration of 0.006 μM . To evaluate the binding between recombinant GST–XIAP protein and embelin using the MicroCal™ iTC₂₀₀ System, embelin had to be 10 – 15 more concentrated. Therefore, 200 nM embelin was prepared in 5 mM phosphate buffer containing 0.15% DMSO. A total of 18 injections of 200 nM embelin were introduced by pipette into the cell unit containing recombinant GST–XIAP protein. Origin® scientific plotting software was used to analyse the calorimetric data generated.

As a negative control, a total of 18 injections of 5 μM EDTA was introduced by pipette into the cell unit containing 0.5 μM calcium. Analysis was possible using the Origin® scientific plotting software.



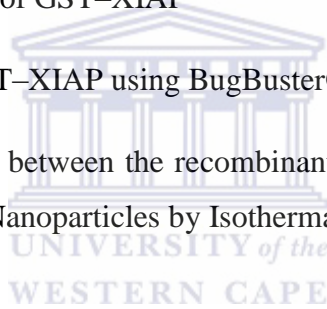
CHAPTER 3: RESULTS

- 3.1. Evaluating the expression levels of XIAP in human cancer cells
 - 3.1.1 Introduction
 - 3.1.2 Western blot analysis of XIAP expression in various human cancer cell lines

- 3.2. Evaluating the apoptotic effects of ceramide as an apoptotic inducer
 - 3.2.1 Introduction
 - 3.2.2 Characterization of conjugated nanoparticles
 - 3.2.3 Morphological changes in MCF7 and HepG2 cancer cells upon treatment
 - 3.2.4 Induction of apoptosis on MCF7 and HepG3 cancer cells as a result of the treatment options
 - 3.2.5 Evaluating the cellular uptake of AuNP-E and AuNP-P-E
 - 3.2.5.1 Inductively Coupled Plasma-Optical Emission Spectrometry
 - 3.2.5.2 Transmission Electron Microscopy

- 3.3. Cloning of XIAP into His-tagged expression vector system
 - 3.3.1 Introduction
 - 3.3.2 The isolation of total RNA from MCF7 breast cancer cells
 - 3.3.3 PCR amplification of XIAP
 - 3.3.4 Sub-cloning of XIAP into pGEM-T Easy vector
 - 3.3.5 Colony PCR screening of XIAP positive clones
 - 3.3.6 Sequence analysis of XIAP positive clones
 - 3.3.7 XIAP release from pGEM-XIAP by restriction digestion
 - 3.3.8 Preparation of the pET28a expression vector for DNA ligation

- 3.3.9 Screening of XIAP positive clones by colony PCR
- 3.4. Affinity purification of recombinant His–XIAP
 - 3.4.1 Introduction
 - 3.4.2 Screening for the expression of XIAP
 - 3.4.3 Purification of His–XIAP recombinant protein using the Ni–NTA His–Bind® resins
- 3.5. Affinity purification for recombinant GST XIAP
 - 3.5.1 Introduction
 - 3.5.2 Expression screen of GST–XIAP
 - 3.5.3 Sequence analysis of GST–XIAP
 - 3.5.4 Purification of GST–XIAP using BugBuster® GST–Bind Purification Kit
- 3.6. Evaluating the interaction between the recombinant GST–XIAP Protein and embelin and embelin Conjugated Nanoparticles by Isothermal Titration Calorimetry (ITC)
 - 3.6.1 Introduction
 - 3.6.2 ITC analysis



3.1. Evaluating the expression levels of XIAP in human cancer cells

3.1.1. Introduction

XIAP is the best and thoroughly characterized human IAP (Holcik *et al.*, 2003; Fischer and Schulze–Osthoff, 2005²). It consists of three BIR regions as well as a RING domain (Holcik *et al.*, 2003; Schimmer, 2004). Tamm and colleagues have previously reported that XIAP was widely expressed in mammalian tumour cell lines (Tamm *et al.*, 2000). The aim of this section was to determine XIAP expression levels among various mammalian cancer cell lines that were available in our laboratory. This was later used to identify cancer lines where XIAP was expressed at both low and high levels. Identified low and high XIAP expressing cancer cells were treated with embelin and embelin conjugates to investigate embelin's inhibitory effect on XIAP.

3.1.2. Western blot analysis of XIAP expression in various human cancer cell lines

The panel of human cancer cell lines that were investigated included A5495, H157, HepG2, HeLa, HT29 as well as MCF7. Proteins were extracted as described in **Section 2.20** to evaluate XIAP expression using the XIAP monoclonal antibody.

Samples were analysed on a 1D SDS PAGE gel prior to western blot analysis. According to **Figure 3.1** a distinct band was visible in all the available cell lines. These bands had a size of approximately 70 kDa. Non-specific bands were detected as their sizes were smaller when compared to the size of the XIAP protein. It may be deduced, from **Figure 3.1**, that successful protein extraction using CytoBuster™ Protein Extraction Reagent was achieved. Confirmation of this 70 kDa band to be XIAP was achieved by Western Blot Analysis.

The extracted protein samples were used for Western Blot analysis to determine XIAP expression. **Figure 3.2** shows XIAP expression in various mammalian cancer cell lines available. High XIAP expression was observed in H157 and MCF7 whereas low XIAP expression was observed in A5495, HepG2, HeLa and HT29 mammalian cancer cell lines.

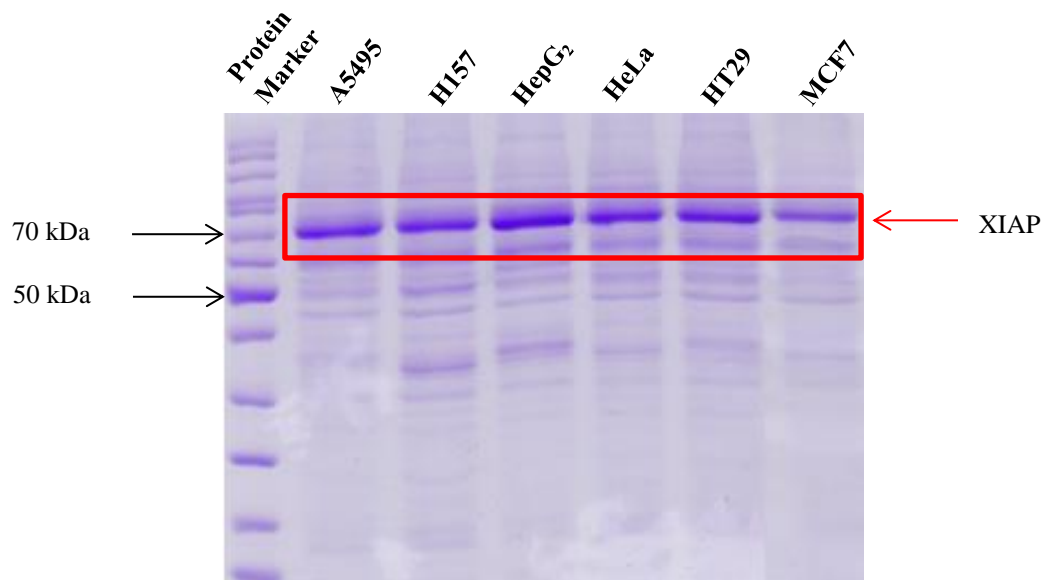


Figure 3.1: 1D SDS polyacrylamide gel electrophoresis of proteins extracted from available mammalian cancer cells. Proteins were extracted from confluent cells by using CytoBuster™ Protein Extraction Reagent.

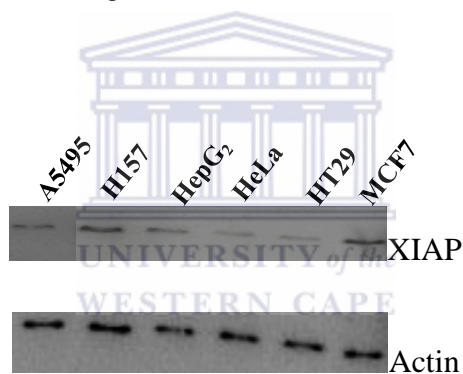


Figure 3.2: Western Blot of XIAP expression in mammalian cancer cells. The XIAP monoclonal antibody was used to determine the levels of XIAP expression in various mammalian cancer cells available, Actin antibody was used to verify equal loading.

The results obtained from western blot analysis were quantified using the ImageJ Software (www.imagej.nih.gov/ij/). The densitometry data for the band intensity for expression of the XIAP protein were used to construct a bar graph. **Figure 3.3** shows high density values for the XIAP protein in cells lines H157, MCF7, with A5495 displaying the most intensity. Low density values were detected in HeLa, HT29, with HepG₂ displaying the least intensity.

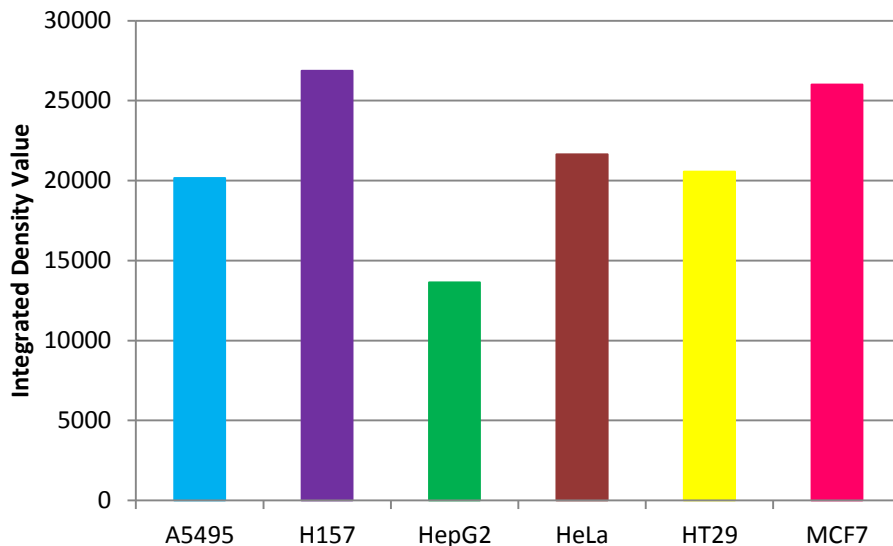


Figure 3.3: Densitometry data for XIAP Protein Expression. XIAP protein expression levels were quantified for the respective cancer cell lines available in the laboratory. Quantification was possible with the ImageJ software.

3.2. Evaluating the apoptotic effects of ceramide as an apoptotic inducer

3.2.1. Introduction

Inhibitors of apoptosis proteins (IAPs) are a family of anti-apoptotic proteins where they mainly function in regulating caspase activity. IAPs regulate apoptosis directly by inhibiting caspase 3 and/ caspase 7 thereby preventing the main execution phase of apoptosis. IAPs also prevent the intrinsic apoptotic pathway by caspase 9 inhibition (Riedl *et al.*, 2001).

The X-chromosome linked inhibitor of apoptosis protein (XIAP) is the best (Schimmer, 2004) and most thoroughly characterized human IAP (Fischer and Schulze-Osthoff, 2005²). XIAP overexpression protects cells from different apoptotic triggers and may lead to cancer (Holcik *et al.*, 2003).

Embelin is a cell-permeable, small molecular weight inhibitor of XIAP which was identified via computational screening (Nikolovska-Coleska *et al.*, 2004²). Embelin or 2,5-dihydroxy-3-undecyl-1,4-benzoquinone was isolated from the plant *Embelia ribes* (Siegelin *et al.*, 2009) which has been used to treat inflammatory disease as well as fever for many years (Pathan and Bhandari, 2011). Embelin targets XIAP's BIR3 domain thereby blocking the

inhibitory effect of XIAP on caspases, and consequently promotes apoptosis (Nikolovska–Coleska *et al.*, 2004²).

Current cancer treatment options are distributed non-specifically in the body. As they affect both the cancerous and normal cells, the achievable dose within the tumour is limited. This results in suboptimal treatment due to excessive toxicities (Cho *et al.*, 2008).

The use of nanoparticles for medical purposes is based on their quantum properties, their ability to absorb and carry other compounds and mainly their surface-to-mass ratio which is much larger when compared to other nanoparticles. The surface of nanoparticles is large and functional in that they are able to bind, absorb and carry compounds such as drugs, probes and proteins (de Jong and Borm, 2008).

As XIAP is inhibited by embelin (Nikolovska–Coleska *et al.*, 2004¹; Nikolovska–Coleska *et al.*, 2004²), the objective of this section was to evaluate the inhibitory effect of embelin on XIAP when embelin was conjugated to gold nanoparticles (AuNP–E) as well as conjugation of embelin and a specific cancer targeting peptide to gold nanoparticles (AuNP–P–E). MCF7 and HepG2 cells were cultured and treated as described in **Section 2.5**.

3.2.2. Characterization of conjugated gold nanoparticles

Gold nanoparticles (sized 14 nm) were synthesized and supplied by Dr. Franklin Keter (Mintek). **Figure 3.4** indicates a schematic representation of an unconjugated gold nanoparticle when compared to gold nanoparticles conjugated with embelin (AuNP–E) and gold nanoparticles biconjugated with embelin and the cancer targeting peptide LTVSPWY (AuNP–P–E).

Gold nanoparticles (AuNPs) were conjugated with embelin (AuNP–E) as well as a cancer targeting peptide LTVSPWY (Shahidi and Sioud, 2003) and embelin (AuNP–P–E) and supplied by Dr. Franklin Keter (Mintek). **Table 3.1** shows the optical properties for AuNP–E and AuNP–P–E. The data comprised of UV Vis spectra (**Figure 3.5**) and TEM (**Figure 3.6**) were generated by Dr. Keter post synthesis.

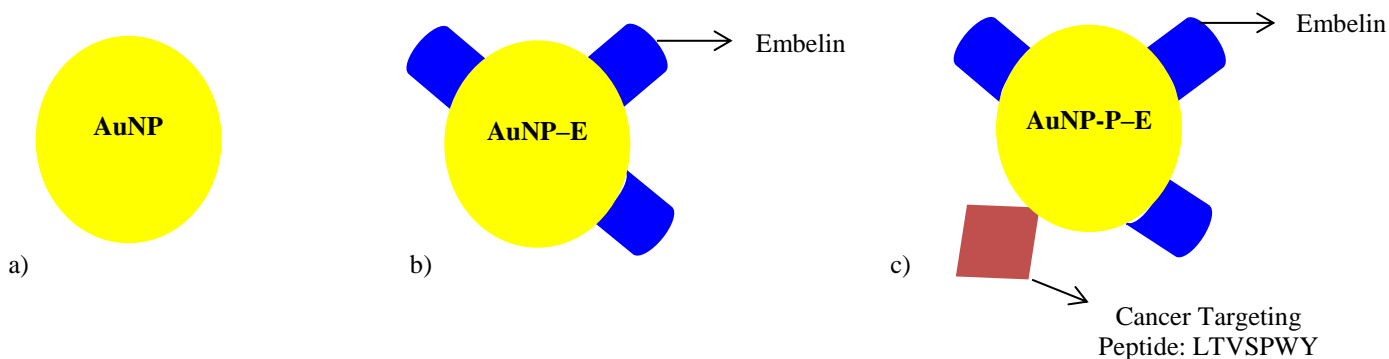


Figure 3.4: A schematic representation of gold nanoparticles before and after conjugation. Panel (a) shows an un conjugated nanoparticle. Panel (b) shows gold nanoparticle conjugated with embelin (AuNP-E). Panel (c) shows a gold nanoparticle biconjugated with embelin and the cancer targeting peptide LTVSPWY (AuNP-P-E).

Table 3.1: Optical Properties of AuNP-E and AuNP-P-E

Features	AuNP-E	AuNP-P-E
UV Absorbance	519 nm	524 nm
Concentration (OD)	2.5094	1
½ OD	563 nm	575 nm
Citrate Concentration	1.14%	1.14%

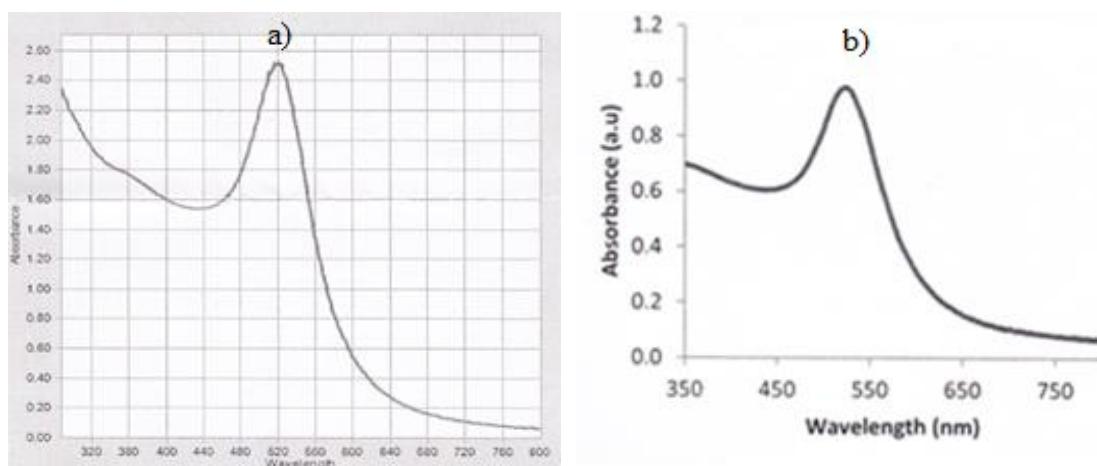


Figure 3.5: UV Vis spectra for (a) AuNP-E and (b) AuNP-P-E. A single peak is visualized in both spectra at a wavelength of 519 nm and 524 nm respectively. The absorbance of embelin-AuNP is approximately 2.5 whereas the absorbance of the peptide-embelin-AuNP is approximately 1.0.

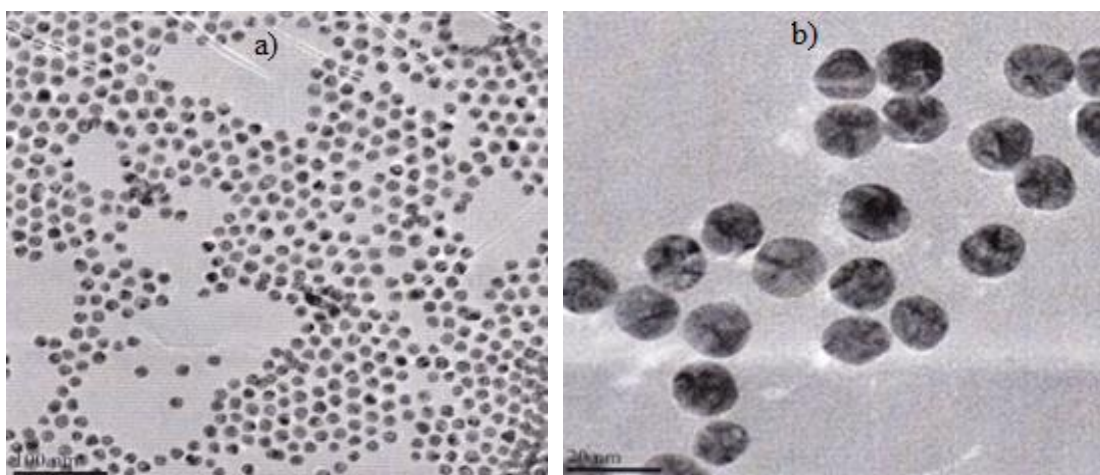


Figure 3.6: TEM data for (a) AuNP-E and (b) AuNP-P-E. The magnification for the embelin-AuNP and peptide-embelin-AuNP was at 100 nm and 20 nm respectively.

Figure 3.5 (a) and (b) shows the absorbance spectra for AuNP-E and AuNP-E-P, respectively. The optical absorption spectra occurred in the range of 300 – 800 nm for AuNP-E and 350 – 800 nm for AuNP-E-P. The AuNP-E had an absorbance of 2.5 corresponding to a wavelength of 519 nm (**Table 3.1**). The AuNP-E-P had an absorbance of 1.0 corresponding to a wavelength of 524 nm (**Table 3.1**). **Figure 3.6** it was observed that the conjugated nanoparticles were distributed uniformly and resembled a spherical shape.

3.2.3. Morphological changes in MCF7 and HepG2 cancer cells upon treatment

MCF7 and HepG2 cancer cells were cultured and treated as described in **Section 2.5**. **Figure 3.7** and **Figure 3.8** shows the changes in morphology for the HepG2 and MCF7 cells respectively post 24 hour treatment.

Post treatments both HepG2 and MCF7 cells treated with embelin, AuNP-E and AuNP-P-E resembled the untreated cells. Therefore, no morphological differences were detected when compared to the untreated controls. It was also observed that the treatments involving ceramide, cells shrunk, rounded up and there were cells that detached from the surface of the well. It may be deduced that ceramide was responsible for the changes in morphology.

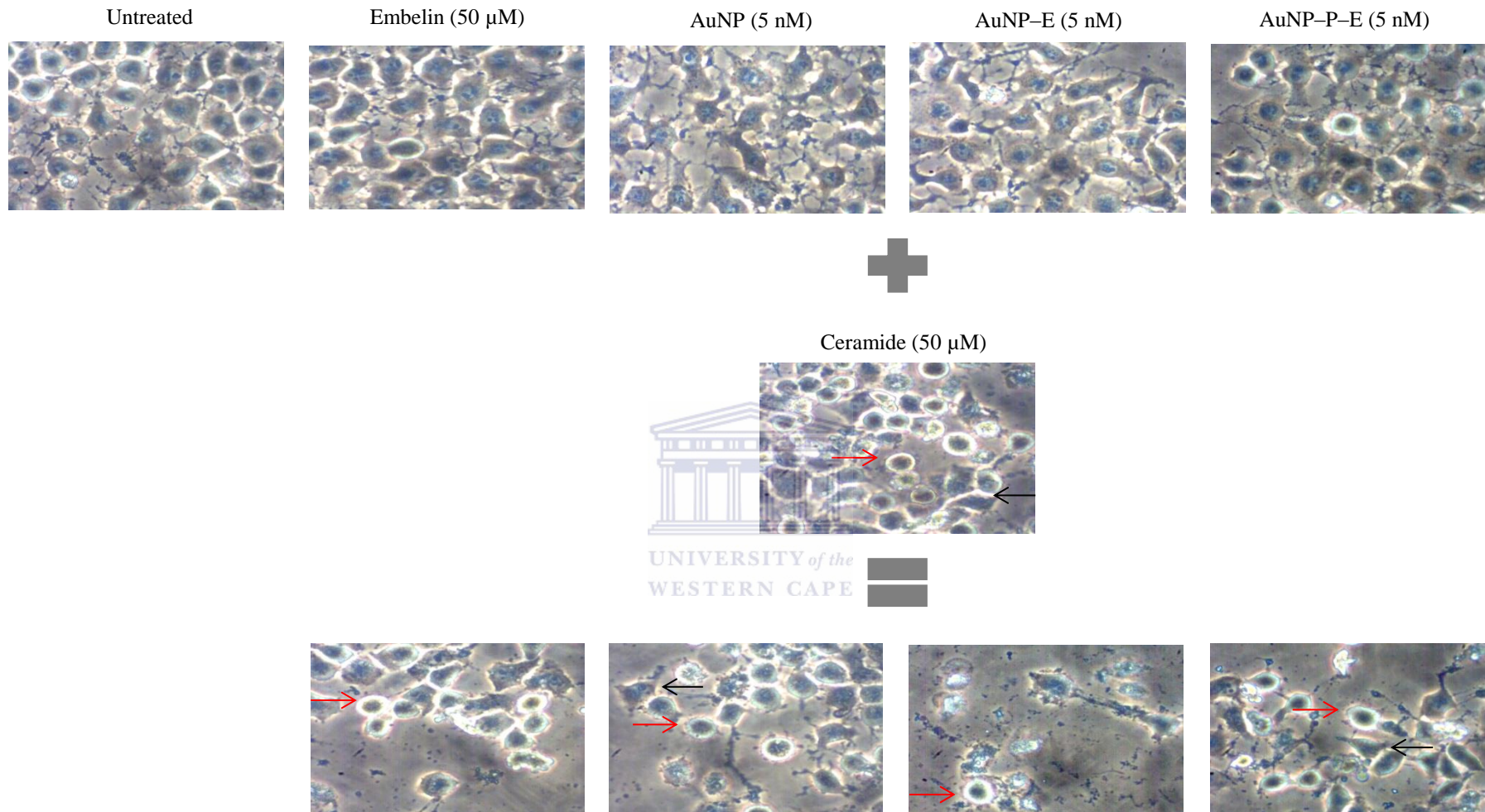


Figure 3.7: Morphology of HepG2 liver cancer cells treated with embelin, AuNP-E or AuNP-P-E as well as co-treatments with ceramide. Morphological differences, observed using a Nikon TMS light microscope with a 20X magnification, included shrinkage of cells (black arrows) as well as rounded detached cells (red arrows).

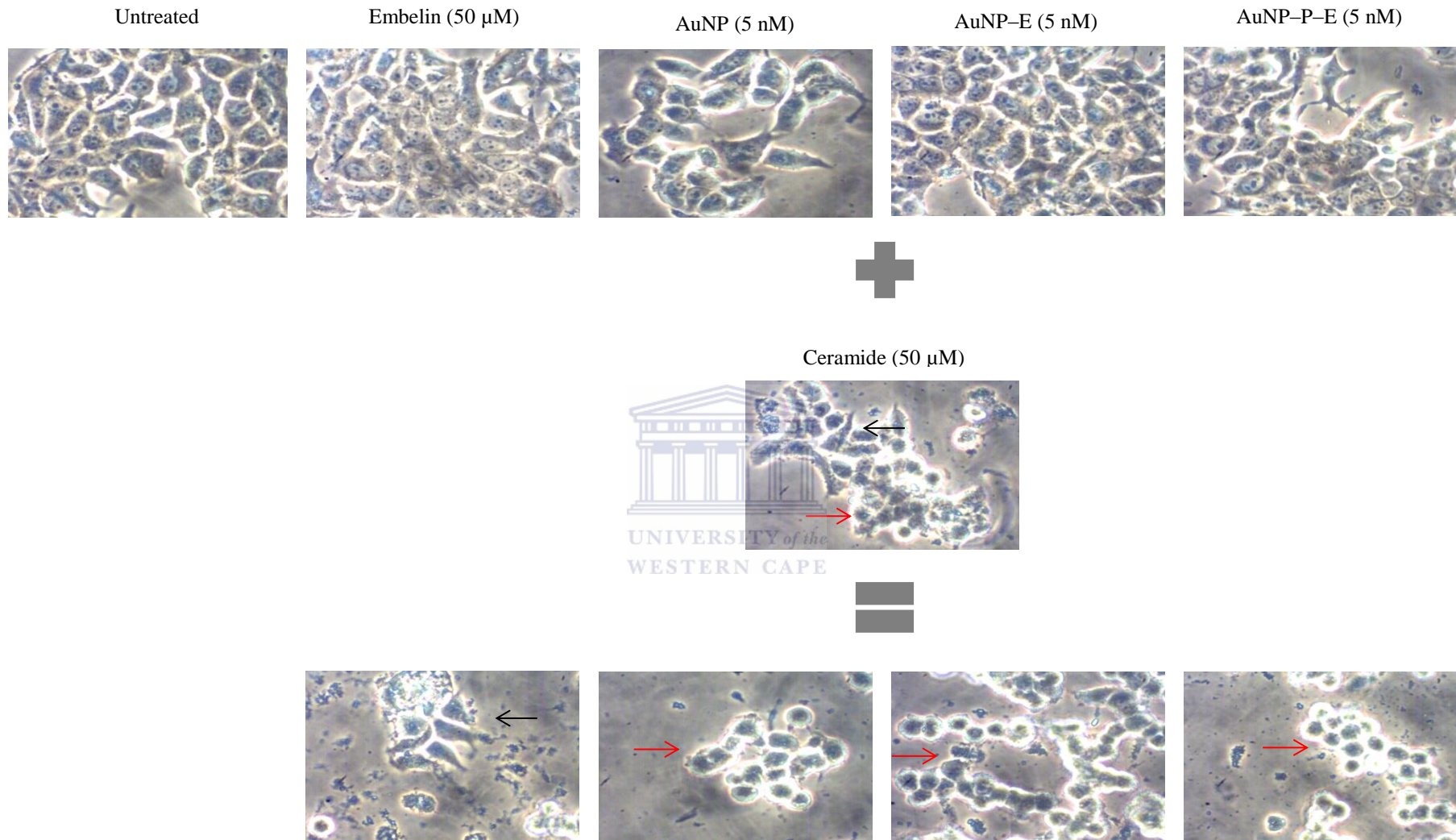


Figure 3.8: Morphology of MCF7 breast cancer cells treated with embelin, AuNP-E or AuNP-P-E as well as co-treatments with ceramide. Morphological differences, observed using a Nikon TMS light microscope with a 20X magnification, included shrinkage of cells (black arrows) as well as rounded detached cells (red arrows).

3.2.4. Induction of apoptosis on MCF7 and HepG2 cancer cells as a result of the treatment options

Apoptosis was assayed by flow cytometry using the FACScan (BD Biosciences) flow cytometer (**Section 2.5**). Cells were harvested and stained with APOPercentage™ dye. This assay is used for detection and measurement to monitor the occurrence of apoptosis in mammalian cells where cells undergoing apoptosis are stained. The data obtained was used to construct bar graphs depicting the percentage of cell death (**Figure 3.9**).

The percentage of apoptosis for the respective treatments showed the same trend for both the HepG2 and MCF7 cancer cell lines. Individual ceramide treatments yielded percentages of apoptosis close to 60%. It was observed that co-treatments comprised of ceramide and embelin conjugates yielded percentages of apoptosis above 50%. The highest percentage of apoptosis arose from the AuNP-E + ceramide treatment. This was followed by AuNP-P-E + ceramide and embelin + ceramide yielded the lowest percentage of apoptosis of the trio.



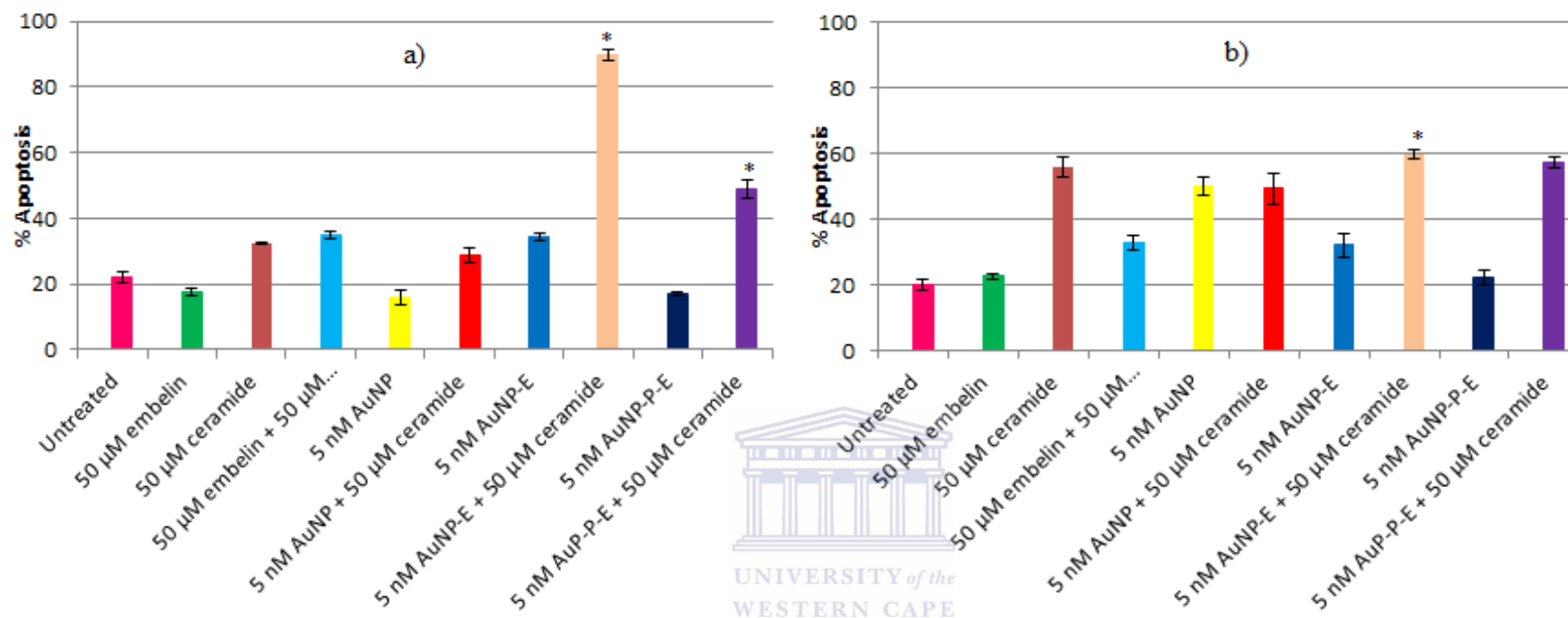


Figure 3.9: Indications of apoptosis of (a) HepG2 and (b) MCF7 cancer cells as a result of the various treatment options. Post 24 hour treatments, cells were stained with APOPercentage™ dye. Cells that were positive for apoptosis were quantified by flow cytometry using the FACScan. Data was obtained in triplicate and were used to construct histograms for HepG2 and MCF7 cancer cells (mean ± SD; n = 3).

3.2.5. Evaluating the cellular uptake of AuNP-E and AuNP-P-E

MCF7 and HepG2 cancer cells were treated for 24 hours with AuNP-E and AuNP-P-E. To evaluate the uptake of the gold nanoparticles two techniques were used, namely, Inductively Coupled Plasma–Optical Emission Spectrometry (ICP–OES) and Transmission Electron Microscopy (TEM).

3.2.5.1. Inductively Coupled Plasma–Optical Emission Spectrometry

MCF7 and HepG2 cancer cells cultured and treated as described in **Section 2.6** for ICP–OES Analysis. The objective of ICP–OES was to determine the concentration (**Figure 3.10 (a)**) and percentage of gold taken up (**Figure 3.11 (b)**) by the treated cancer cells. This was achieved using the Varian 1600 ES instrument and the ICP expert 11 software.

When comparing the concentration of gold present post treatment, for both MCF7 and HepG2 cancer cells, more gold was present in the AuNP–P–E treatment when compared to the AuNP–E treatment. Hence, the percentage of gold detected was higher in the AuNP–P–E treatment (**Figure 3.10 (a)** and **Figure 3.11 (b)**).

In both treatments, the concentration of gold present in the cells present indicates that embelin was taken up by the cancerous cell. However, an increased in gold concentration present post AuNP–P–E treatment suggests that targeted delivery of embelin to the XIAP site was achieved by the presence of the targeting peptide.

3.2.5.2. Transmission Electron Microscopy

MCF7 breast and HepG2 liver cancer cells were cultured and treated as described in **Section 2.7**. Post 24 hour treatments cells were harvested and prepared for TEM Analysis. Analysis was performed by the National Health Laboratory Services (Tygerberg Hospital, Cape Town). The objective of TEM was to visualize the uptake of gold in the treated HepG2 (**Figure 3.10**) and MCF7 (**Figure 3.11**) cancer cells. This was achieved using the JEOL JEM–1011 Electron Microscope instrument and the cis analysis program iTEM imaging software.

Images of untreated HepG2 and MCF7 cells were captured were the bar was represented at 20 μm . Cells treated with 5 nM AuNP as well as co–treated with 5nM AuNP–P–E + 50 μM ceramide had images captured at a magnification of 10 μm . The lower magnification

indicated the presence of the AuNPs within the organelles (inserts: the bar was represented at 2 μm).



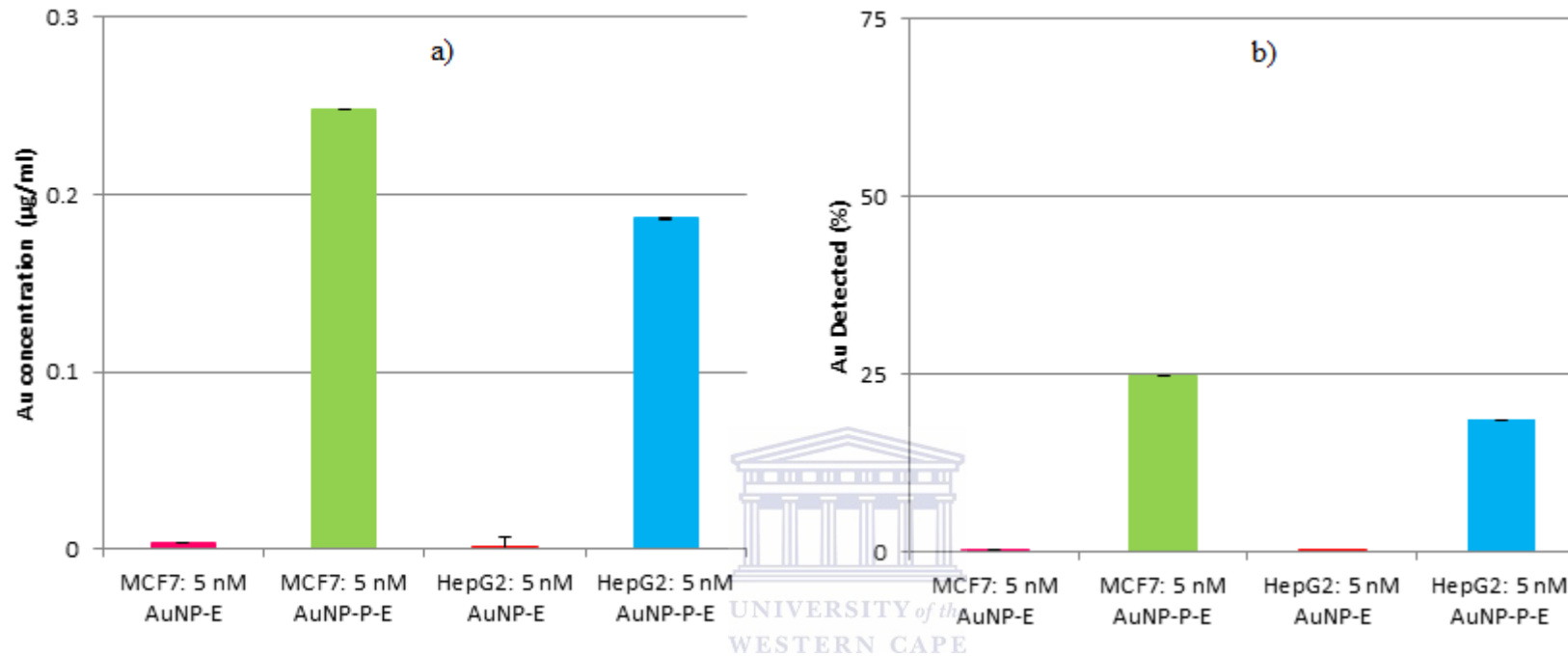


Figure 3.10: Evaluating the presence of gold in MCF7 breast and HepG2 liver cancer cells treated with AuNP-E and AuNP-P-E. Post 24 hour treatment, cells were prepared for ICP analysis. The average of the data obtained were used to determine the (a) concentration and (b) percentage of gold present in the treated cells (mean \pm SD; n = 2).

It was observed that the concentration of gold was higher in the AuNP-P-E when compared to AuNP-E (**Figure 3.10 (a)**). The percentage of gold taken up post treatments was also higher in the AuNP-P-E when compared to AuNP-E (**Figure 3.10 (b)**).

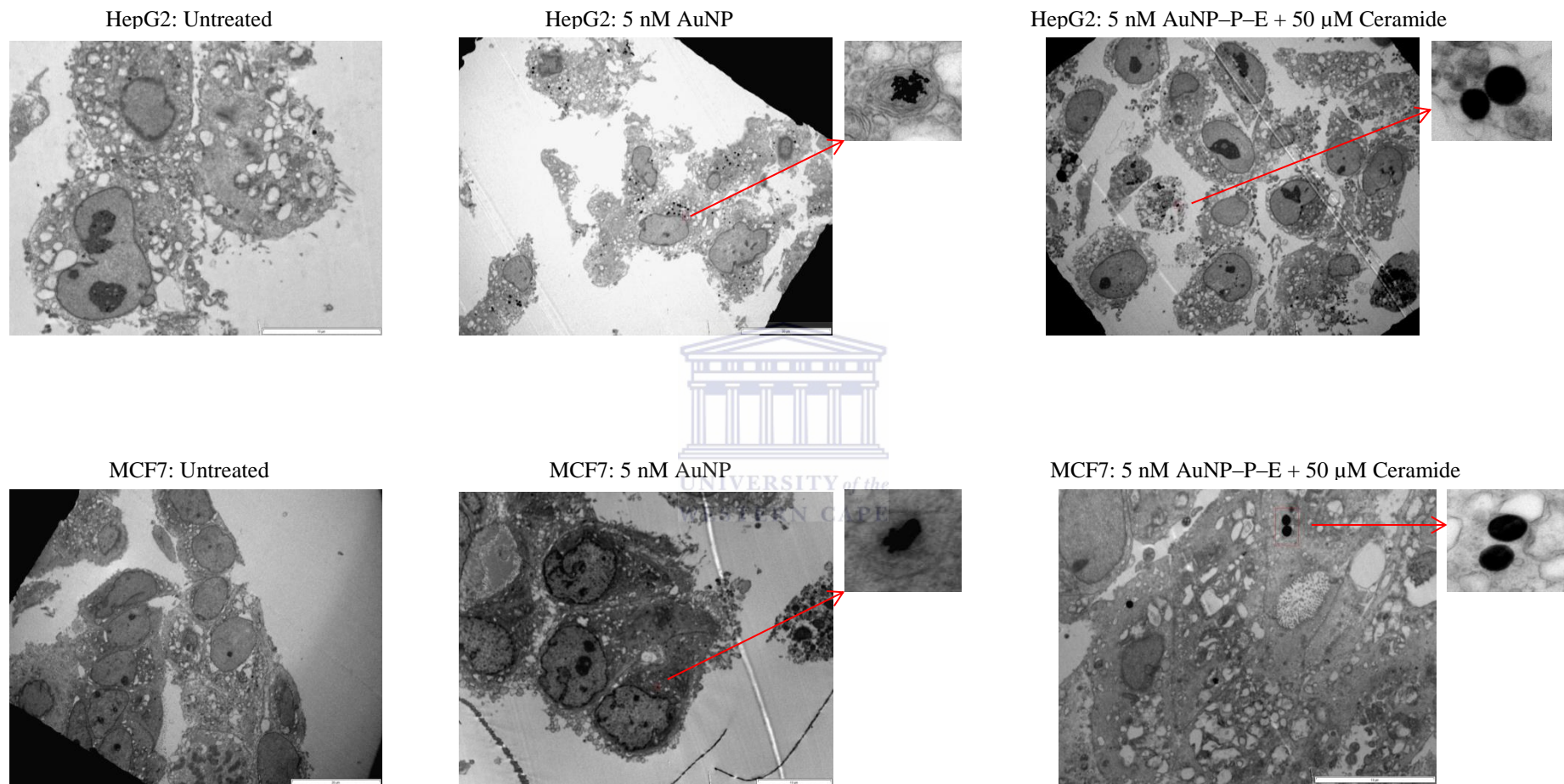


Figure 3.11: Evaluating the uptake of AuNP-E and AuNP-P-E in HepG2 and MCF7 cells. Post 24 hour treatment, cells were prepared for TEM analysis. Images of HepG2 and MCF7 untreated cells were captured where the bar was represented at 20 μ m. Images of cells treated with AuNPs were captured where the bar was represented at 10 μ m. The inserts were taken at 5 μ m to indicate the uptake of the AuNPs.

3.3. Cloning of XIAP into a His-tagged Expression Vector System

3.3.1. Introduction

To evaluate the binding of embelin, AuNP-E and AuNP-P-E to XIAP, it was necessary to express and purify recombinant XIAP protein. Therefore the objective of this section was to express and purify recombinant human XIAP protein using the pET28a expression vector.

3.3.2. The isolation of total RNA from MCF7 breast cancer cells

As shown in **Section 3.1.2 Figure 3.1** XIAP was over expressed in MCF7 breast cancer cells. MCF7 cells were cultured in 25 cm² flasks at 5% CO₂ and 37 °C until confluent (**Section 2.3**). Total RNA was isolated using Machery-Nagel's NucleoSpin® Tri Prep Kit (**Section 2.9**). The RNA was electrophoresed on a 1% agarose gel (**Figure 3.12**). Two major bands representing the two RNA subunits (i.e. 28 S and 18 S) were observed on **Figure 3.12**. Both the 28 S and 18 S subunits remained intact. A third band was present and less visible than the other bands. This band represents the 5 S subunit.

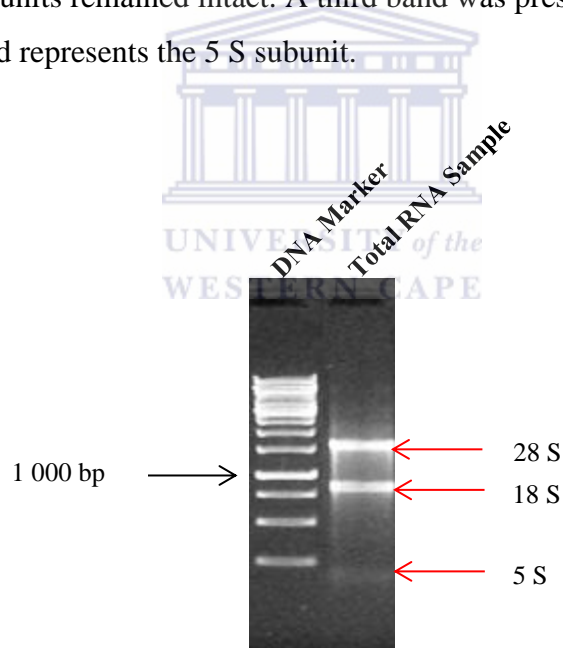


Figure 3.12: Total RNA isolated from MCF7 mammalian breast cancer cells. RNA was isolated using the NucleoSpin® TriPrep Kit. The first lane is the DNA marker and the second lane is the total RNA. The three red arrows on the right indicate RNA subunits (28 S, 18 S and 5 S) present in the total RNA sample.

3.3.3. PCR amplification of XIAP

The total RNA sample was used to synthesize cDNA using the First Strand cDNA Synthesis Kit for RT-PCR (AMV) as described in **Section 2.9**. The resulting cDNA was used to PCR

amplify XIAP's coding region (as described in **Section 2.12**) using XIAP specific primers as described in **Section 2.11**.

The PCR amplified product was electrophoresed on a 1% agarose gel (**Figure 3.13**) and the gel image was captured (**Section 2.9.1**). The PCR amplification indicates a PCR product for the XIAP gene at approximately the expected size of 1494 bp. The PCR amplified product was excised and gel purified (**Section 2.14**). The purified product was ligated into the pGEM-T Easy Vector System.

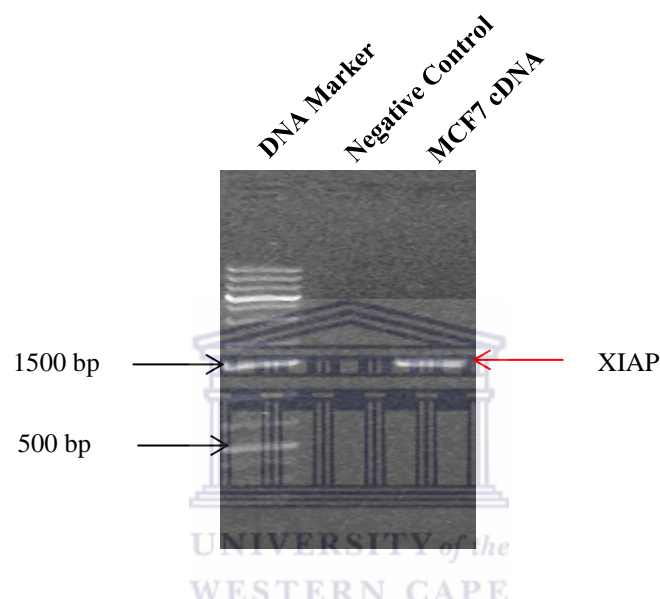


Figure 3.13: PCR amplification of XIAP with the use of gene specific primers. The first lane of the agarose gel shows the 1kb DNA marker, the second the negative control (no cDNA present) and the third lane the PCR product generated with MCF7 cDNA as the template.

3.3.4. Sub-cloning of XIAP into pGEM-T Easy Vector

The amplified XIAP PCR product purified using the NucleoSpin® Extract II PCR Clean-Up Gel Extraction Kit as described in **Section 2.14**. The purified DNA was used in a sub-cloning experiment ligating the XIAP PCR product into the pGEM-T Easy vector. The ratio of insert:vector used was 3:1 (**Table 2.5**) and the ligation reaction was used to transform *E. coli* competent cells as described in **Section 2.15.3**.

3.3.5. Colony PCR screening of XIAP positive clones

The resulting pGEM-XIAP transformed colonies were screened for the presence of XIAP by colony PCR using XIAP specific primers (**Section 2.15.4**). The PCR products were

electrophoresed on a 1% agarose gel (**Figure 3.14**) and the image was captured. The amplified products were at the expected size of 1494 bp for XIAP.

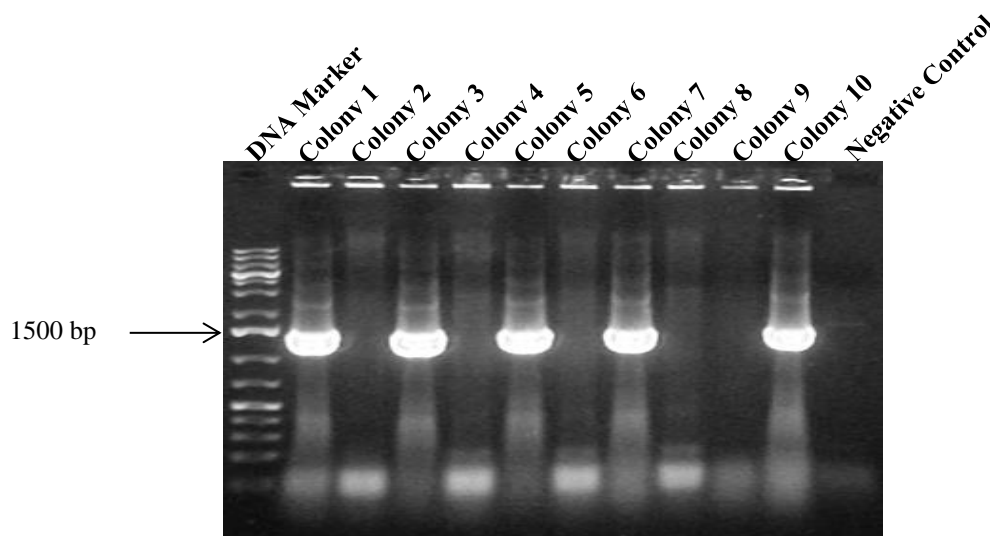


Figure 3.14: Colony PCR screening for XIAP positive clones. Ten clones (numbered 1 – 10) were screened. The last lane shows the negative control where no template DNA was added to the PCR reaction.

3.3.6. Sequence analysis of XIAP positive clones

Clones that were positive for XIAP were cultured LB–ampicillin and 20% v/v glycerol stocks were prepared (**Section 2.15.6**). These clones were used to streak LB–ampicillin agar plates. Agar plates that contained positive clones were sent to Inqaba Biotec for DNA sequencing analysis. Two clones per plate were selected and sequenced in the forward and reverse orientation with the use of M13 sequencing primers. The DNA sequences received from Inqaba Biotec were analysed using BLAST (Altschul *et al.*, 1990) analysis. The BLAST analysis (**Figure 3.15**) for the XAIP clone 3 showed a 99% identity when compared to the original XIAP sequence. From the sequencing data three single mutations were observed.

Homo sapiens X-linked inhibitor of apoptosis (XIAP), transcript variant 1, mRNA
 Sequence ID: [reflNM_001187.3](#) Length: 8460 Number of Matches: 1

Range 1: 160 to 1650		GenBank	Graphics	Next Match	Previous Match
Score	Expect	Identities	Gaps	Strand	
2737 bits(1482)	0.0	1488/1491(99%)	0/1491(0%)	Plus/Plus	
Query 1	ATGACTTTTAACAGTTTTGAAGGATCTAAAACCTTGTACCTGCAGACATCAATAAGGAA	60			
Sbjct 160	ATGACTTTTAACAGTTTTGAAGGATCTAAAACCTTGTACCTGCAGACATCAATAAGGAA	219			
Query 61	GAAGAATTTGTAGAAGAGTTTAAATAGATTA AAAA CTTTGTAAATTTTCCAGTGGTAGT	120			
Sbjct 220	GAAGAATTTGTAGAAGAGTTTAAATAGATTA AAAA CTTTGTAAATTTTCCAGTGGTAGT	279			
Query 121	CCTGTTTCAGCATCAACACTGGCACGAGCAGGGTTTTCTTTATACTGGTGAAGGAGATAAC	180			
Sbjct 280	CCTGTTTCAGCATCAACACTGGCACGAGCAGGGTTTTCTTTATACTGGTGAAGGAGATAAC	339			
Query 181	GTGCGGTGCTTTAGTTGTATGCAGCTGTAGATAGATGGCAATATGGAGACTCAGCAGTT	240			
Sbjct 340	GTGCGGTGCTTTAGTTGTATGCAGCTGTAGATAGATGGCAATATGGAGACTCAGCAGTT	399			
Query 241	GGAGACACAGGAAAGTATCCCAAAATGCGAGATTTATCAACGGCTTTTATCTTGAAAAT	300			
Sbjct 400	GGAGACACAGGAAAGTATCCCAAAATGCGAGATTTATCAACGGCTTTTATCTTGAAAAT	459			
Query 301	AGTCCACGCACTACAAATCTGGTATCCAGAATGGTCACTACAAAGTTGAAAACATAT	360			
Sbjct 460	AGTCCACGCACTACAAATCTGGTATCCAGAATGGTCACTACAAAGTTGAAAACATAT	519			
Query 361	CTGGGAAGCAGAGATCATTTTGCCTTAGACAGGCCATCTGAGACACATGCAGACTATCTT	420			
Sbjct 520	CTGGGAAGCAGAGATCATTTTGCCTTAGACAGGCCATCTGAGACACATGCAGACTATCTT	579			
Query 421	TTGAGAAGTGGGAGGTTGTAGATATATCAGACACCATATACCCGAGGAACCCCTGCCATG	480			
Sbjct 580	TTGAGAAGTGGGAGGTTGTAGATATATCAGACACCATATACCCGAGGAACCCCTGCCATG	639			
Query 481	TATAGTGAAGAGCTAGATTAAAGTCTTTTCAGAACTGGCCAGACTATGCTCACTAACC	540			
Sbjct 640	TATAGTGAAGAGCTAGATTAAAGTCTTTTCAGAACTGGCCAGACTATGCTCACTAACC	699			
Query 541	CCAAGAGAGTTAGCAAGTGTGGACTCTACTACACAGGTATTGGTGACCAAGTGCAGTGC	600			
Sbjct 700	CCAAGAGAGTTAGCAAGTGTGGACTCTACTACACAGGTATTGGTGACCAAGTGCAGTGC	759			
Query 601	TTTTGTTGGTGGAAAACGAAAAATGGGAACCTTGTGATCGTGCCTGGTCAGAACAC	660			
Sbjct 760	TTTTGTTGGTGGAAAACGAAAAATGGGAACCTTGTGATCGTGCCTGGTCAGAACAC	819			
Query 661	AGCGCACACTTTCCCTAATTCCTTTCTTTGTTTTGGGCGGGAATCTTAATATTCGAAGTGAA	720			
Sbjct 820	AGCGCACACTTTCCCTAATTCCTTTCTTTGTTTTGGGCGGGAATCTTAATATTCGAAGTGAA	879			
Query 721	TCGTGCTGTGAGTTCTGATAGGAATTTCCCAAAATTCACAAATCTTCCAGAAATCCA	780			
Sbjct 880	TCGTGCTGTGAGTTCTGATAGGAATTTCCCAAAATTCACAAATCTTCCAGAAATCCA	939			
Query 781	TCCATGGCAGATTATGAAGCAGGATCTTTACTTTTGGGACATGGTATACTCAGTTAAC	840			
Sbjct 940	TCCATGGCAGATTATGAAGCAGGATCTTTACTTTTGGGACATGGTATACTCAGTTAAC	999			
Query 841	AAGGAGCAGCTTGCAAGAGCTGGATTTTATGCTTTAGGTGAAGGTGATAAAGTAAAGTGC	900			
Sbjct 1000	AAGGAGCAGCTTGCAAGAGCTGGATTTTATGCTTTAGGTGAAGGTGATAAAGTAAAGTGC	1059			
Query 901	TTTCACTGTGGAGAGGGCTAAGTGAATGGTGGCCAGTGAAGACCCCTGGGAACAACAT	960			
Sbjct 1060	TTTCACTGTGGAGAGGGCTAAGTGAATGGTGGCCAGTGAAGACCCCTGGGAACAACAT	1119			
Query 961	GCTAAATGGTATCCAGGGTGCAAAATATCTGTTAGAACAGAAAGGGACAGAATATATAAAC	1020			
Sbjct 1120	GCTAAATGGTATCCAGGGTGCAAAATATCTGTTAGAACAGAAAGGGACAGAATATATAAAC	1179			
Query 1021	AATATTCATTTAACTCAATTCACCTTGAGGAGTGTCTGGTAAAGAACTACTGAGAAAACCCA	1080			
Sbjct 1180	AATATTCATTTAACTCAATTCACCTTGAGGAGTGTCTGGTAAAGAACTACTGAGAAAACCCA	1239			
Query 1081	TCCTAACTAGAAGAAITGATGATACCATCTTCCAAAATCCCTATGGTACAAGAGCTATA	1140			
Sbjct 1240	TCCTAACTAGAAGAAITGATGATACCATCTTCCAAAATCCCTATGGTACAAGAGCTATA	1299			
Query 1141	CGAATGGGTTCAAGGACATTAAGAAAATAATGGAGGAAAAAATTCAGATATCT	1200			
Sbjct 1300	CGAATGGGTTCAAGGACATTAAGAAAATAATGGAGGAAAAAATTCAGATATCT	1359			
Query 1201	GGGAGCAACTATAAATCACTTGAGGTTCTGGTTGCAGATCTAGTGAATGCTCAGAAAGAC	1260			
Sbjct 1360	GGGAGCAACTATAAATCACTTGAGGTTCTGGTTGCAGATCTAGTGAATGCTCAGAAAGAC	1419			
Query 1261	AGTATGCAAGATGAGTCAAGTCAAGTTCATTACAGAAAGAGATTAGTACTGAAGAGCAG	1320			
Sbjct 1420	AGTATGCAAGATGAGTCAAGTCAAGTTCATTACAGAAAGAGATTAGTACTGAAGAGCAG	1479			
Query 1321	CTAAGGCGCTGCAAGAGGAGAAGCTTTGCAAAATCTGTATGGATAGAAATATTGCTATC	1380			
Sbjct 1480	CTAAGGCGCTGCAAGAGGAGAAGCTTTGCAAAATCTGTATGGATAGAAATATTGCTATC	1539			
Query 1381	GTTTTTGTTCCTTGTGGACATCTAGTCACTTGTAAACAAATGTGCTGAAGCAGTTGACAAG	1440			
Sbjct 1540	GTTTTTGTTCCTTGTGGACATCTAGTCACTTGTAAACAAATGTGCTGAAGCAGTTGACAAG	1599			
Query 1441	TGTCCATGTGCTACACAGTCAATTAATTTCAAGCAAAAAATTTTATGTCT	1491			
Sbjct 1600	TGTCCATGTGCTACACAGTCAATTAATTTCAAGCAAAAAATTTTATGTCT	1650			

Figure 3.15: BLAST sequence analysis of a positive clone 3 for XIAP. The red boxes indicate the three mutations. The database utilized two query fields. The Query field indicates the DNA sequence of the clone of interest whereas the Subject field indicates the DNA sequence for the original XIAP gene to which the clone of interest was compared.

The DNA sequences received from Inqaba Biotec were translated into protein sequences using ExPASy (<http://www.expasy.org>). A pairwise sequence alignment of the original XIAP gene and pET28a–XIAP (**Figure 3.16**) was generated. Two mutations were observed in the translated sequence. Should the mutations have resulted in an amino acid change, the folding formation of XIAP may be affected.

1	MTFNSFEGSKTCVPADINKEEEFVEEFNRLKTIYVIFPSPGSPVSASTLARAGFLYTGEEDT	60 Query
1	MTFNSFEGSKTCVPADINKEEEFVEEFNRLKTIYVIFPSPGSPVSASTLARAGFLYTGEEDT	60 P98170
61	VRCFSCHAAVDRWQYGDSAVGRHRKVPSPNCRFINGFYLENSATQSTNSGIQNGQYKVENY	120 Query
61	VRCFSCHAAVDRWQYGDSAVGRHRKVPSPNCRFINGFYLENSATQSTNSGIQNGQYKVENY	120 P98170
121	LGSRDHFALDRPSETHADYLLRTGQVVDISDTIYPRNPAMYSEEARLKSFQNWPDYAHLT	180 Query
121	LGSRDHFALDRPSETHADYLLRTGQVVDISDTIYPRNPAMYSEEARLKSFQNWPDYAHLT	180 P98170
181	PRELASAGLYYTIGIGDQVQCFCCGGKLNWPCDRAWSEHRRHFPNCFVLRNLRNIRSE	240 Query
181	PRELASAGLYYTIGIGDQVQCFCCGGKLNWPCDRAWSEHRRHFPNCFVLRNLRNIRSE	240 P98170
241	SDAVSSDRNFPNSTNLPNPSMADYEARIFTFGTIVYISVNKEQLARAGFYALGEGDKVKC	300 Query
241	SDAVSSDRNFPNSTNLPNPSMADYEARIFTFGTIVYISVNKEQLARAGFYALGEGDKVKC	300 P98170
301	FHCGGGLTDWRPSEDPWEQHAKWYPGCKYLLEQKQGEYINNIHLTHSLEECLVRTEKTP	360 Query
301	FHCGGGLTDWKPSEDPWEQHAKWYPGCKYLLEQKQGEYINNIHLTHSLEECLVRTEKTP	360 P98170
361	SLTRRIDDTIFQNPMVQEAIRMGFSFKDIKKIMEEKIQISGSNYKSLEVLVADLVNAQKD	420 Query
361	SLTRRIDDTIFQNPMVQEAIRMGFSFKDIKKIMEEKIQISGSNYKSLEVLVADLVNAQKD	420 P98170
421	SMQDESSQTSLSQKEISTEEQLRRLQEEKLCCKICMDRNIAIVFVPCGHLVTCKQCAEAVDK	480 Query
421	SMQDESSQTSLSQKEISTEEQLRRLQEEKLCCKICMDRNIAIVFVPCGHLVTCKQCAEAVDK	480 P98170
481	CPMCYTVITFKQKIFMS	497 Query
481	CPMCYTVITFKQKIFMS	497 P98170

Figure 3.16: Pairwise protein sequence of the translated DNA sequence obtained for a positive XIAP clone and XIAP protein sequence. The translated sequences were compared to the protein sequence of human XIAP. The red boxes indicate mutations.

3.3.7. XIAP release from pGEM–XIAP by restriction digestion

In order for the ligation of the XIAP fragment into pET28a (**Section 2.16**), pGEM–XIAP plasmid DNA was digested with restriction enzymes (*XhoI* and *NdeI*) to release the XIAP insert (**Section 2.15.7**).

Clone 3 of pGEM–XIAP was selected for sequencing. The sequences were analysed prior to plasmid DNA preparation using Promega’s Wizard® *Plus* SV Miniprep DNA Purification

System (Section 2.15.6). The digested DNA was electrophoresed on a 1% agarose gel and the image was captured using the Kodak Digital Science 1D System (Figure 3.17).

The undigested plasmid (Figure 3.17, lane 2) indicates three bands which represents the three forms of plasmid namely the supercoiled, nicked and linear. The digested plasmid (Figure 3.17, lane 3) was achieved using restriction enzymes *XhoI* and *NdeI*. Three bands can be visualized where the first band indicates linearized vector, the second band indicates the digested vector and the third band indicates the XIAP insert which was released successfully.

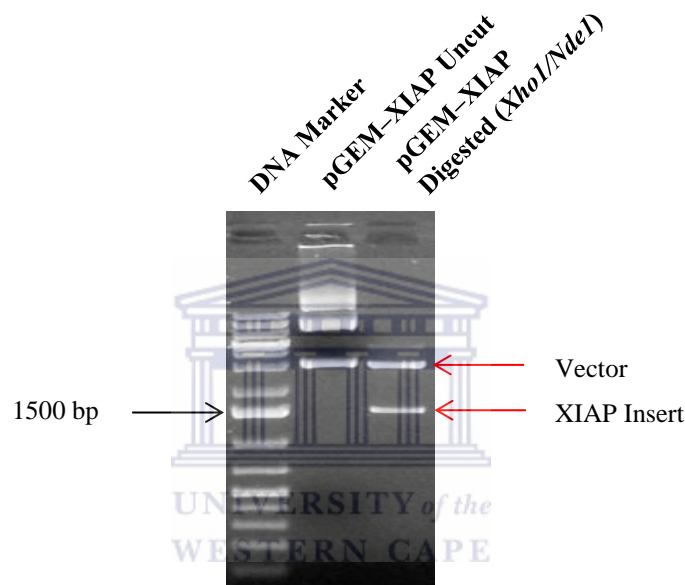


Figure 3.17: Restriction digestion of pGEM-XIAP. Plasmid DNA was digested with *XhoI* and *NdeI*. The first lane of the agarose gel shows the DNA marker, the second the undigested pGEM-XIAP plasmid DNA and the third lane the pGEM-XIAP plasmid DNA. Indicated by the arrows are the pGEM-T Easy vector and the XIAP insert.

3.3.8 Preparation of the pET28a expression vector for DNA ligation

For ligation of the XIAP fragment into pET28a expression vector (Section 2.16.3), both the pGEM-XIAP and pET28a vector were digested with restriction enzymes *XhoI* and *NdeI* as described in Section 2.16.2. As pGEM-XIAP was digested and resulted in successful release of XIAP the pET28a vector was digested with enzymes *XhoI* and *NdeI* (Section 2.16.2). The digested pET28a vector was electrophoresed on a 1% agarose gel and the image was captured using the Kodak Digital Science 1D System (Section 2.9.1). The undigested plasmid (Figure 3.17, lane 2) indicates three bands which represents the three forms of plasmid namely the

supercoiled, nicked and linear. The digested pET28a vector produced a single band representing an intact and linear plasmid.

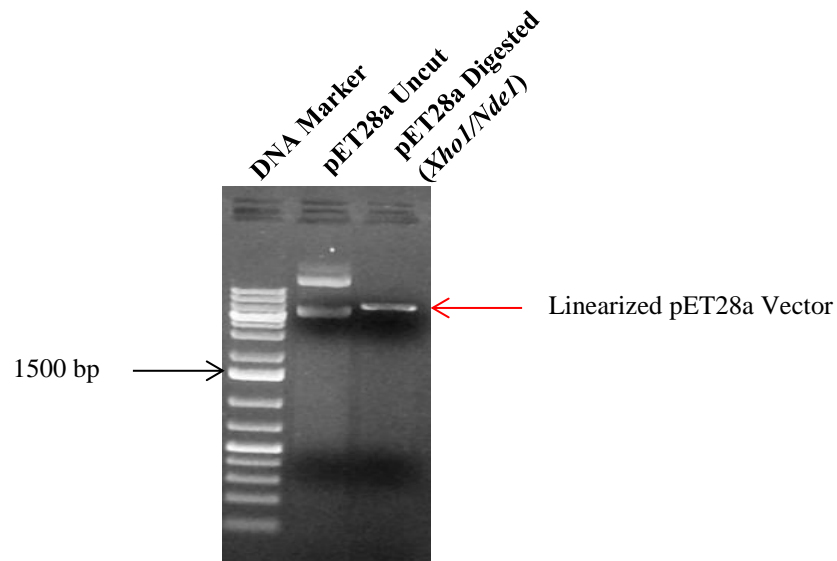


Figure 3.18: Restriction digestion of the pET28a expression vector. The first lane of the agarose gel shows the DNA marker, the second the uncut pET28a vector and the third lane the pET28a vector digested with *XhoI* and *NdeI*. Indicated by the arrow is the linearized pET28a vector.

The linearized pET28a vector was gel purified as described in **Section 2.14**. XIAP from pGEM–XIAP was ligated into the linearized pET28a Expression Vector. The ratio of insert:vector used was 3:1 (**Table 2.6**) and the ligation reaction was used to transform *E. coli* competent cells (**Section 2.16.4**).

3.3.9 Screening of XIAP positive clones by colony PCR

The resulting transformed colonies were screened for the presence of XIAP by colony PCR (**Figure 3.19**). Gene specific primers were used to detect the presence of the insert (**Section 2.11**). The PCR products were electrophoresed on a 1% agarose gel and the image was captured using the Kodak Digital Science 1D System (**Section 2.9.1**). The amplified products were at the expected size of 1494 bp for XIAP.

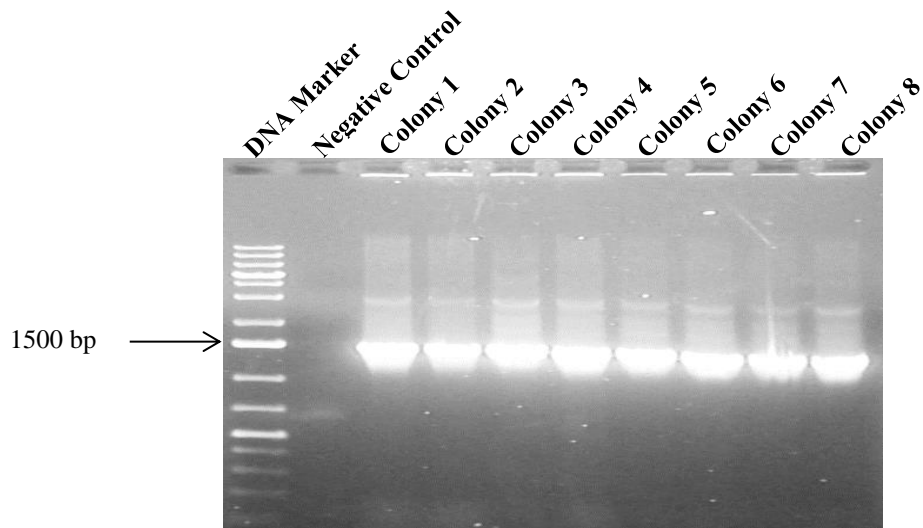


Figure 3.19: Colony PCR screen for XIAP positive clones. Ten clones (numbered 1 – 10) were screened. The second lane shows the negative control where water was used as the template in the PCR reaction.

3.4. Affinity purification of recombinant His–XIAP

3.4.1. Introduction

Upon successful ligation of XIAP into the linearized pET28a vector, the objective of this section was to express XIAP in *E. coli* and purify the protein using the Ni–NTA His–Bind® Resin since the protein will be expressed as a His–tagged fusion protein.

3.4.2. Screening for the expression XIAP

The colony PCR amplification results in **Figure 3.19** indicated the presence of XIAP in all the clones selected. From this data, clone 4 was selected to screen for XIAP as described in **Section 2.15.6**.

XIAP has a size of approximately 57 kDa. Therefore, His–XIAP was expected to be visualized at approximately 63 kDa. Also, it was expected to distinguish XIAP expression between the uninduced and induced samples. According to **Figure 3.20** XIAP expression levels were similar with the exception of clone 3. Addition of IPTG resulted in an increased expression of XIAP when compared to the uninduced sample.

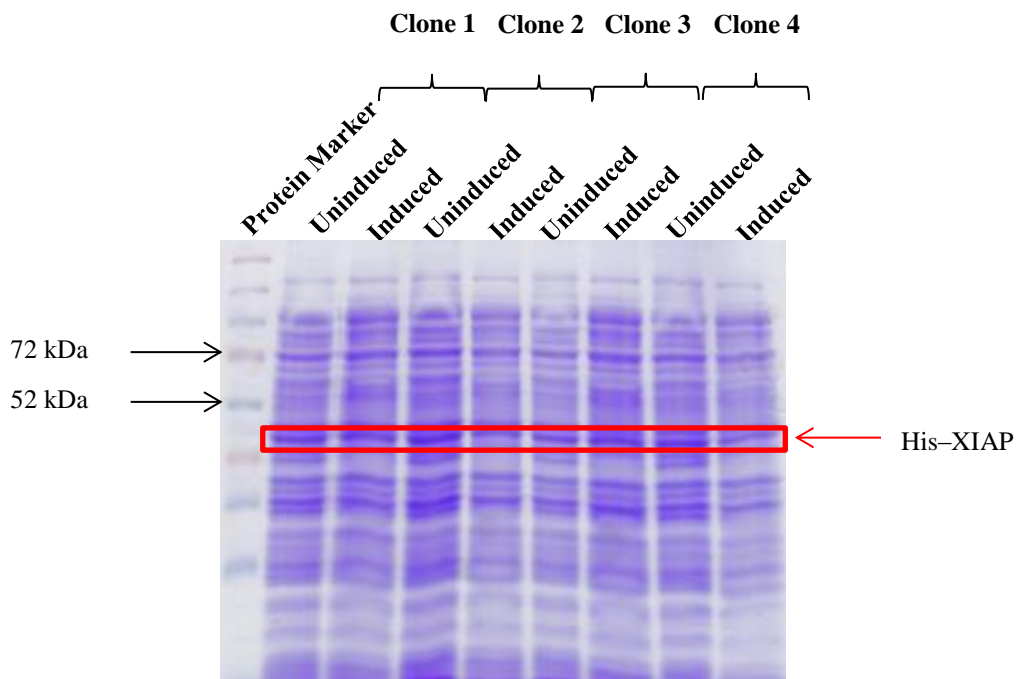


Figure 3.20: Expression screen for His-XIAP protein. Four colonies (numbered clone 1 – 4) were selected. Induction was achieved with 1 mM IPTG.

3.4.3. Purification of His-XIAP recombinant protein using the Ni-NTA His-Bind® Resin

From the expression screen, clone 3 was selected for recombinant purification of His-XIAP (Figure 3.21) with the aid of Novagen's Ni-NTA His-Bind® Resin supplied by Merck (Section 2.18.1).

When comparing the concentration of protein present in the lysate sample to the eluted samples, it was observed that very little protein was eluted. Purification of the XIAP-His protein was attempted using the HIS-Select® Nickel Affinity Gel to purify more of the recombinant His-XIAP protein and at increased efficiency when using the Novagen's Ni-NTA His-Bind® Resin. This purification experiment was unsuccessful as protein was present in the lysate sample but absent in the eluted samples (data not shown).

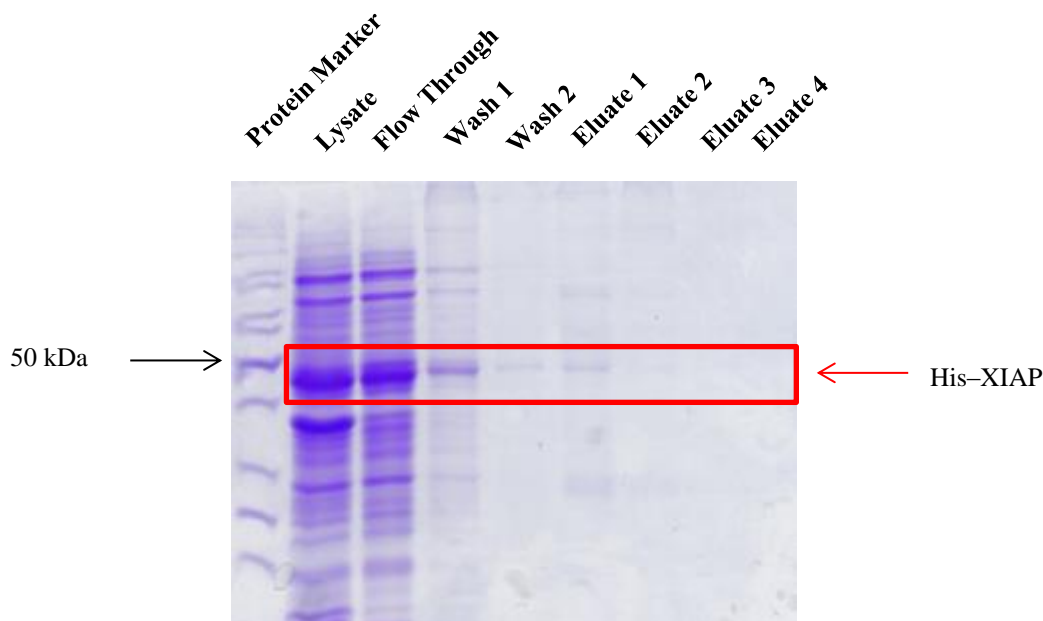


Figure 3.21: Purification of the His-XIAP protein using Ni-NTA His-Bind® Resin.

Lane 1 shows the protein marker, lane 2 shows the lysate, lane 3 shows the flow through, lanes 4 and 5 the two washes and lanes 6 to 10 the eluted His-XIAP protein.

3.5. Affinity purification for recombinant GST-XIAP

3.5.1. Introduction

The objective of this section was to express and purify the recombinant XIAP protein. Recombinant XIAP was required to evaluate its binding to (i) embelin post conjugation of embelin to gold nanoparticles and (ii) biconjugation of embelin and specific cancer targeting peptide to gold nanoparticles. Expression and purification of recombinant XIAP was carried out as described in **Section.17**. As purification of His-XIAP was unsuccessful, the pGEX-XIAP construct was purchased from Addgene. The purchased construct was used for expression and purification of GST-XIAP protein as described in **Section 2.19**.

3.5.2 Expression screen of GST-XIAP

Upon receiving the construct, the step involved screening for XIAP. This was achieved as described in **Sections 2.19.1** up to and including **Section 2.19.3**. Suspected positive clones were selected to screen for the presence of GST-XIAP (**Figure 3.22**).

XIAP has a size of approximately 57 kDa. Therefore, GST-XIAP was expected to be visualized at approximately 83 kDa. It was expected to distinguish XIAP expression between

the uninduced and induced samples. According to **Figure 3.22** XIAP expression levels were higher in the induced samples when compared to the uninduced samples. Expression was increased due to the addition of 0.2 mM IPTG. Of the 4 clones selected, clone 3's induced sample showed a higher level of XIAP expression.

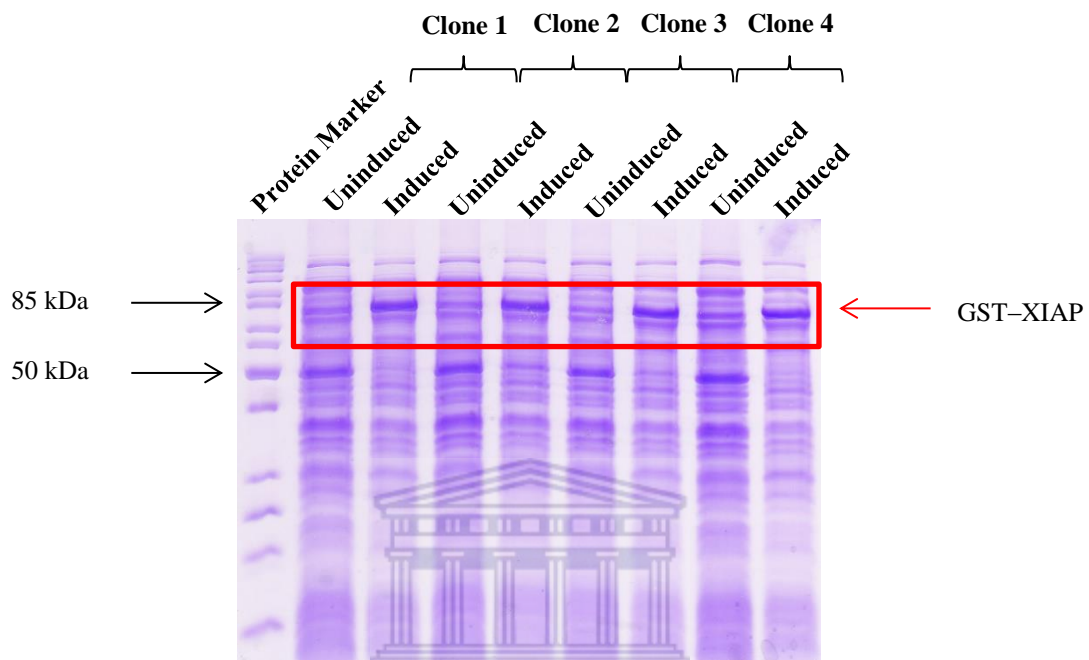


Figure 3.22: Expression screen for GST-XIAP protein. Four colonies (numbered colony 1 – 4) were selected. Induced samples were clearly distinguished from uninduced samples. Induction was achieved with 0.2 mM IPTG.

3.5.3. Sequence analysis of GST-XIAP

From the expression screen (**Figure 3.22**) clone 3 was selected for large scale purification after sequence analysis. Glycerol stocks were used to streak LB-ampicillin agar plates which were sent to Inqaba Biotec for sequencing. Sequence analysis was carried out as described in **Section 3.3.6**. However, pGEX specific sequencing primers were used. A pairwise sequence alignment of the translated DNA sequence for XIAP (**Figure 3.23**) was generated.

Sequencing data obtained from Inqaba Biotec was translated into protein sequences using ExPASy. A pairwise sequence alignment was generated of the original XIAP gene and GST-XIAP. From **Figure 3.23** no mutations were observed in the translated sequences.

1	MTFNSFEGSKTCVPADINKEEEFVEEFNRLKTFANFPGSGSPVSASTLARAGFLYTGEEDT	60	Query
1	MTFNSFEGSKTCVPADINKEEEFVEEFNRLKTFANFPGSGSPVSASTLARAGFLYTGEEDT	60	P98170
61	VRCFSCHAAVDRWQYGDSAVGRHRKVPNCRFINGFYLENSATQSTNSGIQNGQYKVENY	120	Query
61	VRCFSCHAAVDRWQYGDSAVGRHRKVPNCRFINGFYLENSATQSTNSGIQNGQYKVENY	120	P98170
121	LGSRDHFALDRPSETHADYLLRTGQVVDISDTIYPRNPAMYSEEARLKSFQNWPDYAHLT	180	Query
121	LGSRDHFALDRPSETHADYLLRTGQVVDISDTIYPRNPAMYSEEARLKSFQNWPDYAHLT	180	P98170
181	PRELASAGLYYTIGIGDQVQCFCGCKLKNWPCDRAWSEHRRHFPNCFVLRNLNIRSE	240	Query
181	PRELASAGLYYTIGIGDQVQCFCGCKLKNWPCDRAWSEHRRHFPNCFVLRNLNIRSE	240	P98170
241	SDAVSSDRNFPNSTNLPNPSMADYEARI FT FGTWIYSVNKEQLARAGFYALGEGDKVKC	300	Query
241	SDAVSSDRNFPNSTNLPNPSMADYEARI FT FGTWIYSVNKEQLARAGFYALGEGDKVKC	300	P98170
301	FHCGGGLTDWKPSEDPWEQHAKWYPGCKYLLEQKQGEYINNIHLTHSLEECLVRTTEKTP	360	Query
301	FHCGGGLTDWKPSEDPWEQHAKWYPGCKYLLEQKQGEYINNIHLTHSLEECLVRTTEKTP	360	P98170
361	SLTRRIDDTIFQNPMVQEAIRMGFSFKDIKKIMEEKIQISGSNYKSLEVLVADLVNAQKD	420	Query
361	SLTRRIDDTIFQNPMVQEAIRMGFSFKDIKKIMEEKIQISGSNYKSLEVLVADLVNAQKD	420	P98170
421	SMPDESSQTSLQKEISTEEQLRRLQEEKLCIKMDRNIIVFVPCGHLVTCKQCAEAVDK	480	Query
421	SMQDESSQTSLQKEISTEEQLRRLQEEKLCIKMDRNIIVFVPCGHLVTCKQCAEAVDK	480	P98170
481	CPMCYTVITFKQKIFMS	497	Query
481	CPMCYTVITFKQKIFMS	497	P98170

Figure 3.23: Pairwise protein sequence of the translated DNA sequence for a positive clone of XIAP from the pGEX-4T-2 vector. The translated sequences were compared to the protein sequence of human XIAP.

3.5.4 Purification of GST-XIAP using BugBuster® GST-Bind Purification kit

From the expression screening (**Figure 3.22**), clone 3 was selected for sequencing. Post sequence analysis, cell extraction preparation and purification of GST-XIAP (**Section 2.19.4**) was carried out using Novagen's BugBuster® GST-Bind Purification Kit supplied by Merck (**Figure 3.24**).

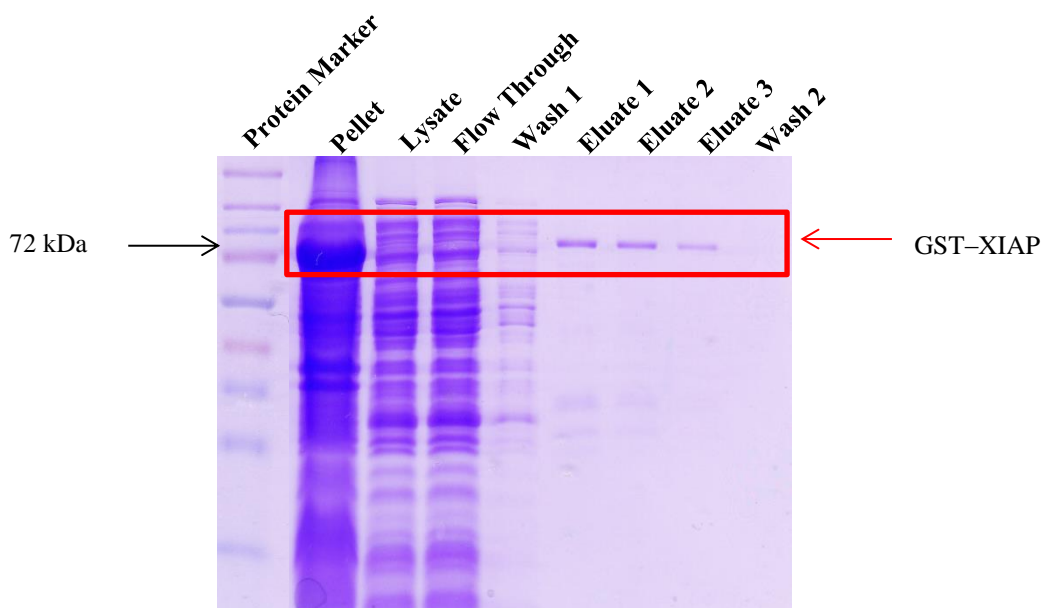


Figure 3.24: Purification of the GST–XIAP protein using the BugBuster® GST–Bind Purification kit. Lane 1 shows the protein marker, lane 2 shows the pellet, lane 3 shows the lysate, lane 4 shows the flow through, lane 5 shows the first wash sample, lanes 6 to 8 shows the eluted GST–XIAP protein and lane 9 shows the second wash sample.

3.6. Evaluating the interaction between the recombinant GST–XIAP protein and embelin and embelin conjugated nanoparticles by Isothermal Titration Calorimetry (ITC)

3.6.1. Introduction

Binding affinities and stoichiometries between proteins and nanoparticles are highly relevant in understanding protein–nanoparticle interactions and their biological consequences. The rate at which the respective protein binds to or dissociates from the nanoparticle, determines the interaction with receptors and hence its biological effects (Cerdervall *et al.*, 2007). The objective of this section is to evaluate the thermodynamics of recombinant GST–XIAP and embelin–conjugated gold nanoparticles using Isothermal Titration Calorimetry (ITC).

3.6.2. ITC analysis

The binding interaction between the recombinant GST–XIAP protein and embelin was evaluated by ITC using the MicroCal™ iTC₂₀₀ System and analysed using Origin® scientific

plotting software. As a negative control, a binding experiment was carried out between calcium and EDTA.

The control experiment consisted of calorimetric titration of 0.5 μM calcium with 5 μM EDTA. The experiment consisted of 18 injections of EDTA into the cell already filled with calcium. The injections were made over a period of 120 minutes. For each injection of EDTA into the cell containing calcium, Origin® takes a record and presents it graphically as shown in Figure 3.23 (a). Here each peak is a representation of an injection. The data is represented as μcal per second versus time in minutes.

Figure 3.25 shows the raw calorimetric data obtained per injection of 5 μM EDTA into the calorimetric cell containing 0.5 μM calcium. A total of 18 injections of EDTA were injected into the calcium over a period of 60 minutes. The number of injections corresponded to reference points which served the foundation for the construction of the sigmoidal curve (**Figure 3.26**) which was used to obtain the thermodynamics as a result of the binding interactions between EDTA and calcium.

In the experimental setup attempting to study the interaction between embelin and GST–XIAP, 200 nM embelin was injected into the unit cell containing 6 nM recombinant GST–XIAP protein. The injections were recorded and are represented graphically as shown in Figure 3.24. When comparing **Figure 3.24 (a)** to **Figure 3.25**, it was observed that the raw calorimetric data of **Figure 3.24 (a)** differed to that of **Figure 3.24** in that the peaks representing heat interaction was present in **Figure 3.24 (a)** but absent in **Figure 3.25**. The raw calorimetric data from Figure 3.24 was insufficient to construct a titration plot. Hence, it was unable to calculate the binding constant, the heat change or entropy change.

Figure 3.27 shows the raw calorimetric data obtained per injection of 200 nM embelin into the calorimetric cell containing 6 nM fused GST–XIAP recombinant protein. When comparing **Figure 3.27** to **Figure 3.25**, there are no similarities to the data generated. **Figure 3.27** generated no reference points for the construction of the sigmoidal curve. Hence, it was unable to obtain the thermodynamics of the binding, if there existed, between embelin and the fused GST–XIAP recombinant protein.

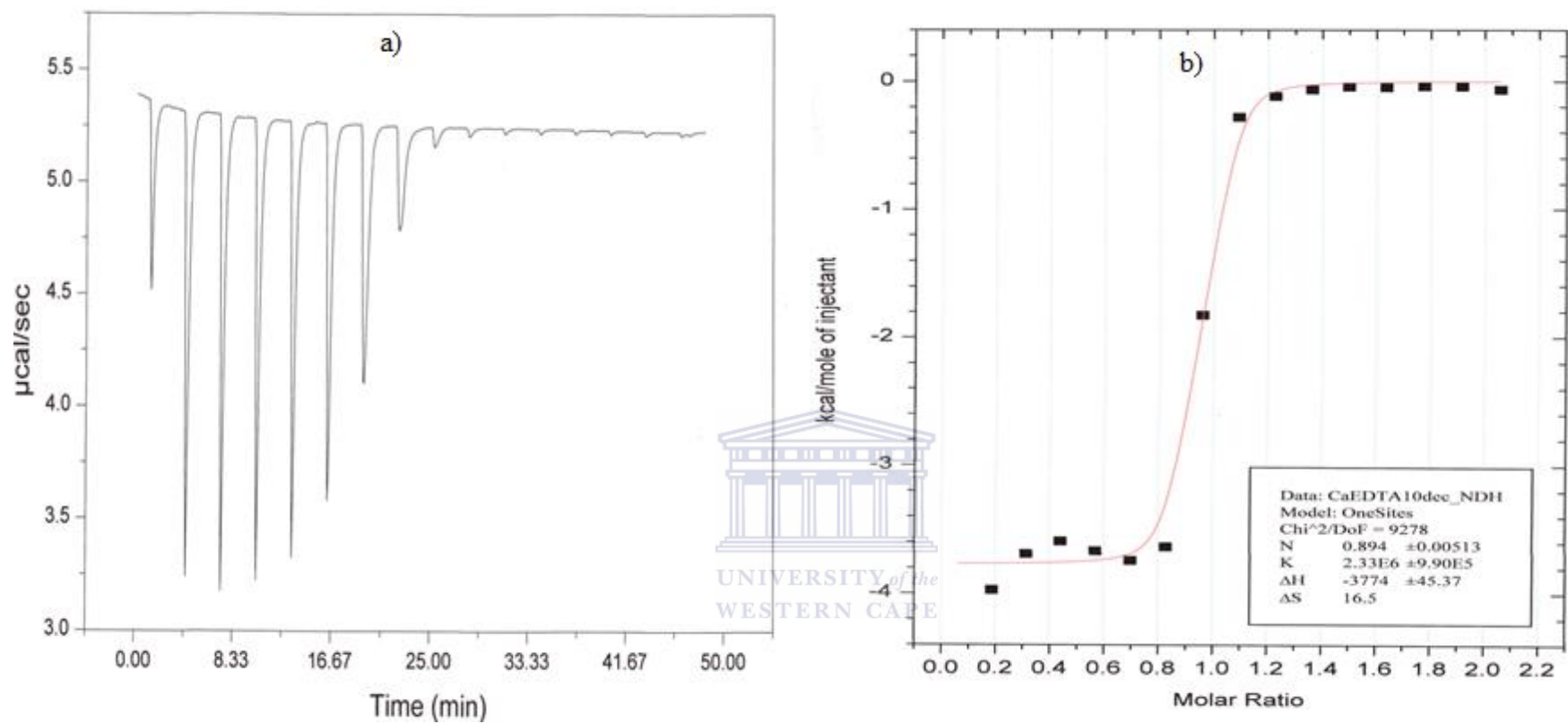


Figure 3.25: ITC titration data describing the interaction of EDTA with calcium. Panel (a) shows the raw calorimetric data obtained during the injection of 5 μM EDTA into the calorimetric cell containing 0.5 μM calcium. Panel (b) shows the titration plot from the integrated raw data of the curve in panel (a). The solid line represents the squares which best fits the data.

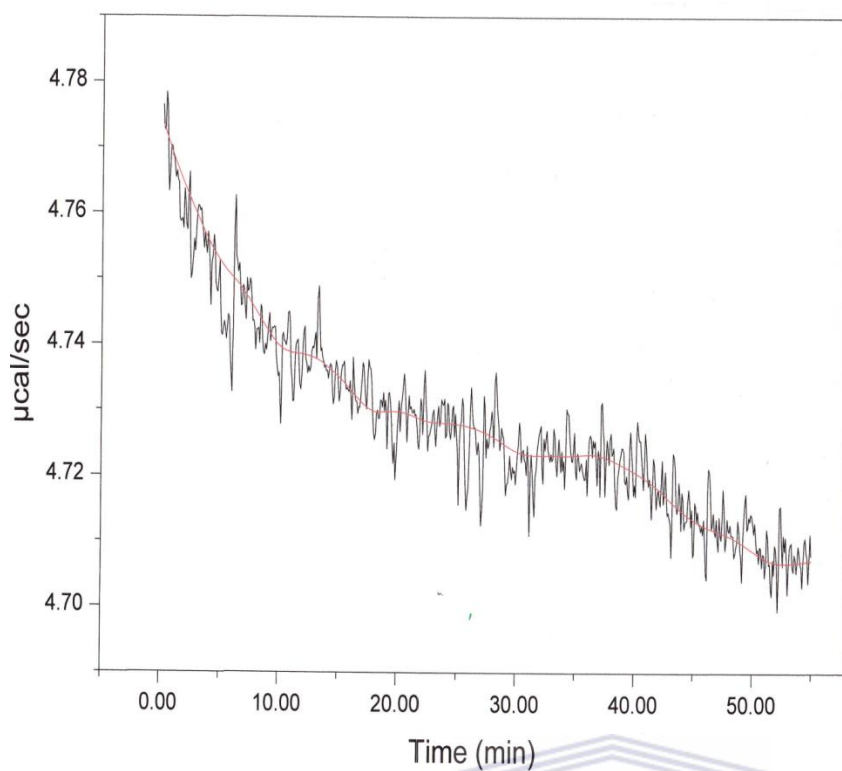


Figure 3.26: ITC titration data describing the interaction of recombinant GST–XIAP protein and embelin. This indicates the raw calorimetric data obtained during the injection of 200 nM embelin into the calorimetric cell containing 6 nM recombinant GST–XIAP protein. Both the GST–XIAP protein and embelin were prepared in 5 mM sodium phosphate, buffer at pH 7.4, containing 0.15% DMSO.

WESTERN CAPE

CHAPTER 4:DISCUSSION

- 4.1. Synthesis and characterization of gold nanoparticles
- 4.2. The expression levels of XIAP in human cancer cell lines
- 4.3. The cytotoxic effects of AuNP-E and AuNP-P-E
- 4.4. Evaluating cellular uptake of AuNPs
- 4.5. Expression and purification of recombinant XIAP protein
- 4.6. Protein-Protein interactions
 - 4.6.1 Isothermal Titration Calorimetry
 - 4.6.2 Applications of ITC to study the Protein-Nanoparticle interactions
- 4.7. Investigating the binding between the recombinant GST-XIAP and embelin
- 4.8. Conclusion
- 4.9. Future Directions



CHAPTER 4:DISCUSSION

XIAP is considered to be the most potent and versatile caspase inhibitor within the IAP family (Hui *et al.*, 2010). XIAP blocks the induction of apoptosis by inhibiting initiator caspase 9 (Nikolovska–Coleska *et al.*, 2004) and effector caspases 3 and 7 (Deveraux *et al.*, 1997; Mufti *et al.*, 2007).

Nikolovska–Coleska and colleagues over–expressed XIAP in Jurkat cells by transfecting these cells with a plasmid encoding the human XIAP gene. Jurkat cells that stably over–express XIAP became resistant to apoptosis induced by etoposide when compared to untransfected Jurkat cells. Treatment with 2.5 μM etoposide for 72 hours resulted in 94.3% cell death in untransfected cells whereas only 59% of the transfected cells died. When increasing the concentration of etoposide to 10 μM , 85% of the transfected cells were killed. These results demonstrated that XIAP over–expression protected the Jurkat cells from etoposide–induced apoptosis and cytotoxicity (Nikolovska–Coleska *et al.*, 2004²). It can therefore be concluded the the over–expression of XIAP in cancer cells contributes to the resistance of these cells to apoptosis, which is a characteristic of cancer cells.

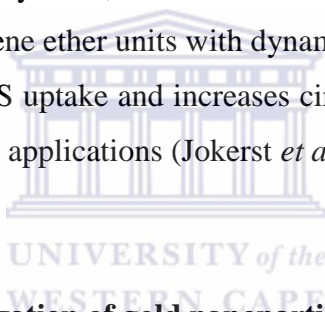
Hui and colleagues therefore considered XIAP as one of the leading targets for anti–cancer drug development (Hui *et al.*, 2010), since the successful inhibition of XIAP can promote the destruction of cancer cells through anti–cancer drug induced apoptosis.

Embelin is a potent, non–peptidic, cell permeable small molecule inhibitor of XIAP. It has been shown to possess both anti–tumour and anti–inflammatory properties (Joshi *et al.*, 2007; Siegelin *et al.*, 2009). Embelin inhibits XIAP by binding to its BIR3 domain (Nikolovska–Coleska *et al.*, 2004¹; Nikolovska–Coleska *et al.*, 2004²). Embelin consist of a quinone and hydroquinone groups on the same ring. It also has a long alkyl side chain which confers solubility in non–polar phase (Joshi *et al.*, 2009).

Although drugs such as embelin and their derivatives are promising anti–cancer agents, a major obstacle in the treatment of cancer is the non–specific delivery of such anti–cancer drugs. Therefore this study aimed at investigating the application of gold nanoparticles (AuNPs) for the targeted delivery of embelin to cancer cells. The main advantage of targeted drug delivery is to improve the therapeutic efficacy of the anti–cancer drug. Other advantages include the lowering of the required dose of the anti–cancer drug whilst reducing side effects (Papasanani *et al.*, 2012).

Cancer targeting peptides have been shown to specifically bind to cancer cells. The cancer targeting peptide consisting of the following 7 amino acids LTVSPWY was previously identified and shown to exhibit preferential binding to and internalization into breast cancer cells (Shadidi and Sioud, 2003²). The aim was to use this peptide to target the delivery of embelin into the cells using AuNPs as a drug carrier. To achieve this AuNPs were biconjugated with embelin and the cancer targeting peptide.

When using nanoparticles for drug delivery, there are several challenges that can obstruct nanoparticles from reaching their target. For example the uptake of nanoparticles by the reticuloendothelial system (RES) results in nanoparticles shuttled out of circulation to the liver, spleen or bone marrow as well as nonspecific binding of nanoparticles to non-targeted or non-diseased areas. Concerns about the toxicity of nanoparticles often arise due to nanoparticle accumulation in the RES. Therefore, the addition of PEG to the nanoparticle surface, a process known as PEGylation, can reduce many of these challenges. PEG is a coiled polymer of repeating ethylene ether units with dynamic conformations. The addition of PEG to nanoparticles reduces RES uptake and increases circulation time of the nanoparticles in both drug delivery and imaging applications (Jokerst *et al.*, 2011).



4.1. Synthesis and characterization of gold nanoparticles

The advantages of using nanoparticles as delivery vehicles include their high stability, high drug loading capacity, the feasibility of incorporating both hydrophobic and hydrophilic substances as well as the feasibility of using various administration routes to deliver the nanoparticles (Gelperina *et al.*, 2005).

Gold compounds have been used in medicine throughout history. The advantages of using AuNPs in Nanotechnology include the easy, simple, cheap, safe and reliable synthesis methods (Patra *et al.*, 2010).

According to Abdelhain and colleagues the most widely used method for characterizing optical properties and electronic structure of nanoparticles is by UV-visible absorption spectroscopy where the absorption bands are related to the width of the nanoparticles (Abdelhain *et al.*, 2012). UV-vis data were provided for both the AuNP-E and AuNP-P-E as represented in Figure 3.5 (a) and Figure 3.5 (b), respectively.

AuNP-E and AuNP-P-E were also characterized by Transmission Electron Microscopy (TEM). Figure 3.6 (a) shows the TEM image of the AuNP-E and Figure 3.6 (b) shows the TEM image of AuNP-P-E. The TEM images show that the conjugated nanoparticles had a spherical shape and were uniformly distributed. The initial size of the nanoparticles were 14 nm. Theoretically, little to no change in nanoparticle size should be observed upon conjugation. It must be noted that no experiments were conducted to determine the size of the nanoparticles post conjugation.

4.2. The expression levels of XIAP in human cancer cell lines

In this study the expression levels of XIAP was investigated in 6 human cancer cell lines (A5495, H157, HepG2, HeLa, HT29 and MCF7). Tamm and colleagues investigated the expression of the IAP family of anti-apoptotic genes (cIAP1, cIAP2 and XIAP) within the NCI panel of 60 human tumour cell lines. They compared expression of cIAP1, cIAP2 and XIAP at mRNA and protein levels. It was observed that mRNA levels of cIAP1, cIAP2 and XIAP did not correlate to the respective protein levels. It was also observed that cIAP1 and XIAP were expressed in most of the human cancer cell lines analysed (Tamm *et al.*, 2000). Using Western blot analysis, Tamm and colleagues observed higher XIAP levels in renal cancer and melanoma cell lines, whereas low XIAP levels typically present in the Central Nervous Systems (CNS) tumour cell lines.

From Figure 3.2 and Figure 3.3 it can be concluded that the expression levels of XIAP were significantly higher in H157 and MCF7 cells when compared to A5495, HepG2, HeLa and HT29 cells. It was observed that XIAP expression for HT29 resulted in shared consensus between the data generated in this study and that reported by Tamm and colleagues. However it was observed that XIAP expression in MCF7 cells was not in agreement with the findings of Tamm and colleagues which reported low expression of XIAP in MCF7 cells, whereas this study found high expression of XIAP in these cells. Based on the results in Figure 3.2 MCF7 and HepG2 cells were used as models of cell lines that expressed high and low levels of XIAP, respectively.

4.3. The cytotoxic effects of AuNP-E and AuNP-P-E

The effects of ceramide, embelin, AuNP, AuNP-E and AuNP-P-E were investigated in MCF7 breast and HepG2 liver cancer cells. Figure 3.7 and Figure 3.8 shows the morphological effects, of the various treatments, for HepG2 and MCF7 cancer cells, respectively. Apoptosis was investigated for both HepG2 and MCF7 cancer cells (Figure 3.9). Treatments with embelin, AuNP, AuNP-E and AuNP-P-E did not have any effect on the cell morphology as the morphology of these cells resembled that of the untreated cells. This suggests that embelin, AuNP, AuNP-E and AuNP-P-E did not have any observable effect on MCF7 and HepG2 cell morphology at the concentrations tested. According to the statistical analysis, the data obtained for AuNP-E and AuNP-P-E are similar to the data obtained for the untreated cells. This was observed for both the MCF7 and HepG2 cells. Therefore, the data obtained were statistically significant.

Ceramide induced morphological changes (cell shrinkage, cell rounding and cell detachment), which were indicative of apoptosis. Co-treatment of cells with ceramide and embelin, ceramide and AuNP-E, or ceramide AuNP-P-E enhanced the effect of ceramide on the morphology of the cells since an increased number of cells were affected by these co-treatments. This is more evident in HepG2 cells co-treated with ceramide and AuNP-E which show that a high number of cells detached from the surface of the culture plate.

Stock solutions of embelin and ceramide were prepared in DMSO. Even though a vehicle control was not included in the cell culture experiments, the concentration of DMSO post treatment was below 0.15 % (v/v). This concentration was proved to be non-toxic to the cells by Dr. Meyer (data not shown). Therefore, it may be concluded that the morphological changes observed in the treatments consisting of ceramide was as a result of the effects of ceramide.

Based on Figure 3.9 approximately 60% of MCF7 and HepG2 cells treated with 50 μ M ceramide stained positive for apoptosis. Treatments with embelin, AuNP, and AuNP-E did not induce apoptosis in HepG2 cells. However, MCF7 cells treated with AuNP were more susceptible to the effects of AuNP, with approximately 30% of the cells being positive for apoptosis. MCF7 and HepG2 cells co-treated with ceramide and AuNP-P-E did not enhance the effect of ceramide on the cells. However, co-treatment with ceramide and AuNP-E enhanced the effect of ceramide in HepG2 cells. The percentage apoptotic cells increased from 50% (single ceramide treatment) to 90% (co-treatment with ceramide and AuNP-E).

This increased cell death in response to co-treatment with ceramide and AuNP-E was not observed in MCF7 cells.

4.4. Evaluating cellular uptake of AuNPs

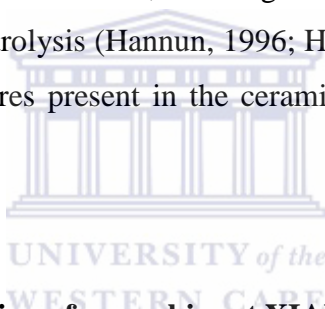
ICP-OES was also used to determine the percentage of gold present in the cells treated with AuNP-E and AuNP-P-E. Based on Figure 3.10 (a) the concentration of gold in both MCF7 breast and HepG2 liver cancer cells were significantly higher in cells treated with AuNP-P-E (~0.25 µg/ml) compared to cells treated with AuNP-E (~0.01 µg/ml). This demonstrates that gold nanoparticles conjugated with the cancer targeting peptide is taken up more efficiently by the cells compared to gold nanoparticles without the cancer targeting peptide. MCF7 cells have taken up more gold than HepG2 cells, which may be due to the fact that these cells express higher levels of the targeting molecule for the peptide.

Based on the ICP-OES results, AuNP-P-E appear to be more effective in delivering embelin to cancer cells. The expectation is that AuNP-P-E should therefore also be more cytotoxic than AuNP-E nanoparticles. However, the results generated using the APOPercentage™ assay (Figure 3.9) is not in agreement with this. The possibility exists that the nanoparticles could have been taken up by the vesicles. Therefore, they were not accessible to the mitochondria as observed in Figure 3.11. Alternatively, since AuNP-P-E nanoparticles are biconjugated with the cancer targeting peptide and embelin, it is possible that these particles do not carry high amounts of embelin into the cells or that the embelin is not functional (which could be as a consequence of bioconjugation) and is therefore not able to inhibit XIAP. Even though AuNP-E nanoparticles are not taken up by the readily as AuNP-P-E nanoparticles, these nanoparticles carry more embelin into the cells (since these particles are only conjugated with embelin and not the peptide as well) and are therefore more effective in blocking the effects of XIAP.

Co-treatment with ceramide and AuNP-E induced higher levels of apoptosis in HepG2 cells compared to cells co-treated with ceramide and AuNP-P-E, while apoptosis induced by co-treatment with ceramide and AuNP-E was lower in MCF7 than HepG2 cells. Co-treatment with ceramide and AuNP-P-E was more effective in HepG2 cells compared to MCF7 cells. This can possibly be ascribed to the fact that HepG2 cells express low levels of XIAP. Consequently, embelin will have a bigger effect on these cells, compared to MCF7 cells,

which express high levels of this protein. In other words, the amount of embelin delivered to the cells was sufficient to block XIAP in HepG2 cells, but not in MCF7 cells.

Cells treated with AuNP or co-treated with ceramide and AuNP-P-E were evaluated by TEM to verify the presence of AuNP within cells. AuNPs were observed in clumps in the perinuclear space within the membrane bound organelles in both the HepG2 and MCF7 cancer cells treated with AuNP's (Figure 3.11). However, AuNPs were absent in HepG2 and MCF7 cancer cells (Figure 3.11) co-treated with ceramide and AuNP-P-E. Structures, which are likely to be lipid rafts, were present in the cytoplasm of these cells. These lipid rafts are absent in the untreated control cells and cells treated with AuNP. It is therefore likely that these lipid rafts are the consequence of ceramide treatment. Sphingolipids, the family of membrane lipids, have important structural roles in regulating fluidity and sub-domain structures of the lipid bilayer (Ogretmen and Hannun, 2004). With sphingomyelin as the main lipid plasma membrane of mammalian cells, it is a given that ceramide is a major source resulting from sphingomyelin hydrolysis (Hannun, 1996; Herr and Debatin, 2001). Therefore, it was concluded that the structures present in the ceramide treated cells were likely to be lipid rafts.



4.5. Expression and purification of recombinant XIAP protein

Based on the results obtained for ICP-OES and the APOPercentage™ assay (as discussed in Section 4.5), the nanoparticles biconjugated with embelin and the targeting peptide may not be able to bind to XIAP. To investigate the interaction between XIAP and embelin, XIAP and AuNP-E and XIAP and AuNP-P-E, recombinant XIAP protein was required. The human XIAP gene cloned was into the pET28a protein expression vector to produce a Histidine-tagged XIAP fusion protein which may be used to study the interaction between XIAP and embelin, XIAP and AuNP-E, and XIAP and AuNP-P-E.

The XIAP gene was cloned from the MCF7 human breast cancer cell line. This was achieved by isolating total RNA (Figure 3.12) for the generation of cDNA (Figure 3.13). XIAP gene specific primers were used to PCR amplify the cDNA which resulted in a DNA fragment with a size of ~1500 bp (Figure 3.12). This is likely to be XIAP as XIAPs expected size is 1494 bp. The PCR amplified product was ligated into the pGEM-T Easy PCR cloning vector and positive clones were identified by colony PCR (Figure 3.14). The colony PCR screen

shows that 9 (colony number 1, 3, 5, 7 and 10) of the 10 colonies were positive for the XIAP gene. Colony number 8 failed to produce the ~1500 bp amplicon and therefore does not contain the XIAP gene.

DNA sequence analysis (Figure 3.15) of colony 3 showed that this clone was 99% identical to the XIAP gene sequence (NM_001167.2) used to design the primers. Three base changes C to T at position 101, A to G at position 826, and A to G at position 932 was detected. These base changes are unlikely to be artefacts of the sequence reactions since the clone was sequenced in the forward and reverse direction with the M13 forward and M13 reverse primers and both sequences produced the same base changes. These base changes could also be the result of PCR artefacts caused by the incorporation of the incorrect bases during PCR amplification (caused by high dNTP concentrations and *Taq* polymerase errors) of XIAP gene from the MCF7 cDNA library. However, since the same base changes were identified in clone number 10 it can be concluded that these base changes are not the result of PCR artefacts, but are more likely to be base changes or mutations in the MCF7 cells.

The translation of the DNA sequence for colony 3 into protein sequence shows two mutations in the protein sequence at positions 34 and 176 (Figure 3.16). At position 34 the valine residue was changed to alanine, while the valine residue in position 176 was changed to isoleucine. Since valine, alanine and isoleucine are all non-polar, aliphatic residues (Garrett and Grisham, 2005) these mutations are not expected to have major effects on the XIAP protein. The third mutation within the DNA sequence was not detected in the protein sequence. It can therefore be concluded that the third mutation may be a silent mutation as it does not cause a change in the amino acid.

Restriction digestion of the pGEM-XIAP plasmid DNA, with *XhoI* and *NdeI*, released a DNA fragment of ~1500 bp (Figure 3.16). As the fragment had the expected size for XIAP, it was sub-cloned into the pET28a expression vector previously digested with *XhoI* and *NdeI* (Figure 3.18). Positive clones were identified by PCR amplification (Figure 3.19). All 8 colonies that were screened produced a ~1500 bp fragment, suggesting that they all contained the XIAP gene. Four of these clones (Clone number 1, 2, 3 and 4) were selected for a small-scale protein expression analysis.

Figure 3.20 shows the results for the protein expression screen on the above mentioned clones. The presence of a prominent 47 kDa protein can be seen in the protein samples. This is the expected size for the XIAP-Histidine tagged protein. However, there is no clear

evidence that this protein is induced in the presence of IPTG, since the intensity of the 47 kDa band is the same in the uninduced and induced samples. Western blot analysis was used to confirm the presence of XIAP in these samples (data not shown).

A large scale expression (Figure 3.21) of the XIAP–Histidine tagged protein was attempted using the Novagen Ni–NTA His–Bind® Resin. Figure 3.21 clearly shows the presence of a 47 kDa protein in the lysate and flow through. The intensity of the 47 kDa protein is the same in the lysate and flow through suggesting that the protein did not bind the resin efficiently. This is confirmed by the fact that a 47 kDa protein was also collected in the first wash. Very low amounts of a 47 kDa protein was eluted in Eluate 1. In an attempt to optimize the binding efficiency different concentrations of imidazole was used. Unfortunately, this proved to be an unsuccessful task (data not shown). As purification of the XIAP–Histidine tagged protein was unsuccessful using the Ni–NTA His–Bind® Resin as well as different imidazole concentrations, purification was attempted using the HIS–Select® Nickel Affinity Gel (Sigma–Aldrich). The HIS–Select® resulted in unsuccessful purification (data not shown) as insufficient protein was eluted.

Hexa–histidine tags and glutathione S–transferase (GST) tags are commonly used for the purification of recombinant proteins (Scheich *et al.*, 2003), but these tags are not equally effective in purifying recombinant proteins.

Braun and colleagues compared the efficiency of 4 affinity tags (namely GST, Maltose Binding Protein (MBP), Hexa–histidine and Calmodulin Binding Protein (CBP)) for application in the purification of recombinant proteins under denaturing and non–denaturing conditions. The purification of 36 different proteins was evaluated using all 4 affinity tags. Under non–denaturing conditions only 4 of the 32 proteins purified by the 6×His–tag were detected via Coomassie stained SDS PAGE and 15 of the 32 proteins were detected by Western blot analysis. Of the 4 proteins, only MAX and p16^{INK4a} were reasonably pure (i.e. 70%). All His–tagged proteins were lost in the flow through and/or could not be eluted from the matrix. This was true for both Ni²⁺ and Co²⁺ matrices and with a broad range of imidazole concentrations ranging between 200 and 500 mM or 5 mM EDTA used for the elution in the presence of 500 mM NaCl. Possible reasons for the low success rate of His–tagged protein purification could be due to protein loss in the flow through and/or the protein not efficiently eluted from the resin. Under non–denaturing conditions for the GST–tagged proteins: 26

proteins of the 32 were purified with a yield of at least 300 ng protein per ml of culture, while 22 of these proteins produced a yield of > 1 µg protein per ml of culture (Braun *et al.*, 2002).

The Braun study demonstrated that GST is more suitable for the purification of recombinant proteins. Consequently, a DNA construct (pGEX-4T-2-XIAP) that can be used to express recombinant GST-XIAP fusion protein was purchased from Addgene.

An expression screen was performed on 4 clones to identify clones that express the GST-XIAP protein. The expected size of GST-XIAP is 76 kDa. Figure 3.21 shows the expression of a ~75 kDa in the induced protein samples. Although this protein was also present in the uninduced protein samples, it is clear that the intensity of the 76 kDa protein was higher in the induced samples. Clone number 3 was used for large scale expression and purification of the GST-XIAP recombinant protein.

Figure 3.23 shows purification of the GST-XIAP recombinant protein using Novagen's BugBuster® GST-Bind Purification Kit (Merck). A protein band corresponding to the approximate size of 75 kDa was present in the Pellet (insoluble protein), Lysate (soluble protein), Flow through, the first Wash as well as Eluates 1, 2 and 3. No GST-XIAP was present in the Second wash. The fact that the 75 kDa protein band is so intense in the Pellet suggests that a large amount of the protein is expressed in inclusion bodies.

Inclusion bodies produced in *E. coli* are composed of densely packed denatured protein molecules. Inclusion bodies are formed from partially folded protein intermediates and are composed of aggregates of mostly single polypeptide. This assists in isolating and purifying protein aggregates of mostly single polypeptide types. This helps in isolating and purifying protein aggregates to homogeneity prior to solubilisation and refolding. Proteins occurring in the form of inclusion bodies possess native-like secondary structures (Singh and Panda, 2005).

Although the Lysate (soluble protein) contained the 75 kDa protein band, a large quantity of the protein was still present in the Pellet. This protein is also present in the Flow through, suggesting that the protein do not bind to the resin efficiently. Nonetheless, the amount of protein present in Eluates 1, 2 and 3 are significantly more than the His-XIAP protein purified using the Ni-NTA His Bind® Resin.

4.6. Protein–Protein Interactions

Technologies that can be used to analyse the interaction between biomolecules or biomolecules and drugs are very important for pharmaceutical drug development as well as the study of biology (Wienken *et al.*, 2010). Isothermal Titration Calorimetry (ITC) and Surface Plasmon Resonance (SPR) are two technologies that can be used to perform these studies.

4.6.1. Isothermal Titration Calorimetry

ITC is a sensitive technique capable of measuring heat absorption or heat release as a result of the interaction between the two reacting species (Toshima *et al.*, 2005; Olsen 2006; Bouchemal, 2008). ITC has been applied to determine stability constants, stoichiometry and interaction enthalpies. In certain experiments ITC had been used to determine entropies, Gibbs free energies as well as heat capacity changes (Bouchemal, 2008).

In an ITC experiment, it is necessary to have the addition of reactant to a sample solution that contains other reactants required for that reaction. After addition of the reactants, heat may either be absorbed or released. Heat reactions are monitored by ITC as peaks of power versus time per injection. Development of ITC data analysis methods is one of the most important researches in the field of thermodynamics for protein ligand interaction studies (Saboury, 2006).

ITC is becoming a reliable tool for the characterization of intermolecular interactions. Both high and low affinity interactions may be quickly and accurately characterized by ITC. In this technique reactive materials may be studied not only in solution but also as particulate suspensions since turbidity or sample colour has no influence the measurements. The thermodynamic parameters of the interactions can be measured without immobilization, modification or labelling of the binding partners and there is no molecular weight restrictions with this technology (Bouchemal, 2008).

4.6.2. Applications of ITC to study for Protein–Nanoparticle Interactions

ITC may be used to investigate the thermodynamics of protein–nanoparticle interactions (Lynch and Dawson, 2008). The protein of interest can be injected into the sample cell containing a solution of the nanoparticles onto which the ligand for the protein was conjugated.

Information on the binding affinities and stoichiometries for different combinations of proteins and nanoparticles are regarded as highly relevant in the field of nanotechnology. It must be considered that nanoparticles used to deliver drugs will encounter countless biomolecules (including proteins) in bodily fluids and intracellular environments that are not necessarily the target of the nanoparticle. Knowledge of the critical parameters that determine the interaction of nanoparticles with the intended target or ligand is therefore important to assess their biological effects. Rates of association and dissociation are likely to have considerable differences depending on the protein, the ligand and the type of particle. The association rate constants of some complexes approach the limit of diffusion-control whereas conformational changes upon binding may also slow the process by magnitude orders.

4.7. Investigating the binding between the recombinant GST–XIAP and embelin

XIAP is a known target of embelin. However, the conjugation of embelin AuNPs could have diminished the binding efficiency of embelin for XIAP. As discussed in Section 4.5, the failure of AuNP–P–E to enhance ceramide-induced apoptosis (even though it is taken up by cells more effectively than AuNP–E) could be due to the fact that embelin conjugated to AuNP–P–E is not able to bind XIAP. Attempts were made to study the interaction between the AuNP–P–E and XIAP, using the MicroCal™ iTC200 System. As a positive control, a binding experiment was carried out between calcium and EDTA.

A curve was fitted to the data as shown in Figure 3.23 (b). This normalized data is represented as kcal/mol of EDTA versus the molar ratio. From the curve the numbers of peaks, representing the EDTA injections, were calculated to be 0.894 ± 0.00513 , the binding constant at $2.33 \times 10^6 \text{ M}^{-1} \pm 9.90 \times 10^5$, heat change at $-3774 \text{ cal/mole} \pm 45.37$ and entropy change at $16.5 \text{ cal/mole/deg}$.

However, the ITC result for GST–XIAP and embelin failed to show that there is interaction between the drug and the protein. A possible reason for the failed experiment could be the low concentration of the recombinant GST–XIAP protein. The following equation was used to determine the desired concentration of the recombinant GST–XIAP protein:

$$M = 10 \times K_d$$

where M represents the concentration required for GST–XIAP protein and K_d the dissociation constant between XIAP and embelin.

For the experiment to be carried out successfully, the required concentration of the recombinant GST–XIAP protein is 4 μM . The concentration of GST–XIAP was 6 nM, which is approximately 7 fold less than the concentration required to study the interaction between embelin and GST–XIAP. However, because the quantities of recombinant GST–XIAP protein purified in this study were so low, it was not possible to carry out the experiment.

The presence of the GST tag could also have interfered with the experimental procedure. It may be considered to perform an additional experiment where the interaction between embelin and XIAP is investigated after the removal of the GST tag from the fusion protein. Alternatively, SPR can be used to study the interaction between XIAP and embelin. SPR is an optical phenomenon which can be used for detecting and measuring the concentration of the counterpart, or for characterising the kinetics and affinity of binding, by monitoring the change in optical properties during binding and dissociation (Lofas and Johnson, 1990). An example of SPR is the Biocore T200 (GE Healthcare). It uses the principle of SPR to study protein–protein and protein–drug interactions. The advantages of SPR over ITC is that it requires less of the potential ligands and seeing that the purification of GST–XIAP is problematic SPR may be a better alternative.

4.8. Conclusion

The objective of this study was to develop AuNP's that can be used to target the delivery of embelin to cancer cells and enhance the pro–apoptotic effects of ceramide. AuNP's were synthesized and conjugated with embelin and the cancer targeting peptide with the following amino acid sequence: LTVSPWY. This study showed that cancer cells very efficiently take up AuNP conjugated with this peptide. AuNP conjugated with embelin significantly enhanced the pro–apoptotic effects of ceramide and can therefore be used to kill cancer cells more effectively. However, AuNP biconjugated with embelin and the targeting peptide failed to enhance the pro–apoptotic effects of ceramide. It is likely that biconjugation with the targeting peptide lowered the embelin loading on the particles and consequently these particles are not able to deliver embelin efficiently to the cells.

Even though this study requires further optimization, it successfully demonstrated that AuNP conjugated with embelin could be used to enhance the effects of anti-cancer drugs.

4.9. Future Directions

The present study has limitations that need to be addressed. The investigation into the interaction between XIAP and embelin, XIAP and AuNP-E and XIAP and AuNP-P-E was not completed in this study. The limiting factor was the amount of interaction of recombinant XIAP. Therefore the purification of recombinant GST-XIAP will need to be optimized. The removal of the GST tag from the GST-XIAP fusion protein can possibly also resolve the problems experienced with ITC. Alternatively, instead of using ITC, these interactions may also be studied by SPR.

Compared to AuNP-E, AuNP-P-E was not very effective in promoting ceramide induced apoptosis in the cancer cells. It is likely the molar ratio's of AuNP:targeting peptide:embelin used in the synthesis of the nanoparticle resulted in the particle carrying more of the peptide and less of the embelin. It would therefore be advisable to optimise the molar ratio's of the AuNP, targeting peptide and embelin in order to produce a nanoparticle that can target the cancer cells efficiently, but still carry sufficient quantities of embelin to the cells.

Finally, the treatments with AuNP-P-E as well as AuNP-P-E and ceramide should be tested on other cancer cell lines as well. Also, apoptosis induction should also be investigated using anti-cancer drugs.

REFERENCES

- Abdelhalim, M. A. K., Mady, M. M. and Ghannam, M. M. (2012) Physical properties of different gold nanoparticles: ultraviolet–visible and fluorescence measurements, *Journal of Nanomedicine and Nanotechnology*, **3**: 1–5
- Ahn, K. S., Sethi, G. and Aggarwal, B. B. (2007) Embelin, and inhibitor of X chromosome–linked inhibitor–of–apoptosis–protein, blocks Nuclear Factor–kB (NF–kB) signalling pathway leading to suppression of NF–kB–regulated anti–apoptotic and metastatic gene products, *Molecular Pharmacology*, **71**: 209–219
- Aina, O. H., Liu, R., Sutcliffe, J. L., Pan, C–X and Lam, K. S. (2007) From combinatorial chemistry to cancer targeting peptides, *Molecular Pharmaceutics*, **4**: 631–651
- Allen, T. M. (2002) Ligand–targeted therapeutics in anticancer therapy, *Nature: Cancer Reviews*, **2**: 750–763
- Altschul, S. F., Gish, W., Miller, W., Myers, E. W. and Lipman, D. J. (1990) Basic local alignment search tool, *Journal of Molecular Biology*, **215**: 403–410
- Andrieu–Abadie, N., Gouaze, V., Salvayre, R. and Levade, T. (2001) Ceramide in apoptosis signalling: relationship with oxidative stress, *Free Radical Biology and Medicine*, **31**: 717–728
- Bachur, N. R., Gordon, S. L. and Gee, M. V. (1978) A general mechanism for microsomal activation of quinone anticancer agents to free radicals, *Cancer Research*, **38**: 1745–1750
- Blagosklonny, M. V. (2004) Prospective strategies to enforce selectively cell death in cancer cells, *Oncogene*, **23**: 2967–2975
- Bolton, J. L., Trush, M. A., Penning T. M., Dryhurst, G. and Monks, T. J. (2000) Role of quinones in toxicology, *Chemical Research Toxicology*, **13**: 135–160
- Bouchemal, K. (2008) New challenges for pharmaceutical formulations and drug delivery system characterization using isothermal titration calorimetry, *Drug Discovery Today*, **13**: 960–972

Braun, P., Hu, Y., Shen, B., Halleck, A., Koundinya, M., Harlow, E. and LaBaer, J. (2002) Proteome-scale purification of human proteins from bacteria, *Proceedings of the National Academy of Sciences*, **99**: 2654–2659

Brigger, I., Dubernet, C. and Couvreur, P. (2002) Nanoparticles in cancer therapy and diagnosis, *Advanced Drug Delivery Reviews*, **54**: 631–651

Brown, J. M. and Attardi, L. D. (2005) The role of apoptosis in cancer development and treatment response, *Nature Reviews: Cancer*, **5**: 231–237

Cai, W., Gao, T., Hong, H. and Sun, J. (2008) Applications of gold nanoparticles in cancer nanotechnology, *Nanotechnology, Science and Application*, **1**: 17–32

Carter, J. C. and Church, F. C. (2009) Obesity and breast cancer: the roles of peroxisome proliferator-activated receptor- γ and plasminogen activator inhibitor-1, PPAR Research, article ID 345320

Cedervall, T., Lynch, I., Lindman, S., Berggard, T., Thulin, E., Nilsson, H., Dawson, K. A. and Linse, S. (2007) Understanding the nanoparticle-protein corona using methods to quantify exchange rates and affinities of proteins for nanoparticles, *Proceedings of the National Academy of Sciences*, **104**: 2050–2055

Chen, M. and Wang, J. (2002) Initiator caspases in apoptosis signalling pathways, *Apoptosis*, **7**: 313–319

Chen, J., Nikolovska-Coleska, Z., Wang, G., Qiu, S. and Wang, S. (2006) Design, synthesis and characterization of new embelin derivatives as potent inhibitors of X-linked inhibitor of apoptosis proteins, *Bioorganic and Medicinal Chemistry Letters*, 5805–5808

Cho, K., Wang, X., Nie, S., Chen, Z. G. and Shin, D. M. (2008) Therapeutic nanoparticles for drug delivery in cancer, *Clinical Cancer Research*, **14**: 1310–1316

Christian, P., Von der Kammer, F., Baalousha, M. and Hofmann, T. (2008) Nanoparticles: structure, properties, preparation and behaviour in environmental media, *Ecotoxicology*, **17**: 326–343

Cretney, E., Takeda, K. and Smyth, M. J. (2007) Cancer: novel therapeutic strategies that exploit the TNF-related apoptosis-inducing ligand (TRAIL)/TRAIL receptor pathway, *International Journal of Biochemistry and Cell Biology*, **39**: 280–286

- de Jong, W. H. and Borm, P. J. A. (2008) Drug delivery and nanoparticles: applications and hazards, *International Journal of Nanomedicine*, **3**: 133–149
- Deveraux, Q. L., Takashi, R., Salvesen, G. S. and Reed, J. C. (1997) X-linked IAP is a direct inhibitor of cell-death proteases, *Nature*, **188**: 300–304
- Deveraux, Q. L. and Reed, J. C. (1999) IAP family of proteins—suppressors of apoptosis, *Genes and Development*, **13**: 239–252
- Deveraux, Q. L., Stennicke, H. R., Salvesen, G. S. and Reed, J. C. (1999) Endogenous Inhibitors of Caspases, *Journal of Clinical Immunology*, **19**: 388–398
- Ferlay, J., Shin, H. R., Bray F, Forman, D., Mathers, C. and Parkin, D. M. (2010) Estimates of worldwide burden of cancer 2008: GLOBOCAN 2008, *International Journal of Cancer*, **127**: 2893–2917
- Fesik, S. W. (2005) Promoting apoptosis as a strategy for cancer drug discovery, *Nature: Cancer Reviews*, **5**: 876–885
- Fischer, U. and Schulze–Osthof, K. (2005¹) Apoptosis–based therapies and drug targets, *Cell Death and Differentiation*, **12**: 942–961
- Fischer, U. and Schulze–Osthof, K. (2005²) New approaches and therapies targeting apoptosis in disease, *Pharmacological Reviews*, **57**: 187–215
- Friedrich, K., Wieder, T., Van Haefen, C., Radetzki, S., Janicke, R., Schulze–Osthoff, K., Dorken, B. and Daniel, P. T. (2001) Overexpression of caspase–3 restores sensitivity for drug–induced apoptosis in breast cancer cell lines with acquired drug resistance, *Nature: Oncogene*, **20**: 2749–2760
- Fry, D. C. and Vassilev, L. T. (2005) Targeting protein–protein interactions for cancer, *Journal of Molecular Medicine*, **83**: 995–963
- Gao, Z., Tian, Y., Wang, J., Yin, Q., Wu, H, Li, Y. M. and Jiang, X. (2007) A dimeric Smac/DIABLO peptide directly relieves caspase 3 inhibition by XIAP – dynamic and cooperative regulation of XIAP by Smac/DIABLO, *Journal of Biological Chemistry*, **282**: 30718–30727

- Garcia, M., Jemal, A., Ward, E. M., Center, M. M., Hao, Y., Siegelin, R. L. and Thun, M. J. (2007) Global Cancer Facts and Figures 2007, *American Cancer Society*
- Garrett, R. H. and Grisham, C. M. (2005) *Biochemistry: Amino Acids*, Third Edition, Singapore: Thomson Learning, Inc.
- Gelperina, S., Kisich, K., Iseman, M. D. and Heifits, L. (2005) The potential advantages of nanoparticle drug delivery systems in chemotherapy of Tuberculosis, *American Journal of Respiratory and Critical Care Medicine*, **172**: 1487–1490
- Gewies, A. (2003) Introduction to apoptosis, ApoReview
- Ghavami, S., Hashemi, M., Ande, S. R., Yeganeh, B., Xiao, W., Eshraghi, M., Bus, C. J., Kadkhoda, K., Wiechec, E., Halayko, A. J. and Los, M. (2009) Apoptosis and cancer: mutations within caspase genes, *Journal of Medical Genetics*, **46**: 497–510
- Ghosh, P., Han, G., De, M., Kim, C. K. and Rotello, V. M. (2008) Gold nanoparticles in delivery applications, *Advanced Drug Delivery Reviews*, **60**: 1307–1315
- Gotter T. G., (2009) Apoptosis and cancer: the genesis of a research field, *Nature Reviews: Cancer*, **9**: 501–507
- Gourishankar, A., Shukla, S., Ganesh, K. N. and Sastry, M. (2004) Isothermal titration calorimetry studies on the binding of DNA bases and PNA base monomers to gold nanoparticles, *Journal of the American Chemical Society*, **126**: 13186–13187
- Green, D. R. and Martin, S. J. (1995) The killer and the executioner: how apoptosis controls malignancy, *Current Opinion in Immunology*, **7**: 694–703
- Haley, B. and Frenkel, H. (2003) Nanoparticles for drug delivery in cancer treatment, *Urological Oncology: Seminars and Originals Investigations*, **26**: 57–64
- Hao, Z. and Mak, T. W. (2010) Type I and type II pathways of Fas-mediated apoptosis are differentially controlled by XIAP, *Journal of Molecular and Cell Biology*, **2**: 63–64
- Hanahan, D. and Weinberg, R. A. (2000) The hallmarks of cancer, *Cell*, **100**: 57–70
- Hannun, Y. A. (1996) Functions of ceramide in coordinating cellular response to stress, *SCIENCE*, 274: 1866–1859

- Hannun, Y. A. and Luberto, C. (2000) Ceramide in the eukaryotic stress system, *TRENDS in Cell Biology*, **10**: 73–80
- Hengartner, M. O. (1996) Programmed cell death in invertebrates, *Current Opinion in Genetics and Development*, **6**: 34–38
- Herr, I. and Debatin, K–M. (2001) Cellular stress response and apoptosis in cancer therapy, *Blood*, **98**: 2603–2614
- Holcik, M., Gibson, H. and Korneluk, R. G. (2001) XIAP: apoptotic brake and promising therapeutic agent, *Apoptosis*, **6**: 253–261
- Hou, X. and Jones, B. T. (2000) *Encyclopedia of Analytical Chemistry*, Inductively Coupled Plasma/Optical Emission Spectrometry, R. A. Meyers Edition, Chichester: John Wiley and Sons Ltd
- Huang, W–C., Chem, C–L., Lin, Y–S. and Lin, C–F (2011) Apoptotic sphingolipid ceramide in cancer therapy, *Journal of Lipids*, 1–15
- Hui, S. K., Tse, M–K., Yang, Y., Wong, B. C–Y and Sze, K–H (2010) Backbone and side–chain ¹H, ¹³C and ¹⁵N assignments of the ubiquitin–associated domain of human X–linked inhibitor of apoptosis protein, *Biomolecular NMR Assignments*, **4**: 13–15
- Igney, F. H. and Krammer, P. H. (2002) Death and anti–death: tumour resistance to apoptosis, *Nature Reviews: Cancer*, **2**: 277–288
- Jiang, Z., Hong, X., Long, H., Hu, J. and Zhai, Z. (2000) Ceramides induce apoptosis in HeLa cells and enhance cytochrome c–induced apoptosis in *Xenopus* egg extracts, *Cellular and Molecular Life Sciences*, **57**: 1117–1125
- Johnson–Thompson, M. C. and Guthrie, J. (2000) Ongoing research to identify environmental risk factors in breast carcinoma, *American Cancer Society*, **88**: 1224–1229
- Joshi, H., Shirude, P. S., Bansal, V., Ganesh, K. N. and Sastry, M. (2004) Isothermal titration calorimetry studies on the binding of amino acids to gold nanoparticles, *Journal of Physical Chemistry B*, **108**: 11535–11540

Joshi, R., Kamat, J. P. and Mukherjee, T. (2007) Free radical scavenging reactions and antioxidant activity of embelin: biochemical and pulse radiolytic studies, *Chemico–Biology Interactions*, **167**: 125–134

Joshi, R., Ghanty, T. K. and Mukherjee, T. (2009) Formation of semiquinone radical in the reaction of embelin (2,5–dihydroxy–3–undecyl–1,4–benzoquinone) with reductants as well as oxidants. Characterization by pulse radiolysis and structure investigation by quantum chemical study, *Journal of Molecular Structure*, **928**: 46–53

Kroemer, G., El–Deiry, W. S., Golstein, P., Peter, M. E., Vaux, D., Vandenabeele, P., Zhivotovsky, B., Blagosklonny, M. V., Malorni, W., Knight, R. A., Piacentini, M., Nagata, S. and Melino, G. (2005) Classification of cell death: recommendations of the Nomenclature Committee on Cell Death, *Cell Death and Differentiation*, **12**: 1463–1467

Ladbury, J. E. and Chowdhry, B. Z. (1996) Sensing the heat: the application of isothermal titration calorimetry to thermodynamic studies of biomolecular interactions, *Chemistry and Biology*, **3**: 791–801

LaCasse, E. C., Baird, S., Korneluk, R. G. and MacKenzie, A. E. (1998) The inhibitors of apoptosis (IAPs) and their emerging role in cancer, *Oncogene*, **17**: 3247–3259

LaVan, D. A., McGuire, T. and Langer, R. (2003) Small–scale systems for *in vivo* drug delivery, *Nature: Biotechnology*, **21**: 1184–1191

Liu, Z., Sun, C., Olejniczak, E. T., Meadows, R. P., Betz, S. F., Oost, T., Herrmann, J., Wu, J. C., and Fesik, S. W. (2000) Structural basis for binding Smac/DIABLO to the XIAP BIR3 domain, *Nature*, **408**: 21–28

Liu, J., Zhang, D., Luo, W., Yu, Y., Yu, J., Jingxia, Z., Zhang, B., Chen, J., Wu, X–R., Rosas–Acosta, G. and Huang, C. (2011) X–linked inhibitor of apoptosis protein (XIAP) mediates cancer cell motility via Rho GDP dissociation inhibition (RhoGDI)–dependent regulation of the cytoskeleton, *Journal of Biological Chemistry*, **286**: 15630–15640

Los, K., Burek, C. J., Stroh, C., Benedyk, K., Hug, H. and Mackiewicz, A. (2003) Anticancer drugs of tomorrow: apoptotic pathways as targets for drug design, *Drug Discovery Today*, **8**: 67–77

- Meng, X. W., Lee, S-H and Kaufmann, S. H. (2006) Apoptosis in the treatment of cancer: a promise kept?, *Current Opinion in Cell Biology*, **18**: 668–676
- Mufti, A. R., Burstein, E. and Duckett, C. S. (2007) XIAP: cell death regulation meets copper homeostasis, *Archives of Biochemistry and Biophysics*, **463**: 168–174
- Myszka, D. G. and Rich, R. L. (2000) Implementing surface plasmon resonance biosensors in drug discovery, *Pharmaceutical Science and Technology Today*, **3**: 310–317
- Nachmias, B., Asshab, Y., Bucholtz, V., Drize, O., Kadouri, L., Lotem, M., Peretz, T., Mandelboim, O. and Ben-Yehuda, D. (2003) Caspase-mediated cleavage converts Livin from an anti-apoptotic to a pro-apoptotic factor: implications for drug-resistant melanoma, *Cancer Research*, **63**: 6340–6349
- Meyer, M., Essack, M., Kanyanda, S. and Rees, J. G. (2008) A low-cost flow cytometric assay for the detection and quantification of apoptosis using an anionic halogenated fluorescein dye, *BioTechniques*, **45**: 317–320
- Nachmias, B., Ashhab, Y. and Ben-Yehuda, D. (2004) The inhibitor of apoptosis protein family (IAPs): an emerging therapeutic target in cancer, *Seminars in Cancer Biology*, **14**: 231–243
- Nikolovska-Coleska, Z., Wang, R., Fang, X., Pan, H., Tomita, Y., Li, P., Roller, P. P., Krajewski, K., Saito, N. G., Stuckey, J. A. and Wang, S. (2004¹) Development and optimization of a binding assay for the XIAP BIR3 domain using fluorescence polarization, *Analytical Biochemistry*, **332**: 261–273
- Nikolovska-Coleska, Z., Xu, L., Hu, Z., Tomota, Y., Li, P., Roller, P. P., Wang, R., Fang, X., Guo, R., Zhang, M., Lippman, M. E., Yang, D. and Wang, S. (2004²) Discovery of Embelin as a cell-permeable, small-molecular weight inhibitor of XIAP through structure-based computational screening of a traditional herbal medicine three-dimensional structure database, *Journal of Medicinal Chemistry*, **47**: 2430–2440
- Ogretmen, B. and Hannun, Y. A. (2004) Biologically active sphingolipids in cancer pathogenesis and treatment, *Nature Reviews: Cancer*, **4**: 604–616
- Olsen, S. N. (2006) Applications of isothermal titration calorimetry to measure enzyme kinetics and activity in complex solutions, *Thermochimica Acta*, **448**: 12–18

- Papasani, M. R., Wang, G. and Hill, R. A. (2012) Gold nanoparticles: the importance of physiological principles to devise strategies for targeted delivery, *Nanomedicine: Nanotechnology, Biology and Medicine*, **8**: 808–814
- Parton, M., Dowsett, M. and Smith, I. (2001) Studies of apoptosis in breast cancer, *British Medical Journal*, **322**: 1528–1532
- Pathan, R., A. and Bhandari, U. (2011) Preparation and characterization of embelin–phosphate complex as effective drug delivery tool, *Journal of Inclusion Phenomena and Macrocyclic Chemistry*, **69**: 139–147
- Patra, C. R., Bhattacharya, R., Mukhopadhyay, D. and Mukherjee, P. (2010) Fabrication of gold nanoparticles for targeted therapy in pancreatic cancer, *Advanced Drug Delivery Reviews*, **62**: 346–361
- Pettus, B. J., Chalfant, C. E. and Hannun, Y. A. (2002) Ceramide in apoptosis: an overview and current perspectives, *Biochimica et Biophysica Acta*, **1585**: 114–125
- Pierce, M. M., Raman, C. S. and Nall, B. T. (1999) Isothermal titration calorimetry of protein–protein interactions, *METHODS*, **19**: 213–221
- Radin, N. S. (2003) Killing tumours by ceramide–induced apoptosis: a critique of available drugs, *Biochemical Journal*, **371**: 243–256
- Raychaudhuri, S. (2010) How can we kill cancer cells: insight from the computational models of apoptosis, *World Journal of Clinical Oncology*, **1**: 24–28
- Riedl, S. J., Renatus, M., Schwarzenbacher, R., Zhou, Q., Sun, C., Fesik, S. W., Liddington, R. C. and Salvesen, G. S. (2001) Structural basis for the inhibition of caspase–3 by XIAP, *Cell*, **104**: 791–800
- Saboury, A. A. (2006) A Review on the ligand binding studies by isothermal titration calorimetry, *Journal of the Iranian Chemical Society*, **3**: 1–21
- Salvesen, G. S. and Dixit, V. M. (1997) Caspases: Intracellular Signalling by Proteolysis, *Cell*, **91**: 443–446
- Schimmer, A. D. (2004) Inhibitor of Apoptosis Proteins: translating basic knowledge into clinical practice, *Cancer Research*, **64**: 7183–7190

Scheich, C., Sievert, V and Bussow, K (2003) An automated method for high-throughput protein purification applied to a comparison of His-tag and GST-tag affinity chromatography, *BMC Biotechnology*, **3**:12

Schimmer, A. D., Welsh, K., Panilla, C., Wang, Z., Krajewska, M., Bonneau, M-J., Pedersen, I. M., Kitada, S., Scott, F. L., Bailly-Maitre, B., Glinsky, G., Scudiero, D., Sausville, E., Salvesen, G., Nefzi, A., Ostresh, J. M., Houghten, R. A. and Reed, J. C. (2004) Small-molecule antagonists of apoptosis suppressor XIAP exhibit broad antitumour activity, *Cancer Cell*, **5**: 25–35

Schimmer, A. D., Dalili, S., Batey, R. A. and Riedl, S J. (2006) Targeting XIAP for the treatment of malignancy, *Cell Death and Differentiation*, **13**: 179–188

Schumacker, P. T. (2006) Reactive oxygen species in cancer cells: live by the sword, die by the sword, *Cancer Cell*, 175–176

Scott, F. L., Denault, J. B., Riedl, S. R. Shin, H., Renucci, M. and Salvesen, G. S. (2005) XIAP inhibits caspase -3 and -7 using two binding sites: evolutionary conserved mechanisms of IAPs, *European Molecular Biology Organization Journal*, **24**: 645–655

Sellers, W. R. and Fisher, D. E. (1999) Apoptosis and cancer drug targeting, *The Journal of Clinical Investigation*, **104**: 1655–1661

Selzner, M., Bielawski, A., Morse, M. A., Rudiger, H. A., Sindram, D., Hannun, Y. A. and Clavien, P-A. (2001) Induction of apoptotic cell death and prevention of tumour growth by ceramide analogues in metastatic colon cancer, *Cancer Research*, **61**: 1233–1240

Shadidi, Mand Sioud, M. (2003¹) Identification of novel carrier peptides for the specific delivery of therapeutics into cancer cells, *Federation of American Societies for Experimental Biology Journal*, **17**: 256–258

Shadidi, M. and Sioud, M. (2003²) Selective targeting of cancer cells using synthetic peptides, *Drug Resistance Updates*, **6**: 363–371

Shabbits, J. A., Hu, Y. and Mayer, L. D. (2003) Tumour chemosensitization strategies based on apoptosis manipulations, *Molecular Cancer Therapeutics*, **2**: 805–813

Shiozaki, E. N. and Yigong, S. (2004) Caspases, IAPs and Smac/DIABLO: mechanisms from structural biology, *TRENDS in Biochemical Sciences*, **39**: 486–494

Siegelin, M. D., Gaiser, T. and Siegelin, Y. (2009) The XIAP inhibitor Embelin enhances TRAIL-mediated apoptosis in malignant glioma cells by down-regulation of the short isoform of FLIP, *Neurochemistry International*, **55**: 423–430

Singh, S. M. and Panda, A. K. (2005) Solubilization and refolding of bacterial inclusion body proteins, *Journal of Bioscience and Bioengineering*, **99**: 303–310

Sinha, R., Kim, G. J., Nie, S. and Shim, D. M. (2006) Nanotechnology in cancer therapeutics: bioconjugated nanoparticles for drug delivery, *Molecular Cancer Therapeutics*, **5**: 1909–1917

Sousa, J. F. and Espreafico, E. M. (2006) Malonoma Survival Strategies: The intrinsic apoptotic pathway—upstream and downstream regulators, *Journal of Morphological Sciences: Functional Anatomy and Cell Biology*, **23**: 43–56

Tamm, I., Kornblau, S. M., Segall, H., Krajewski, S., Welsh, K., Kitada, S., Scudiero, D. A., Tudor, G., Qui, Y. H., Monks, A., Andreeff, M. and Reed, J. C. (2000) Expression and prognostic significance of IAP-family genes in human cancers and myeloid cancers, *Clinical Cancer Research*, **6**: 1796–1803

Thornberry, N. A. and Lazebnik, Y. (1998) Caspases: enemies within, *SCIENCE*, **281**: 1312–1316

Toshima, N., Kanemaru, M., Shiraishi, Y. and Koga, Y. (2005) Spontaneous formation of core/shell bimetallic nanoparticle: a calorimetric study, *Journal of Physical Chemistry B*, **109**: 16326–16331

Trentham-DieDietz, A., Newcomb, P. A., Nichols, H. B. and Hampton, J. M. (2007) Breast cancer risk factors and second primary malignancies among women with breast cancer, *Breast Cancer Research Treatment*, **105**: 195–207

Utreja, P., Jain, S. and Tiwary, A. K. (2010) Novel drug delivery systems for sustained and targeted delivery of anti-cancer drugs: current status and future aspects, *Current Drug Delivery*, **7**: 152–161

Velazques-Campoy, A. and Freire, E. (2006) Isothermal titration calorimetry to determine association constants for high-affinity ligands, *Nature*, **1**: 186–191

Wagenknecht, B., Roth, W., Gulbins, E.m Wolburg, H. and Weller, M. (2001) C2–ceramide signalling in glioma cells: synergistic enhancement of CD95–mediated, caspase–dependent apoptosis, *Cell Death and Differentiation*, **8**: 595–602

Wienken, C. J., Baaske, P., Rothbauer, U., Braun, D. and Duhr, S. (2010) Protein–binding assays in biological liquids using microscale thermophoresis, *Nature Communications*, **1093**: 1–7

Xu, M., Jingrong, C., Fu, H., Proksch, P., Lin, W. and Li, M. (2005) Embelin derivatives and their anticancer activity through microtubule assembly, *Planta Medica*, **71**: 944–958

Yih, T. C. and Al–Fandi, M. (2006) Engineered nanoparticles as precise drug delivery systems, *Journal of Cellular Biochemistry*, **97**: 1184–1190

Ziedan, N. I., Kadri, H. and Westwell, A. D. (2008) The development of Pro–Apoptotic Cancer Therapies, *Medical Reviews in Medicinal Chemistry*, **8**: 711–718



ImageJ:

Rasband, W.S., ImageJ, U. S. National Institutes of Health, Bethesda, Maryland, USA, <http://imagej.nih.gov/ij/>, 1997–2012